Stony Brook University

$G\alpha_q$ Regulation of Cardiac Autophagy

A Dissertation Presented

by

Shengnan Liu

to

The Graduate School

in Partial Fulfillment of the

Requirements

for the Degree of

Doctor of Philosophy

in

Molecular and Cellular Program

Immunology and Pathology Track

Stony Brook University

May 2016

Stony Brook University

The Graduate School

Shengnan Liu

We, the dissertation committee for the above candidate for the

Doctor of Philosophy degree, hereby recommend

acceptance of this dissertation.

Richard Z. Lin, M.D.
Professor, Department of Physiology and Biophysics

Deborah A. Brown, Ph.D.
Professor, Department of Biochemistry and Cell Biology

Ira S. Cohen, M.D., Ph.D.
Leading Professor, Department of Physiology and Biophysics

Wei-Xing Zong, Ph.D.
Professor, Department of Chemical Biology, Rutgers, The State University of New Jersey

Lixin Liu, M.D., Ph.D.
Associate Professor, Department of Anesthesiology

This dissertation is accepted by the Graduate School

Charles Taber
Dean of the Graduate School

Abstract of the Dissertation

$G\alpha_q$ Regulation of Cardiac Autophagy

by

Shengnan Liu

Doctor of Philosophy

in

Molecular and Cellular Biology Program

Immunology and Pathology Track

Stony Brook University

2016

Receptors that activate the heterotrimeric G protein $G\alpha_q$ are thought to play a role in the development of heart failure. Dysregulation of autophagy occurs in some pathological cardiac conditions including heart failure, but whether $G\alpha_q$ is involved in this process is unknown. A cardiomyocyte-specific transgenic mouse model of inducible $G\alpha_q$ activation (termed $G\alpha_q$Q209L) was used to address this question. Autophagy is a quality control and recycling process in which double-membrane vesicles called autophagosomes enclose intracellular materials and send them to lysosomes for degradation. After 7 days of $G\alpha_q$ activation, $G\alpha_q$Q209L hearts contained more autophagic vacuoles than wild type (WT) hearts. Increased levels of proteins involved in autophagy, including Vps34, Beclin1, Atg7, Atg14, p62 and LC3-II, were also seen. Real-time quantitative PCR showed a 4-fold upregulation in p62 mRNA and a small increase in Atg7 mRNA, but mRNAs encoding the other proteins were not transcriptionally upregulated. Inhibition of the Ca^{2+}-dependent protease calpain, whose activity is increased in $G\alpha_q$Q209L hearts, did not block the increase in LC3-II protein, suggesting that increased autophagy is not due to calpain activation.

LysoTracker staining and western blotting showed that the number and size of lysosomes and lysosomal protein levels were increased in $G\alpha_q$Q209L hearts, indicating enhanced lysosomal degradation activity. Importantly, an autophagic flux assay measuring LC3-II turnover indicated that autophagic activity is enhanced in $G\alpha_q$Q209L hearts. $G\alpha_q$Q209L hearts exhibited elevated levels of the Class III phosphoinositide 3-kinase (Vps34) complex. As a consequence, Vps34 activity and phosphatidylinositol 3-phosphate levels were higher in $G\alpha_q$Q209L hearts than WT hearts, thus accounting for the higher abundance of autophagic vacuoles. These results indicate that an increase in autophagy is an early response to $G\alpha_q$ activation in the heart.

To my beloved parents

Guangtian Liu

and

Yan Liu

Table of Contents

List of Figures

List of Abbreviations

4-OHT	4-hydroxytamoxifen
AA	$G\alpha_q$Q209L-AA-hbER
ACE	Angiotensin-converting enzyme
AMPK	AMP-activated protein kinase
AT1	Angiotensin II receptor type 1
ATG	Autophagy-related genes
AVd	Degradative autophagic vacuoles
AVi	Initial autophagic vacuoles
CaMKIIδ	Ca2+/CaM-dependent protein kinase II
CAPN	Calpain
CAPNS1	Calcium-dependent protease small subunit 1
CVD	Cardiovascular disease
DAG	Diacylglycerol
DIC	Differential interference contrast
ER	Endoplasmic reticulum
GNAQ	G protein subunit alpha q
GPCR	G protein coupled receptor
hbER	Hormone binding domain of estrogen receptor
HF	Heart failure
HSP	Heat shock protein
KCNE1	Potassium channel, voltage gated subfamily E regulatory beta subunit 1
KCNQ1	Potassium channel, voltage gated KQT-Like subfamily Q, member 1
IP	Immunoprecipitation
IP_3	Inositol 1,4,5-trisphosphate
IP_3R	Inositol 1,4,5-trisphosphate receptor
LC3	Microtubule-associated proteins 1A/1B light chain 3
MEF	Mouse embryonic fibroblast
mTORC1	Mechanistic target of rapamycin complex 1

NRCM	Neonatal rat cardiomyocyte
PE	Phosphoethanolamine (Chapter 1)
PE	Phenylephrine (Chapter 4)
PI	Phosphatidylinositol
PI(3)P	Phosphatidylinositol 3-phosphate
PI3K	Phosphoinositide 3-kinase
PIP_2	PI 4,5-bisphosphate
PKC	Protein kinase C
PLB	Phospholamban
PLCβ	Phospholipase C β
QL	$G\alpha_q Q209L$
ROS	Reactive oxygen species
SERCA-2	Sarcoplasmic reticulum Ca^{2+} ATPase-2
SR	Sarcoplasmic reticulum
TRPC6	Transient receptor potential cationchannel, subfamily C, member 6
ULK1	unc-51 like autophagy activating kinase 1
UPS	Ubiquitin-proteasome system
α_{1A}-AR	α1A-adrenergic receptor
αMHC	α myosin heavy chain

Acknowledgements

I acknowledge the Molecular and Cellular Biology Program at Stony Brook University, who provided me the chance of studying life sciences in the United States.

I acknowledge my advisor, Dr. Richard Lin, for providing me the opportunity to work in his lab and guiding me through the entire PhD study.

I acknowledge my mentors, Dr. Wei-Xing Zong and Dr. Lisa M. Ballou, for their guidance and training on me. Thanks to Dr. Yaping Jiang, who taught me knowledge about the heart.

I acknowledge my committee members, who never hold back their support and encouragement.

I acknowledge my colleagues, especially Dr. Jian Pan, Dr. Eileen So Carpenter, Nithya Sivaram, and Jennifer DeLeon for providing help in lab and in life.

Special thanks to my friends, Dr. Lin Zhang, Dr. Jiangfang Zhu, Dr. Yeting Zhang, Dr. Song Feng, Dr. Yulin Huang and Dr. Lingling Jiang, who greatly supported me during my hardest time.

My words are plain, but I hold a deep gratefulness for all the people I have encountered during these seven years pursuing my PhD.

Publications

Liu S, Jiang YP, Ballou LM, Zong WX, Lin RZ. Activation of $G\alpha_q$ in cardiomyocytes increases Vps34 activity and stimulates autophagy. *Journal of Cardiovasc Pharmacol*. Revise and resubmit.

Wu CY, Chen B, Jiang YP, Jia Z, Martin DW, **Liu S**, Entcheva E, Song LS, Lin RZ. Calpain-dependent cleavage of junctophilin-2 and T-tubule remodeling in a mouse model of reversible heart failure. *J Am Heart Assoc*. 2014 Jun 23; 3(3).

Lu Z, Jiang YP, Wu CY, Ballou LM, **Liu S**, Carpenter ES, Rosen MR, Cohen IS, Lin RZ. Increased persistent sodium current due to decreased PI3K signaling contributes to QT prolongation in the diabetic heart. *Diabetes*. 2013 Dec; 62(12):4257-65.

Chapter 1. Background

1-1. $G\alpha_q$ in heart failure

1-1-1. Heart failure and its animal models

Heart failure (HF) is a clinical syndrome with primary symptoms including dyspnea, fatigue, exercise intolerance and retention of fluid in the lungs and peripheral tissues (1). According to the World Health Organization, cardiovascular diseases (CVDs) are the leading cause of death, contributing to ~31% of deaths worldwide (2). HF is the leading cause of mortality and morbidity in the United States (1). Despite the development of multiple treatments, therapy for HF remains very unsatisfactory, and the 5-year mortality rate is about 50% (3,4). Thus, there is a need to develop novel preventative and reparative therapies (1).

There are many animal models designed to recapitulate the different types of HF seen in human patients. For example, aortic constriction in mice and rats mimics aortic stenosis-induced HF; coronary artery ligation in pigs and sheep induces dilated ischemic cardiomyopathy; and hypertensive heart disease-induced HF is studied in a spontaneously hypertensive rat (1). Large animal models such as dogs and pigs provide a closer approximation of human HF conditions than rodents. However, small animal models including transgenic mice provide opportunities for studying specific molecular mechanisms of HF (1).

1-1-2. G proteins

G protein-coupled receptors (GPCRs) make up the largest family of transmembrane receptors (5). More than 1,000 GPCRs are encoded in mammalian genomes. The majority of GPCRs are sensory receptors, and about 400-500 GPCRs recognize and transmit signals from hormones, neurotransmitters, and paracrine factors into cells. Only a small fraction of GPCRs (~200) have identified physiological ligands. Most of the others are called "orphan" GPCRs because no endogenous ligands have been identified for them (6).

GPCRs couple to signaling partners known as heterotrimeric G proteins to work coordinately to recognize extracellular ligands and transmit signals into cells. G proteins are composed of three subunits: Gα and a dimer of Gβ and Gγ that never separates. As illustrated in Fig. 1-1, upon activation by a ligand (Step A), the GPCR induces exchange of GDP on Gα to GTP (Step B), which activates Gα. Gβγ then dissociates from Gα-GTP (Step C), and both Gα-GTP and Gβγ subsequently transmit signals through diverse effectors (Step D). Gα subunits have intrinsic GTPase activity that downregulates Gα signaling by converting GTP to GDP (Step E). Gα-GDP then re-associates with Gβγ (Step F) and the system is reset for the next activation cycle.

There are 36 heterotrimeric G proteins identified in mammalian genomes, including 17 Gα subunits categorized into four classes, 7 Gβ subunits, and 12 Gγ subunits (6-8). One GPCR can couple to different types of Gα subunits, and one Gα subunit can associate with different Gβγ subunits; therefore, one GPCR can transmit different signals into a cell based on the combination of G proteins it couples to. Moreover, there are various regulatory mechanisms to fine-tune G protein signaling. All of the above mechanisms enable G proteins to participate in a great number of signaling pathways that generate different cellular responses under different conditions. These complexities also increase the challenge of understanding GPCR signaling.

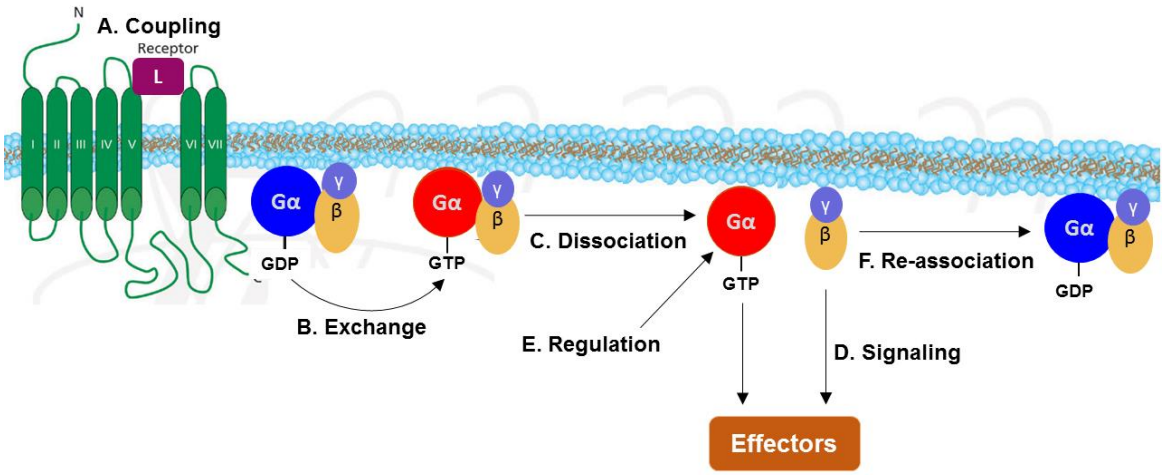

Figure 1-1. G protein signaling.

1-1-3. $G\alpha_q$ in heart failure

The q subtype of the heterotrimeric G protein α subunit, $G\alpha_q$, is activated by a number of receptors whose agonists are upregulated in the progression of heart failure, including angiotensin II and catecholamines (9). Angiotensin II is a main component in the renin-angiotensin-aldosterone pathway, whose activation is important in maintaining cardiac output in the short term but also accelerates cardiac dysfunction in the long term (10). Angiotensin-converting enzyme (ACE) inhibitors and angiotensin receptor blockers are used to lower blood pressure and decrease the heart's workload in heart failure patients (11).

$G\alpha_q$ expression may also play a role in the development of heart failure. A -695/-694 TT/GC polymorphism in the promoter region of GNAQ (the gene encoding $G\alpha_q$ protein) has been reported to associate with human cardiac conditions. The GC allele frequency is around 55% in Caucasians (12,13) and 64% in African Americans (12). The GC site was shown to be a binding site for the Sp-1 transcription factor (12,13). Two conflicting reports have described effects of the GC and TT alleles on the regulation of GNAQ expression. Frey et al. showed that the GC allele increases $G\alpha_q$ expression and results in enhanced activation of the $G\alpha_q$ pathway *in vitro* (13). Moreover, echocardiography studies suggested that the GC allele in Caucasians is associated with a higher risk of increased left ventricular mass but is not significantly associated with wall thickness or systolic dysfunction (13). Liggett et al. showed that the TT allele increases transcriptional activity using a reporter assay, but did not analyze $G\alpha_q$ mRNA levels (12). The authors tracked patient survival and suggested that the TT allele increases the risk of heart failure death in African Americans but not in the Caucasian population (12). These two studies suggest that upregulation of $G\alpha_q$ expression may play a role in the development of cardiac hypertrophy and heart failure in humans, but more studies need to be done to measure the actual transcriptional regulation of GNAQ in patient samples.

Using transgenic mice, it is well established that $G\alpha_q$ mediates cardiac hypertrophy and heart failure induced by pressure overload. Transgenic expression of $G\alpha_q$ alone in cardiomyocytes is enough to stimulate downstream signaling and trigger pathological phenotypes (9,14), and blockade of $G\alpha_q$ signaling prevents pressure

overload-induced heart failure (15). Many pathways downstream of $G\alpha_q$ have been suggested to contribute to the development of hypertrophy and heart failure.

1-1-4. $G\alpha_q$ signaling in the heart

In the cannonical $G\alpha_q$ signaling pathway, $G\alpha_q$ activates phospholipase C β (PLCβ), which hydrolyzes phosphatidylinositol 4,5-bisphosphate (PIP_2) to produce inositol 1,4,5-trisphosphate (IP_3) and diacylglycerol (DAG). IP_3 and DAG are effectors of $G\alpha_q$. IP_3 binds to the IP_3 receptor (IP_3R) to trigger a release of Ca^{2+} from the endoplasmic reticulum (or the sarcoplasmic reticulum (SR) in cardiomyocytes) into the cytosol, and DAG activates conventional and novel isoforms of protein kinase C (PKC). Increased cytosolic Ca^{2+} can also activate conventional PKCs.

In one study, $G\alpha_q$ deficiency in cardiomyocytes led to altered electrophysiological properties, reduced calcium transients, and reduced cardiomyocyte size (16). Thus, it was proposed that persistent stimulation of the $G\alpha_q$ signaling pathway at a low physiological level is an important contributor to the maintenance of cardiomyocyte homeostasis (16). However, contractile function was not reported in this study. In another study, absence of $G\alpha_q$ signaling did not cause any morphological or functional abnormalities in the whole heart (15).

The altered electrophysiology could be explained by the fact that ion channels are regulated by $G\alpha_q$ signaling. Production of DAG induces membrane curvature and the opening of TRPC6, an inwardly and outwardly rectifying channel for Ca^{2+} and Na^+ (17). In addition, activity of the KCNQ1/KCNE1 potassium channel complex has been shown to be strongly inhibited by transient depletion of PIP_2 in a cell line *in vitro* (18). However, whether $G\alpha_q$ activation in cardiomyocytes leads to local or general PIP_2 depletion needs investigation.

Many molecular mechanisms underlying $G\alpha_q$-induced cardiac hypertrophy and heart failure have been proposed. Sarcoplasmic reticulum calcium-ATPase-2 (SERCA2) and the Na^+/Ca^{2+} exchanger withdraw cytosolic calcium back into the SR during contraction cycles. $G\alpha_q$ activation induces cytosolic Ca^{2+} overload through IP_3-induced Ca^{2+} release from the SR and decreased expression of SERCA2 and the Na^+/Ca^{2+} exchanger (9,19). PKCα indirectly upregulates the phosphorylation of

phospholamban (PLB), which inhibits SERCA2 activity and also leads to increased cytosolic calcium (20).

Increased Ca^{2+} leads to loss of mitochondrial membrane potential and the release of reactive oxygen species (ROS) and cytochrome c, which can then lead to cardiomyocyte death. Ca^{2+}/CaM-dependent protein kinase II (CaMKIIδ) and calcineurin, a Ca^{2+}-dependent phosphatase, are proposed mediators in this process. In the mouse, overexpression of catalase targeted to mitochondria prevented cardiac hypertrophy induced by angiotensin II or heart failure induced by $G\alpha_q$ overexpression, indicating that mitochondrial ROS plays important roles in $G\alpha_q$ signaling in the heart (21). Knocking out CaMKIIδ prevented mitochondrial ROS production in $G\alpha_q$-overexpressing transgenic mice and prevented $G\alpha_q$-induced cardiac dysfunction. Treatment of neonatal rat cardiomyocytes (NRCM) with a CaMKIIδ inhibitor reduced mitochondrial ROS production and prevented cell death induced by $G\alpha_q$Q209L, a constitutively active form of $G\alpha_q$ (22).

In NRCM, insulin-like growth factor-II (IGF-II) activated $G\alpha_q$ and induced apoptosis through the activation of calcineurin. Calcineurin induces translocation of Bad to mitochondria and the release of cytochrome c and apoptotic factors. Knockdown of $G\alpha_q$ and calcineurin blocked IGF-II–induced apoptosis (23). In the mouse, pharmacological inhibition of calcineurin by cyclosporin A blunted myocardial hypertrophy induced by $G\alpha_q$ overexpression (24).

Calcium signaling in myocytes is unique compared to other types of cells due to the cytosolic calcium oscillations during contraction. The cytosolic Ca^{2+} concentration increases from ~100 nM at rest to ~1 μM during contraction, with peak Ca^{2+} levels in the cleft between the sarcolemma/T-tuble and the SR reaching approximately 400 μM (25). It remains unclear how calcineurin, CaMKIIδ and PKC differentiate between contractile Ca^{2+} and signaling Ca^{2+}. Two hypotheses are favored: 1) Ca^{2+}-sensitive signaling factors respond to a sustained elevation of diastolic Ca^{2+} concentration; or 2) Ca^{2+} signaling proteins concentrate at microdomains and macromolecular complexes which are inaccessible to contractile Ca^{2+} (25).

In summary, all effectors downstream of $G\alpha_q$ in the cannonical signaling pathway have been reported to contribute to $G\alpha_q$–induced cardiac phenotypes; calcium is of special importance in these pathways.

1-2. Autophagy

1-2-1. General characteristics

Autophagy is an intracellular degradation process, conserved in all eukaryotes, in which double-membrane vesicles called autophagosomes enclose bulk intracellular materials and send them to lysosomes for degradation (26). Under physiological conditions, a basal level of autophagy removes damaged proteins and organelles and recycles their constituent building blocks for other necessary metabolic uses, so that cellular homeostasis is maintained (27). Autophagy is also an essential mechanism for cells to cope with stress. For example, nutrient deprivation, hypoxia, oxidative stress, hormones and exercise are all reported to induce autophagy, which allows the cell to use its own components to produce nutrients and ATP that are necessary for survival (28,29).

The autophagy machinery is composed of 37+ autophagy-related genes (ATG) in yeast (30), the majority of which have mammalian orthologs. Only mammalian proteins are mentioned in this thesis, unless otherwise noted. Eighteen of these proteins organize into 6 protein complexes to execute the core steps of autophagy (Figure 1-2) (31); the other ATG proteins participate in more specific autophagic conditions (30).

1-2-2. Different subtypes of autophagy

Based on how substrates are delivered to lysosomes, autophagy is categorized as macroautophagy, microautophagy and chaperone-mediated autophagy. Macroautophagy is the most studied; in this process, cytoplasmic contents are included into autophagosomes and delivered into lysosomes. Microautophagy takes place locally in lysosomes, where lysosome membrane invagination isolates a small amount of cytoplasm and delivers it into the lysosomal lumen for digestion. In chaperone-mediated autophagy, specific proteins are recognized by chaperones, unfolded and translocated into the lysosome (32). My research focused on macroautophagy.

Based on substrate types, autophagy is categorized as nonselective autophagy, in which bulk materials in the cytoplasm are included into autophagosomes indiscriminately, and selective autophagy, in which only specific substrates are directed into autophagosomes. Different types of selective autophagy based on substrate are mitophagy (mitochondria), glycophagy (glycogen), peroxiphagy (peroxisomes), etc. Different kinds of selective autophagy can happen in the same cell at the same time.

1-2-3. Molecular mechanisms

1) Activation

Autophagy initiates when the ULK1 (unc-51-like autophagy-activating kinase 1) complex (ULK1-Atg13-Atg101-FIP200) is assembled (Figure 1-2). ULK1 is a serine/threonine kinase. In nutritious conditions, mTORC1 binds to and phosphorylates ULK1 and mAtg13 at multiple sites, which inhibits ULK1 activity. Upon starvation, mTORC1 is inactivated and AMPK becomes activated due to low ATP levels. AMPK phosphorylates ULK1 and mAtg13 at multiple sites to activate the ULK1 complex. At the same time, AMPK inhibits mTORC1, thus preventing inhibitory phosphorylation of ULK1 by mTORC1 (33).

2) Autophagosome assembly-nucleation (initiation)

The ULK1 complex dictates the assembly of a complex that contains Vps34, p150, Atg14 and Beclin1. Vps34 and p150 are the catalytic and regulatory subunits, respectively, of Class III phosphatidylinositol (PI) 3-kinase (PI3K). Vps34 phosphorylates PI at the 3' hydroxyl position to generate PI 3-phosphate [PI(3)P]. Atg14 mediates formation of the complex by binding to both Vps34-p150 and Beclin1 and directs it to a subdomain of an intracellular membrane source where nucleation of autophagosome vesicles occurs (34). Binding to Beclin1 and Atg14 greatly increases the lipid kinase activity of Vps34 so that PI(3)P is produced at the nucleation site, leading to recruitment of proteins with PI(3)P binding domains and extension of the growing autophagosomal membrane. The cup-shaped double-membrane sac is called a phagophore or isolation membrane.

It is believed that a pre-existing membrane serves as the nucleation site for autophagosome assembly. Various membrane structures have been proposed to play this role, including Golgi membranes, subdomains of the endoplasmic reticulum (ER), the mitochondrial outer membrane, ER-mitochondria contact sites, and the plasma membrane (35). This may indicate that under different cellular contexts, different types of autophagy take place.

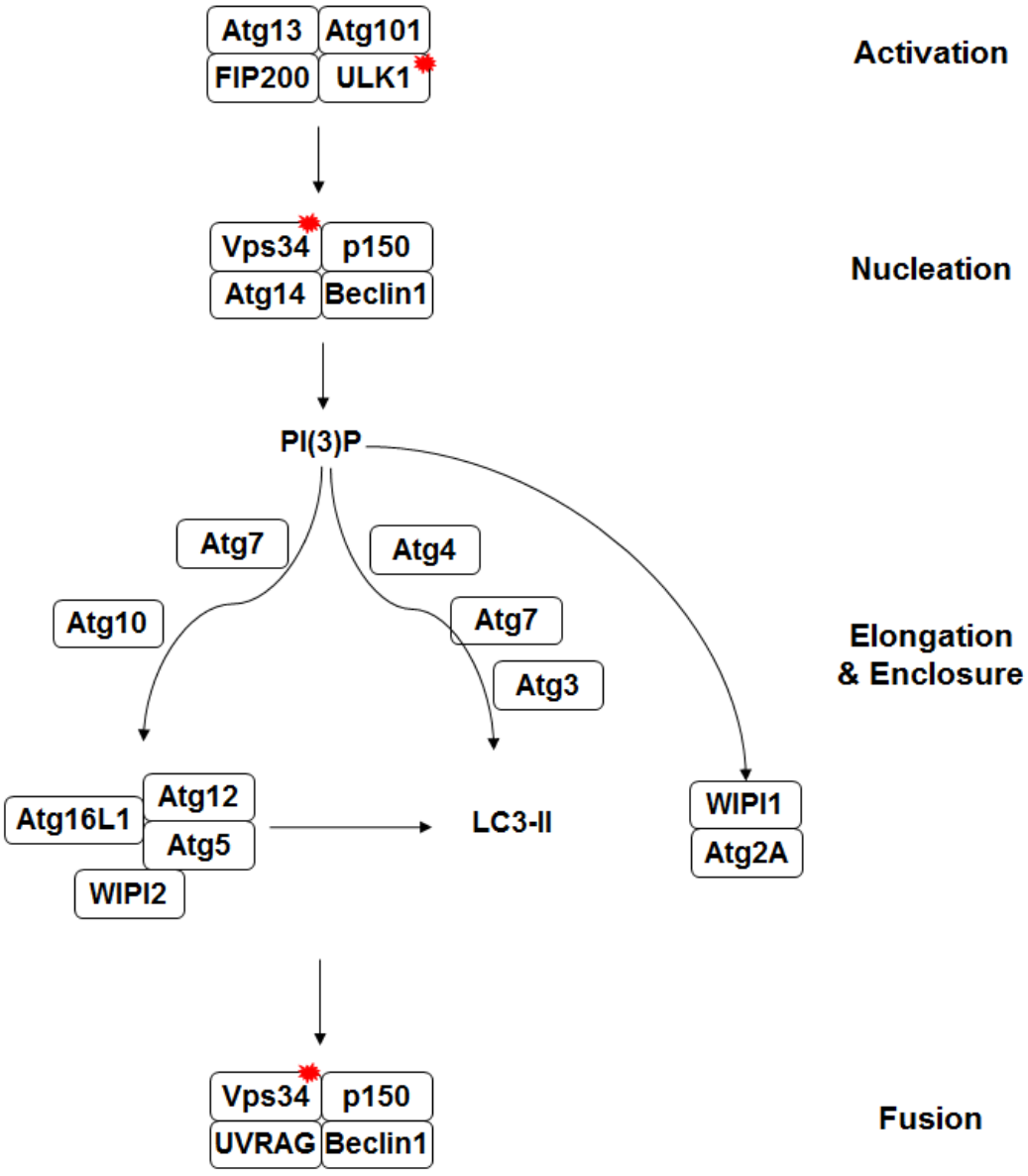

Figure 1-2. Important protein complexes in the autophagic pathway. Red star indicates subunit with kinase activity.

3) Autophagosome assembly-elongation and enclosure

Proteins in two ubiquitin-like conjugation pathways promote phagophore (isolation membrane) elongation, curvature, and closure into an autophagosome (32). In one pathway, Atg7 is the E1-like enzyme and Atg10 is the E2-like enzyme, and they help to assemble an Atg12-Atg5-Atg16L1-WIPI2 complex (Figure 1-2). In the other pathway, Atg7 is the E1-like enzyme and Atg3 is the E2-like enzyme, and the complex Atg12-Atg5 functions as an E3-like enzyme but conjugates phosphatidylethanolamine (PE) to LC3-I. The lipidated protein, LC3-II, then inserts into the lipid bilayer to facilitate membrane elongation (35). LC3-II is also important for the enclosure of the phagophore to make an autophagosome; however, detailed molecular mechanisms for the enclosure event have yet to be discovered.

Recognition and delivery of cargo into the forming autophagosome is mediated by the adaptor proteins p62 (sequestosome 1), NBR1, optineurin, etc. These adaptors bind to ubiquitinated proteins as well as to LC3-II, thus targeting autophagy substrates into autophagosomes (36).

4) Fusion with lysosome

Upon enclosure of the phagophore, autophagosomes travel along the cytoskeleton to fuse with proximal lysosomes. Live-cell microscopy has shown that autophagosomes move along microtubule tracks towards the perinuclear region where late endosomes and lysosomes predominantly locate. The small GTPase Rab7 and its effector protein RILP play critical roles to bridge autophagosomes to the motor protein dynein which carries out this movement. Loss of dynein led to accumulation of LC3-II and impaired autophagic clearance of aggregation-prone proteins (37). Actin was also reported to help autophagosome trafficking, but only in selective autophagy that targets protein aggregates and not in starvation-induced autophagy (37).

When the organelles come into proximity, membrane-tethering complexes and SNARE proteins participate in docking and fusion of autophagosomes and late endosomes/lysosomes.

5) Degradation and recycling

The fusion of autophagosomes and lysosomes creates “autolysosomes”. Autophagic cargos are then degraded by approximately 60 different lysosomal

hydrolases, including sulphatases, glycosidases, peptidases, phosphatases, lipases and nucleases. Various types of hydrolases allow the lysosome to hydrolyse a vast repertoire of biological substrates, including glycosaminoglycans, sphingolipids, glycogen and proteins (38). Soluble catabolites such as carbohydrates and amino acids are then exported to the cytosol by specific transporters, while insoluble lipid catabolites are transported through vesicular trafficking (39).

1-2-4. Autophagy regulation

mTORC1 and AMPK are important nutrient and energy sensors that regulate autophagy. However, in one RNAi screen study, mTOR did not play an important role in the regulation of basal autophagy, which maintains cellular homeostasis (40). This may indicate that the regulation of basal autophagy is different from starvation-induced autophagy. Moreover, based on current findings, Beclin1 posttranslational modification is central to autophagy regulation. Many signaling pathways regulate Beclin1's participation in Class III PI3K complexes and regulation of Vps34 activity, which could bypass the ULK1 complex depending on cellular context (35).

1-2-5. Autophagy in cardiac physiology and pathology

The use of knockout mice has demonstrated that autophagy is essential for normal cardiac function. Cardiac-specific Vps34 knockout mice developed cardiac hypertrophy and died between 5 and 13 weeks of age (41). Cardiac-specific deletion of Atg5 led to mitochondrial dysfunction, development of dilated cardiomyopathy, and early death starting at 6 months of age (42). Moreover, inducible knockout of Atg5 in the adult mouse heart led to left ventricular dilatation and contractile dysfunction, with a disorganized sarcomere structure and mitochondrial misalignment and aggregation (43). These results suggest that autophagy maintains mitochondrial homeostasis in the normal heart and indicate that a deficiency in autophagy can lead to heart failure.

Accumulating evidence suggests that autophagy is dysregulated in CVD. However, whether autophagy is protective or detrimental under these conditions is still under debate (32). Increased autophagic activity was reported in the ischemic myocardium (28,44) and preconditioned heart (28), and was thought to be protective

against ischemia/reperfusion injury (28). However, another study described increased autophagy as a maladaptive response to hemodynamic stress, as inhibition of autophagy attenuated systolic dysfunction in a model of load-induced heart failure (45).

Chapter 2. Activation of $G\alpha_q$ stimulates autophagy in the heart via increasing Vps34 activity

2-1. Introduction

2-1-1. Model systems to study $G\alpha_q$ signaling in the heart

$G\alpha_q$'s role in the heart has been studied in mouse models and different types of cardiomyocytes. Three major types of mouse models are: Transgenic or knockout mice that directly modify $G\alpha_q$ or its activation by GPCRs; pressure overload models in which $G\alpha_q$ has been demonstrated to play important roles; and animals or cardiomyocytes treated with angiotensin II, which activates the $G\alpha_q$-coupled angiotensin II type 1 receptor (AT_1) in the heart.

2-1-2. Summary of our $G\alpha_q$Q209L heart failure model

Our laboratory previously constructed a heart failure model in which $G\alpha_q$ signaling could be turned on and off at will in the heart of adult mice (9). A constitutively active $G\alpha_q$ mutant with defective GTPase activity, $G\alpha_q$Q209L, was fused to a modified hormone-binding domain of the estrogen receptor (hbER), and expressed specifically in cardiomyocytes under control of the α myosin heavy chain (αMHC) promoter. The fusion protein is sequestered by heat shock protein (HSP) 70 and remains inactive under normal conditions; however, it becomes active when the mouse is injected with tamoxifen, which is metabolized to 4-hydroxytamoxifen (4-OHT) *in vivo*. 4-OHT binds to the hbER domain and releases $G\alpha_q$Q209L-hbER from HSP70, and $G\alpha_q$Q209L becomes functional.

Upon $G\alpha_q$ activation by tamoxifen injection, the mice quickly showed decreased cardiac contractility around day 7, dilated cardiomyopathy around day 14, and overt heart failure after 21 days, which was characterized by a 20% increase in body weight due to peripheral edema (9,46). Moreover, many mice died beginning at 14 days of tamoxifen injection, presumably due to heart failure or arrhythmia. Histological examination of the myocardium after 28 days of tamoxifen injections showed increased extracellular space, but no obvious evidence of cellular hypertrophy,

apoptosis or necrosis. Only a minimal increase in interstitial fibrosis was observed. Measurement of capacitance of isolated cardiomyocytes also did not show cardiomyocyte hypertrophy. Cleavage of caspase 3 or poly (ADP-ribose) polymerase, which would indicate apoptosis, was not detected by western blotting after 7 days of tamoxifen injections (9,46).

The heart failure phenotype is caused by $G\alpha_q$ activation of PLCβ, because another mouse strain, $G\alpha_q$Q209L-AA-hbER (called AA), in which two alanine mutations block the ability of $G\alpha_q$Q209L to activate PLCβ, did not show any pathological phenotype (9). $G\alpha_q$ activation led to dephosphorylation of phospholamban (PLB), which binds to and inhibits sarcoplasmic reticulum Ca^{2+} ATPase-2 (SERCA-2) activity. Decreased SERCA-2 activity led to reduced withdrawal of Ca^{2+} from the cytosol into the sarcoplasmic reticulum. The increase in cytoplasmic Ca^{2+} concentration led to activation of calpain, which cleaves junctophilin-2, an important molecule in maintaining T-tubule structure. Thus, T-tubules were disrupted and Ca^{2+} homeostasis was disturbed, which could explain the decreased contractility of $G\alpha_q$Q209L hearts (9,47). The link between PLCβ and PLB is not yet clear. $G\alpha_q$ activation also caused decreased activity of the L-type Ca^{2+} channel, which initiates Ca^{2+} influx and cardiomyocyte contraction. However, this phenotype was not mediated by $G\alpha_q$ activation of PLCβ and was not the cause of heart failure, since it was also observed in AA mice which did not develop heart failure.

Surprisingly, $G\alpha_q$Q209L-induced heart failure was reversed when $G\alpha_q$ signaling was terminated. When tamoxifen injections were stopped after 21 days of administration, the mice which had already demonstrated severe heart failure progressively recovered and reached nearly full cardiac contractility after 14 days of recovery (46,47). Peripheral edema disappeared, extracellular space in the myocardium shrank, and changes in PLB phosphorylation and SERCA-2 activity that were observed in failing $G\alpha_q$Q209L hearts were reversed (46). These results were consistent with our findings that contractility failure was not due to cardiomyocyte death, but rather to a dysfunctional contractile apparatus. Thus, the heart has reparative capacity when detrimental signals are stopped in this case.

2-1-3. Autophagy regulation by $G\alpha_qQ209L$

Autophagy dysregulation has been demonstrated in pressure overload and angiotensin II-treated hearts and cardiomyocytes (21, 45); however, whether $G\alpha_q$ signaling directly regulates autophagy is not clear yet.

2-2. Results

2-2-1. $G\alpha_qQ209L$ activation leads to autophagic protein level increase

We first investigated how autophagic proteins are changed upon continuous $G\alpha_q$ activation in the heart in a time course experiment (Fig. 2-1A). Two autophagy indicators, p62 and LC3-II, were increased on day 1, day 3, and after day 5. Proteins in the core autophagic machinery, i.e., Vps34, Beclin1, Atg7 and Atg5-Atg12 conjugates, all increased after 5 days of tamoxifen injection. Interestingly, ubiquitinated proteins, which are autophagy substrates, also increased greatly after 5 days of tamoxifen injection. More animals were used to confirm this response at three time points (Fig. 2-1B). After 1 tamoxifen injection, p62 and LC3-II levels did not behave in the same manner as in the time course experiment in Fig. 2-1A, which is probably due to variation between animals. After 3 days of tamoxifen injections, p62 and LC3-II levels increased moderately. After 7 days of injections, p62 and LC3-II levels increased greatly, and other proteins in the autophagy machinery also increased (Fig. 2-1B).

Subsequently, mRNA level of these autophagic proteins at day 3 and day 7 were measured (Fig. 2-2). After 3 days of tamoxifen injections, $G\alpha_qQ209L$ hearts showed a 2-fold increase in p62 mRNA as compared to WT hearts (Fig. 2-2A). After 7 days of tamoxifen injections, RT-qPCR showed a 4-fold upregulation in p62 mRNA (Fig. 2-2B), which could account for the increased level of p62 protein in $G\alpha_qQ209L$ hearts. Atg7 mRNA increased slightly, while LC3, Vps34, Beclin1 and Atg14 were not transcriptionally upregulated (Fig. 2-2B). This result suggests that these proteins may be stabilized post-translationally.

In order to have evident and consistent results in the following experiments, I chose to study $G\alpha_qQ209L$ hearts after 7 days of tamoxifen injections.

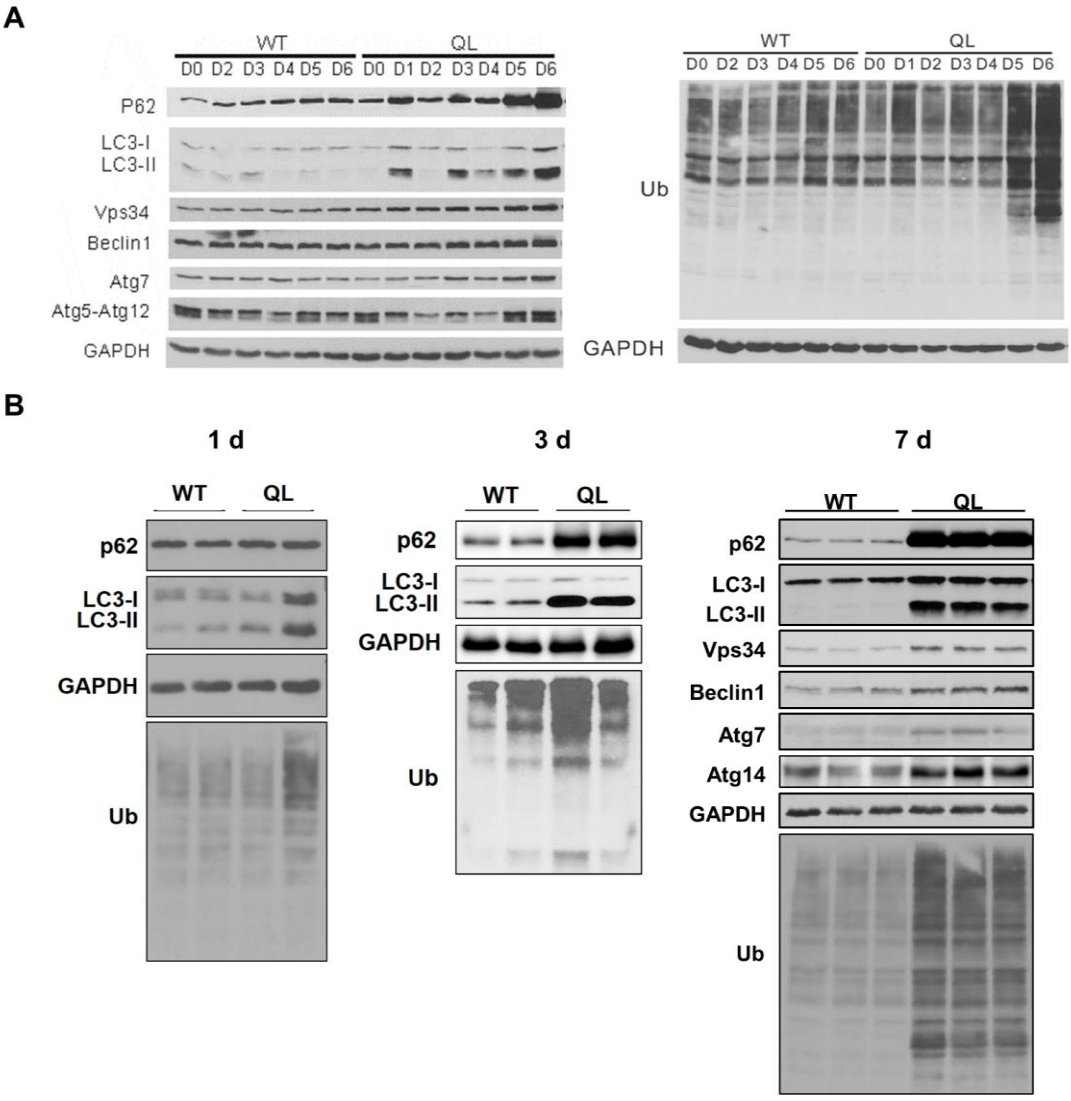

Figure 2-1. Autophagic protein levels are increased in $G\alpha_qQ209L$ hearts. Autophagy-related proteins in heart lysates of mice injected with tamoxifen for the indicated number of days were detected by western blotting using the indicated antibodies. GAPDH is a loading control. (A) A time course experiment in which mice were injected for 1 day (D1) to 6 days (D6). (B) Mice were injected with tamoxifen continuously for the indicated number of days.

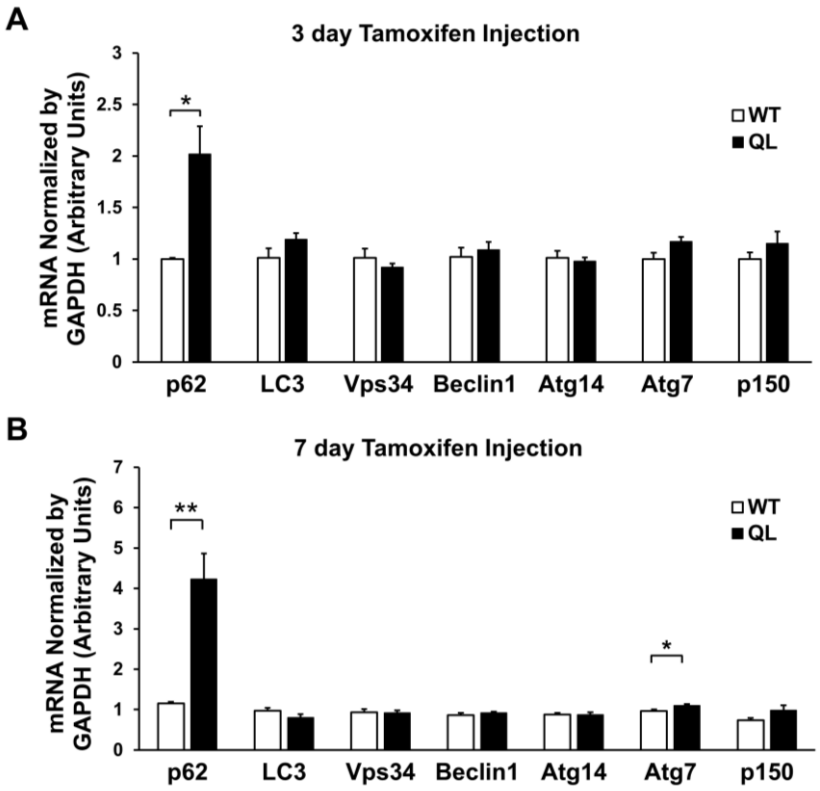

Figure 2-2. Autophagy gene expression is increased in $G\alpha_qQ209L$ hearts. WT and $G\alpha_qQ209L$ (QL) mice were injected with tamoxifen for 3 days (A) or 7 days (B), and the normalized expression of autophagy-related genes in ventricular tissue was determined by RT-qPCR. n=6 mice per group. Error bars show standard error of the mean. *, $p<0.05$; **, $p<0.001$; Student's *t*-test.

2-2-2. Transmission electron microscopy (TEM) study shows that autophagosome formation is increased in $G\alpha_qQ209L$ hearts

Autophagic vacuoles can be characterized into two categories: early or initial autophagic vacuoles (AVi or autophagosomes), which are surrounded by a double membrane and contain undigested cytoplasmic contents; and late or degradative autophagic vacuoles (AVd), which result from the fusion of autophagosomes with endosomes or lysosomes, have a single membrane, and contain electron-dense digested material (48). We next investigated autophagic vacuole formation in tamoxifen-injected $G\alpha_qQ209L$ *vs.* WT mice using TEM.

Low-magnification TEM images showed that the sarcomere structure of the majority of $G\alpha_qQ209L$ cardiomyocytes was severely disrupted (Fig. 2-3A(b,c)),

although there were some areas in which sarcomere structure was relatively well preserved (Fig. 2-3A(c,d)). These results are consistent with our previous finding of contractile failure in these animals (9,46,47). We also observed an increased number of deformed mitochondria in sections of $G\alpha_q$Q209L hearts (Fig. 2-3A(b) and Fig. 2-3D).

We observed many more autophagic vacuoles in $G\alpha_q$Q209L hearts than in WT hearts (Fig. 2-3A and Fig. 2-3B). AVi's containing mitochondria and glycogen were observed in $G\alpha_q$Q209L hearts (Fig. 2-3A(e,h)). Fig. 2-3A(f) shows an AVi containing a mitochondrion fusing with an AVd. One type of very large empty vacuole seemed to have resulted from digestion of several mitochondria (Fig. 2-3A(c,g)) and thus was categorized as AVd. There were also smaller AVd's containing digested cytosolic material (Fig. 2-3A(b,i)). In $G\alpha_q$Q209L hearts, the numbers of AVi and AVd increased proportionally as compared to WT, which indicates that autophagosome maturation is normal in $G\alpha_q$Q209L hearts (Fig. 2-3B and Fig. 2-3C).

Another striking observation is that while WT hearts contained many lipid droplets, $G\alpha_q$Q209L hearts were deficient in this ultrastructure (Fig. 2-3A(a) and Fig. 2-3E). By contrast, we observed more lysosomes in $G\alpha_q$Q209L hearts than in WT hearts (Fig. 2-3A(b), Fig. 2-4C and Fig. 2-3F).

Some abnormal ultrastructures were often observed in $G\alpha_q$Q209L hearts but rarely appeared in WT hearts. Mitochondria enclosed in electron-dense membranes were one such structure (Fig. 2-4A). Under higher magnification, the dense membrane appeared to be a double layer membrane closely contacting the mitochondrion. The thickness of one layer (marked by yellow bars in the figure) is 36.8 nm, close to the thickness of a double membrane seen in a normal autophagosome (Figure 2-3B(e)), which is 38.2 nm. Another abnormality in $G\alpha_q$Q209L hearts was multi-layer membrane structures (Fig. 2-4D). Similar ultrastructures were observed previously in heart samples, and were called "myelin bodies" or "myelin-like structures" (49-51). Although they were proposed to be artificial effects due to fixation during the sample preparation process (52), the larger number of these structures in $G\alpha_q$Q209L hearts may indicate that they are specifically induced by $G\alpha_q$ activation (Fig. 2-4E).

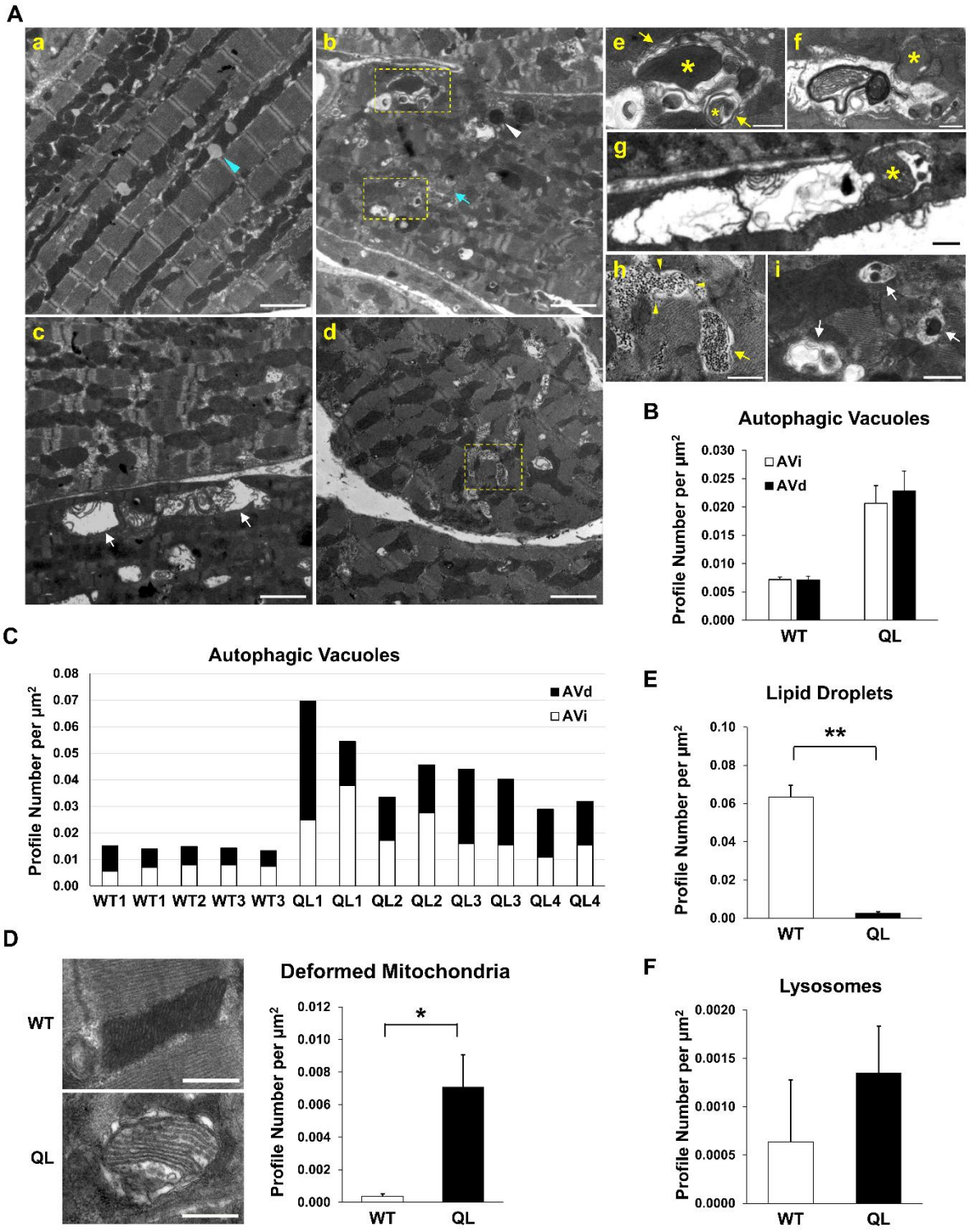

Figure 2-3. Autophagic vacuoles are increased in $G\alpha_qQ209L$ hearts. WT and $G\alpha_qQ209L$ (QL) mice were injected with tamoxifen for 7 days. Heart sections were imaged by TEM. (A) (a-d) Representative images from one WT (a) and three QL (b-d) hearts. Cyan arrow head, lipid droplet; white arrow head, lysosome; cyan arrow, deformed mitochondrion; white arrows, AVd. Bars, 2 µm. (e-i) Higher magnification views of

structures in QL hearts. (e) and (i) are boxed areas in (b); h is boxed area in (d). *, mitochondrion in autophagic vacuole; yellow arrows, AVi; white arrows, AVd; yellow arrow heads, isolation membrane. Bars, 500 nm. (B) Quantification of autophagic vacuoles (AVi and AVd) in WT and QL hearts. 51 images from 5 sections of 3 WT hearts and 102 images from 8 sections of 4 QL hearts were analyzed. Error bars are standard error of the mean. "Profile" stands for the object being counted. (C) Quantification of AVi and AVd in each section. The horizontal axis is labeled with animal identification. (D) Representative images of a normal mitochondrion in a WT heart (top) and a deformed mitochondrion in a QL heart (bottom). Bars, 500 nm. Bar graph on the right shows quantification of deformed mitochondria in WT and QL heart sections. Error bars show standard error of the mean. *, $p<0.05$, unpaired two-tailed *t*-test. (E) Quantification of lipid droplets in WT and QL heart sections. Error bars show standard error of the mean. **, $p<0.01$, unpaired two-tailed *t*-test. (F) Quantification of lysosomes in WT and QL heart sections. Error bars show standard error of the mean. $p=0.40$, unpaired two-tailed *t*-test.

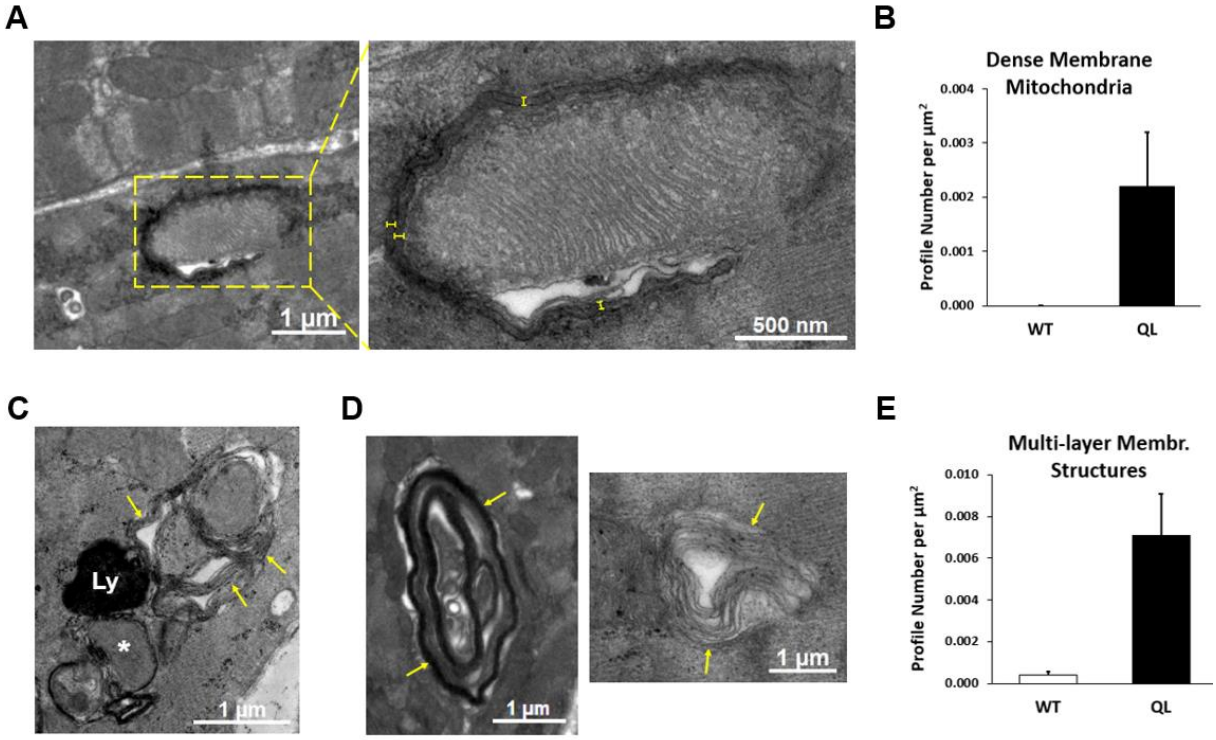

Figure 2-4. Abnormal ultrastructures identified in $G\alpha_qQ209L$ heart. WT and $G\alpha_qQ209L$ (QL) mice were injected with tamoxifen for 7 days. Heart sections were imaged by TEM. (A) A representative image for a mitochondrion enclosed in electronic dense thick membrane structure, which appears to be double layer membrane at higher magnification. The thickness of one layer of the membrane (indicated by yellow bar) was about 36.8 nm, calculated by an average of 7 measurements. (B) Quantification of mitochondria with electronic dense membrane present in WT and QL heart sections. (C) Representative image for lysosome (Ly), mitochondrion enclosed in dense membrane (star), and multi-layer membrane structure (yellow arrows). (D) Two representative images for multi-layer membrane structure (yellow arrows) present in QL hearts. (E) Quantification of the structures (D) present in WT and QL heart sections.

2-2-3. p62 forms aggregates, and does not always colocalize with LC3

p62 transcription has been shown to increase upon a number of cellular stresses (53-55), as it plays a critical role in maintaining cellular homeostasis by forming protein aggregates to sequester harmful proteins such as the negative redox regulator Keap-1 (56,57). To investigate the subcellular distribution of p62, we performed immunofluorescence (IF) microscopy using isolated cardiomyocytes. The signal was very faint in WT cells, but we found that p62 formed large aggregates throughout the sarcoplasm in $G\alpha_q$Q209L myocytes (Fig. 2-5A and Fig. 2-5B). p62 aggregates were also observed in cryosections of $G\alpha_q$Q209L hearts, confirming that they were not an artifact of cardiomyocyte isolation (Fig. 2-5C). Together with the result that p62 transcription is increased in $G\alpha_q$Q209L hearts (Fig. 2-2A and 2-2B), these results suggest that despite increased autophagy, p62 expression and aggregation are induced, which may help fight against the stressed conditions such as elevated reactive oxygen species (ROS) upon $G\alpha_q$ activation.

One important function of p62 is to deliver ubiquitinated autophagy substrates to autophagosomes through its interaction with LC3. Thus, I checked whether LC3 colocalizes with p62. I crossed $G\alpha_q$Q209L mice with a transgenic mouse line which expresses GFP-LC3 in its entire body. In both isolated cardiomyocytes (Fig. 2-5D and 2-5E) and tissue cryosections (Fig. 2-5F), GFP-LC3 formed puncta with no large aggregates upon $G\alpha_q$ activation. Moreover, higher magnification images showed that most of the p62 and LC3 do not colocalize. These results suggest that the aggregated form of p62 may not be delivered to autophagosomes efficiently.

2-2-4. Lysosome function is enhanced

The increased number of autophagosomes and LC3-II upregulation observed in $G\alpha_q$Q209L hearts could be due to impaired clearance of autophagosomes, although the presence of digested material in AVd's and autophagosomes containing mitochondria fusing with AVd's (Fig. 2-3A) would seem to be against this possibility. To confirm that clearance of autophagosome cargo is not impaired in $G\alpha_q$Q209L hearts, we next examined lysosomes by using LysoTracker Red to stain the acidic

organelles in isolated cardiomyocytes. In WT cells, most of the acidic vesicles were small and clustered around the nuclei (Fig. 2-6A). In $G\alpha_qQ209L$ cardiomyocytes, enlarged vesicles appeared around the nuclei and throughout the length of the cell (Fig. 2-6A). The number of acidic vesicles per myocyte was larger in

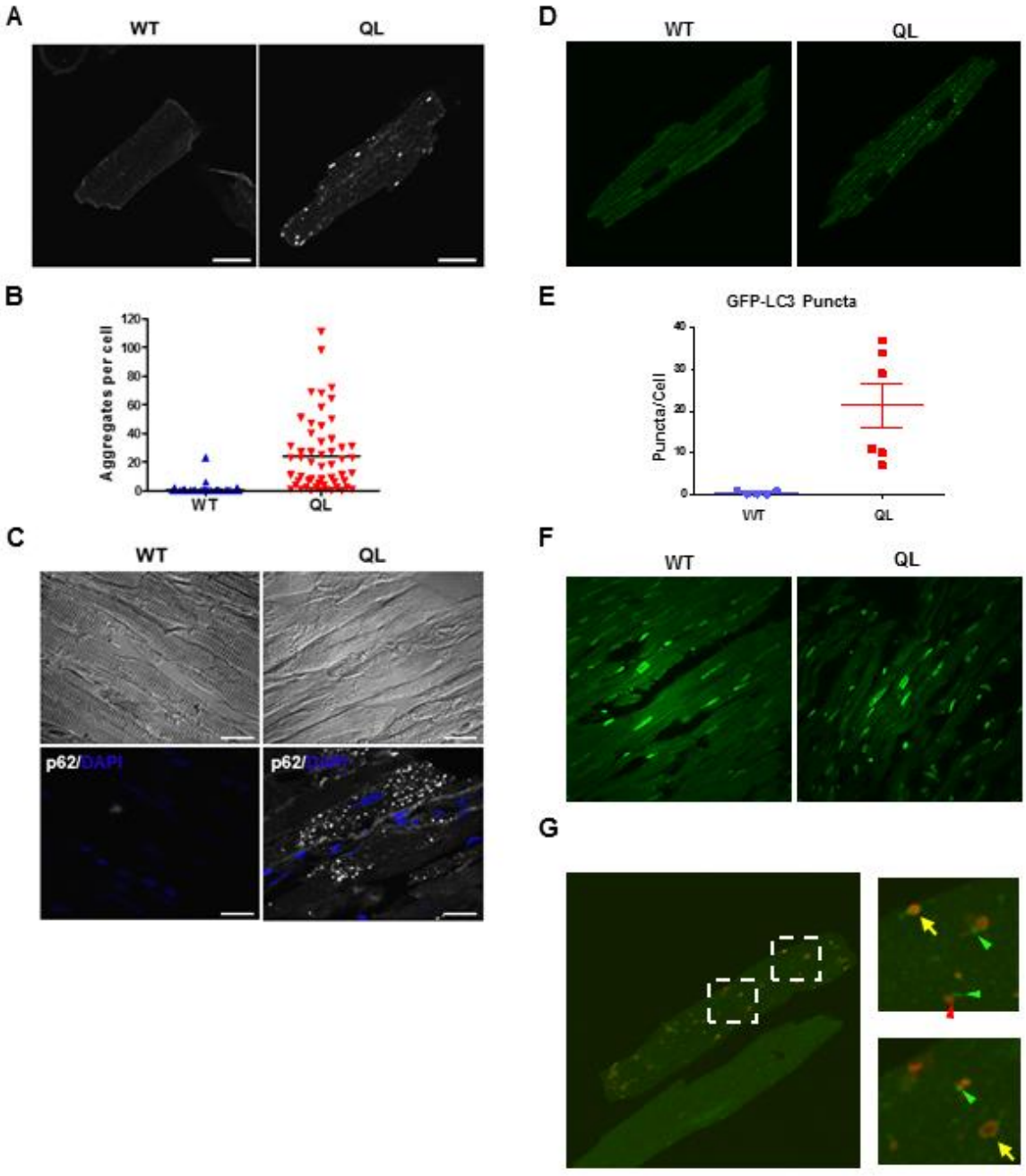

Figure 2-5. p62 forms aggregates in $G\alpha_qQ209L$ hearts and cardiomyocytes. (A-C) WT and QL mice were injected with tamoxifen for 7 days. (A) p62 in isolated

cardiomyocytes was visualized by immunofluorescence microscopy (63x magnification). (B) The number of p62 aggregates per cell was analyzed using CellProfiler 2.0. Cardiomyocytes isolated from 3 WT and 4 QL mice were analyzed. Bars show the mean values. $p<0.0001$, Student's *t*-test. (C) Images of heart cryosections (40x magnification). Upper panels, differential interference contrast images. Lower panels, detection of p62 by immunofluorescence microscopy. Nuclei were counterstained with DAPI. (D-G) $G\alpha_qQ209L$ mice were crossed with GFP-LC3 transgenic mice; the offspring which were homozygous GFP-LC3, with or without $G\alpha_qQ209L$ gene (WT or QL), were injected with tamoxifen for 7 days. (D) GFP-LC3 in isolated cardiomyocytes was visualized by confocal microscopy (63X magnification). (E) The number of GFP-LC3 puncta per cell was analyzed using CellProfiler 2.0. (F) Images of GFP-LC3 pattern in heart cryosections (40x magnification). (G) p62 was immunostained and visualized together with GFP-LC3 in isolated cardiomyocytes. Yellow arrows indicate puncta or aggregates in which p62 and GFP-LC3 colocalizes; green arrows indicate GFP-LC3 positive only puncta; red arrow indicates p62 positive only puncta.

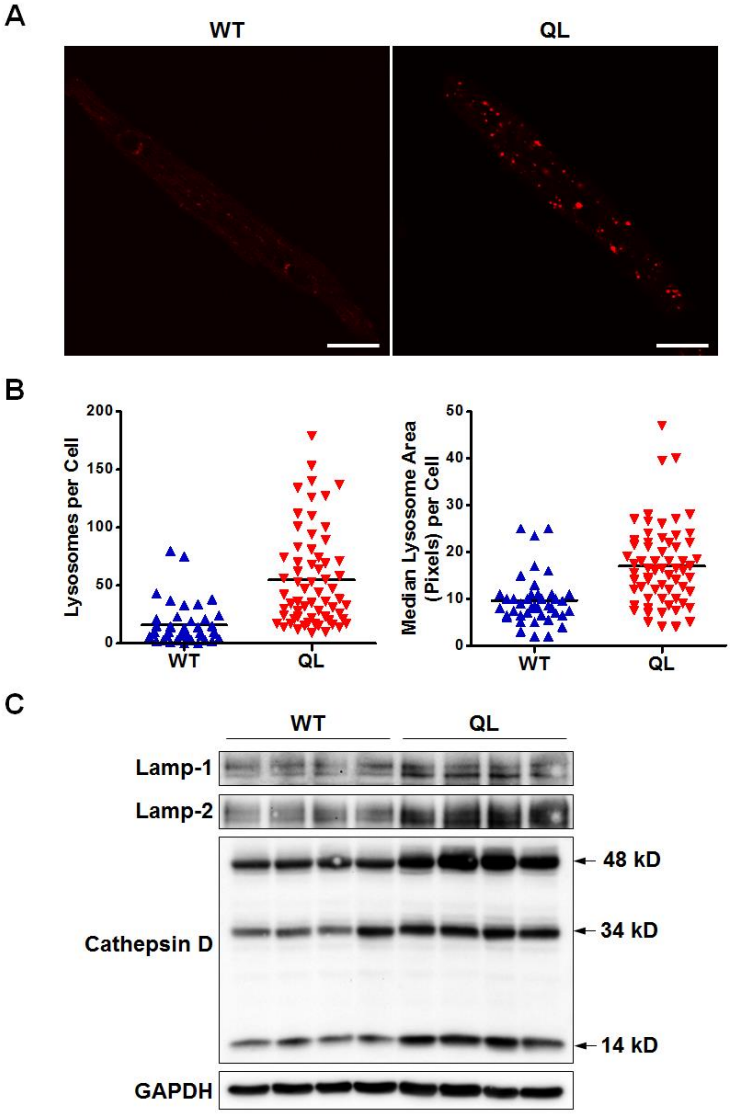

Figure 2-6. Lysosomal activity is enhanced in $G\alpha_qQ209L$ hearts and cardiomyocytes. WT and $G\alpha_qQ209L$ (QL) mice were injected with tamoxifen for 7 days. (A) Isolated cardiomyocytes were loaded with LysoTracker Red and imaged by confocal microscopy (63x magnification). Representative cells are shown. (B) LysoTracker-positive puncta in each cell were analyzed using CellProfiler 2.0. The left panel shows lysosomes per cell; n=41 for WT and n=64 for QL. The right panel shows median lysosome area per cell; n=43 for WT and n=64 for QL. Bars show the mean values. $p<0.0001$, Mann-Whitney test (both panels). (C) Lysosomal proteins in ventricular lysates were detected by western blotting using the indicated antibodies. GAPDH is a loading control.

$G\alpha_qQ209L$ cells than in WT cells (Fig. 2-6A and Fig. 2-6B). Furthermore, the average size of the lysosomes in $G\alpha_qQ209L$ myocytes was larger than in WT cells (Fig. 2-6A and Fig. 2-6B). Western blotting showed that levels of two lysosome-associated membrane proteins (Lamp-1 and Lamp-2) that are important for lysosomal function were elevated in $G\alpha_qQ209L$ hearts (Fig. 2-6C). Importantly, in an active lysosome, immature pro-cathepsin D (52 kDa) is proteolytically cleaved into the intermediate form (48 kDa), which is further cleaved to yield the two subunits of the mature form (34 kDa and 14 kDa) (58). In $G\alpha_qQ209L$ hearts, both the intermediate and mature forms of cathepsin D were increased, while the immature pro-cathepsin D was not detected (Fig. 2-6C). Collectively, these data indicate that lysosomal activity is enhanced in $G\alpha_qQ209L$ hearts.

2-2-5. Autophagic flux is increased

A standard biochemical method used to show autophagic activity is the autophagic flux assay, in which protein accumulates when bafilomycin A1 is used to block lysosomal degradation. This assay was performed on cardiomyocytes isolated from WT and $G\alpha_qQ209L$ hearts. Consistent with our observations in the whole heart (Fig. 2-1D), cardiomyocytes from $G\alpha_qQ209L$ mice showed increased levels of LC3-II as compared to WT in the absence of bafilomycin A1 (Fig. 2-7). More importantly, when the cells were treated with bafilomycin A1, LC3-II increased in both the WT and $G\alpha_qQ209L$ myocytes, indicating that autolysosomes are functional in $G\alpha_qQ209L$ cells (Fig. 2-7).

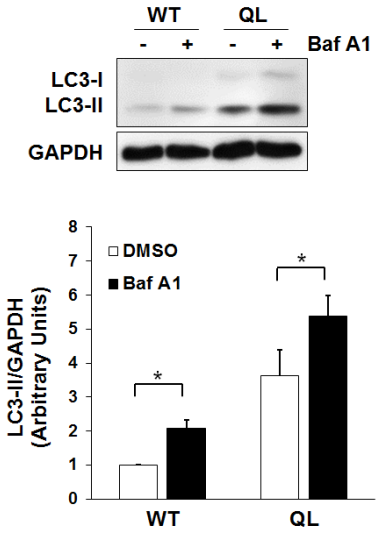

Figure 2-7. Autophagic flux is intact in $G\alpha_qQ209L$ cardiomyocytes. WT and QL mice were injected with tamoxifen for 7 days, and cardiomyocytes isolated from both groups were treated with dimethyl sulfoxide (DMSO) or 100 nM bafilomycin A1 (Baf A1) in ACCIT medium for 6 h. Cell lysates were then analyzed by western blotting using the indicated antibodies (upper panels). The experiment was repeated three times and one representative result is shown. The lower bar graph shows LC3-II band density normalized to GAPDH. The averages of four experiments are shown. n=4 for WT and n=5 for QL. Error bars show standard error of the mean. *, $p<0.05$, Student's *t*-test.

2-2-6. Class III PI3K complex assembly is enhanced and Vps34 activity is increased in $G\alpha_qQ209L$ hearts

The increase in protein expression of Beclin1, Vps34, and Atg14 in $G\alpha_qQ209L$ hearts suggests that the Class III PI3K complex that contains these components is also upregulated. On the other hand, Beclin1 and Vps34 can be found in other functionally distinct complexes (59). To further explore the mechanism of increased autophagic activity in $G\alpha_qQ209L$ hearts, we checked the formation of the autophagy-promoting Beclin1/Vps34/Atg14 complex using coimmunoprecipitation. We found that more Vps34 and Atg14 co-immunoprecipitated with Beclin1 from $G\alpha_qQ209L$ hearts than from WT hearts (Fig. 2-8A and Fig. 2-8B). *In vitro* lipid kinase assays demonstrated that Vps34 activity was also enhanced in Beclin1 immunoprecipitates from $G\alpha_qQ209L$ hearts (Fig. 2-8C and Fig. 2-8D). To determine if these *in vitro* assays correlate with *in vivo* PI(3)P levels, we isolated phospholipids from hearts and used an ELISA assay to measure PI(3)P. PI(3)P levels tended to be higher in $G\alpha_qQ209L$ hearts as compared to

WT hearts in mice injected with tamoxifen for 7 days, and after 14 days of injections there was a statistically significant increase in PI(3)P in $G\alpha_qQ209L$ hearts (Fig. 2-8E). These results suggest that activation of $G\alpha_qQ209L$ in the heart leads to increases in assembly of the autophagy-initiation Beclin1/Vps34/Atg14 complex, Vps34 activity, and production of PI(3)P, which culminates in autophagosome formation.

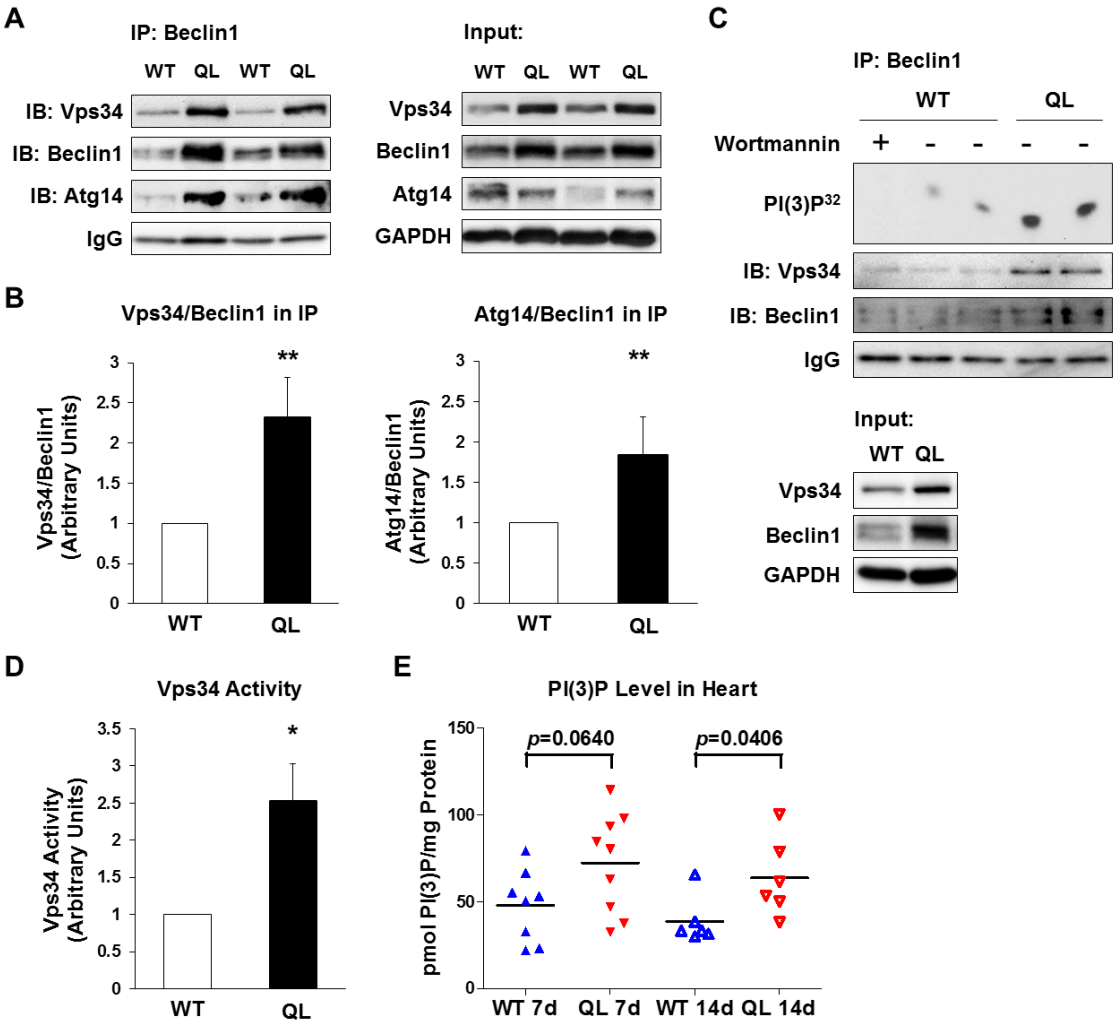

Figure 2-8. Increased formation of the autophagy initiation complex and Vps34 activity in $G\alpha_qQ209L$ hearts. WT and $G\alpha_qQ209L$ (QL) mice were injected with tamoxifen for 7 days except where otherwise noted. (A) Equal amounts of heart lysate protein from two animals in each group were immunoprecipitated (IP) using a Beclin1 antibody. The IPs were analyzed by immunoblotting (IB) using the indicated antibodies (left panels). The right panels ("Input") show western blots of the same lysates without IP. IgG and GAPDH are loading controls. (B) Protein bands from Beclin1 IP/western blots using the method in (A) were quantified by densitometry. Normalized Vps34/Beclin1 (n=5 per group) and Atg14/Beclin1 (n=6 per group) ratios are shown. Error bars show standard error of the mean. **, $p<0.01$, Student's *t*-test. (C) Vps34 activity assay. Heart lysates from one pair of

WT and QL mice were IP'd using a Beclin1 antibody. 75% of each IP was subjected to a Vps34 activity assay. The top panel shows an autoradiograph of ^{32}P-labeled PI(3)P produced in the assays. One assay contained 50 μM wortmannin (WM) to inhibit Vps34. The remainder of each IP was subjected to IB using the indicated antibodies (lower panels). The bottom panels ("Input") show western blots of the same lysates without IP. (D) ^{32}P-labeled PI(3)P produced in Vps34 activity assays (n=3 mice per group) was quantified by scintillation counting and normalized to the WT mean. Error bars show standard error of the mean. *, $p<0.05$, Student's *t*-test. (E) WT and QL mice were injected with tamoxifen for 7 or 14 days. Phospholipids were extracted from frozen hearts and PI(3)P was quantified and normalized to protein level. Each point represents one heart. Bars show the mean values. Significance was determined by Mann-Whitney test.

2-3. Discussion

Following cardiac injury, up-regulation of hormones leads to the activation of GPCRs that promote progression to heart failure. Many reports have shown that activation of receptors coupled to $G\alpha_i$, $G\alpha_s$ or $G\alpha_q$ can modulate autophagy (60). The study of how GPCRs regulate autophagy is complicated by the fact that receptors can couple to multiple types of Gα proteins, and both the Gα and Gβγ dimers that are released upon receptor activation signal to downstream effectors. The transgenic approach I used here studied the effect of activated $G\alpha_q$ in isolation and revealed that $G\alpha_q$ stimulates autophagy in the heart. Our $G\alpha_q$Q209L mice exhibit contractile dysfunction that develops into heart failure (9,46). An increase in cardiac autophagy in this model is consistent with findings in other models of cardiac injury and heart failure (28,32,45,49,61,62).

In contrast to our finding that $G\alpha_q$ stimulates autophagy, Zhang *et al.* used siRNAs to knock down $G\alpha_{q/11}$ in HeLa cells and saw increased autophagy, thus concluding that $G\alpha_q$ inhibits this process (63). The discrepancy between our finding and those of Zhang *et al*. (63) may be due to cell type-specific differences. Studies of molecules in the canonical $G\alpha_q$ signaling pathway have reported mixed effects on autophagy. In non-cardiac cells, elevation of intracellular IP_3 decreased autophagic flux by an unknown mechanism, while the IP_3R was shown to block autophagy by binding to and sequestering Beclin1 in a complex that cannot initiate autophagosome formation (64,65). Similar observations were made in neonatal rat cardiomyocytes (66). Increased cytosolic Ca^{2+} concentration has been reported to induce or inhibit autophagy, depending on cell type (67-69). Similarly, the Ca^{2+}-activated protease calpain, which is 2 times more active in $G\alpha_q$Q209L hearts than WT hearts (47), has been reported to be essential for or inhibitory to autophagy (70,71). It is not clear how the increases in IP_3 and the changes in Ca^{2+} handling that occur in $G\alpha_q$Q209L hearts contribute to the increase in autophagy seen here; calpain's role is discussed in Chapter 3. A second target of $G\alpha_q$ is the Class 1A phosphoinositide 3-kinase PI3Kα, whose activity suppresses autophagy (72,73). PI3Kα is inhibited by binding to $G\alpha_q$Q209L (74,75), which might contribute to the increase in autophagic flux in $G\alpha_q$Q209L hearts. A Gα subunit that is involved in pheromone signaling in yeast, Gpa1, activates Vps34

on endosomes through direct binding (76). Whether $G\alpha_q$ directly regulates Vps34 to control autophagy in mammalian cells is unknown. Due to the multiple effects that are initiated by activation of $G\alpha_q$ signaling, determining which signaling pathway is the dominant driver of autophagy will need further investigation.

We found that $G\alpha_q$Q209L activation increased the level of autophagy-related proteins and the Vps34-Beclin1-Atg14 complex. Several studies have shown that the Vps34-p150-Beclin1-Atg14 interaction stabilizes each component. In yeast, the absence of Vps34, Vps15 (the yeast homolog of p150), or Atg6/Vps30 (the Beclin1 homolog in yeast) all led to degradation of Atg14 (77). In HeLa cells, knockdown of Vps34 reduced the level of Beclin1 and Atg14; knockdown of Beclin1 also reduced the level of Atg14 (78). In HCT 116 human colon cancer cells, knockdown of Atg14 decreased the Beclin1 level (79). It is possible that release of sequestered Beclin1 from non-autophagic complexes (i.e., Beclin1-IP_3R) upon activation of $G\alpha_q$Q209L permits the formation of new Vps34-Beclin1-Atg14 complexes. Stabilization of the proteins in this complex would explain why we observed an increase in protein but not mRNA levels in the $G\alpha_q$Q209L heart. In addition to the Vps34-Beclin1-Atg14 complex, we observed a small increase in Atg7 transcription in $G\alpha_q$Q209L hearts after injection of tamoxifen for 7 days. Other studies have described a stimulatory effect of $G\alpha_q$ on Atg7 transcription. Uveal melanoma cell lines harboring a constitutively active $G\alpha_q$ mutant had a 2.1-fold higher level of Atg7 expression than WT cell lines (80). In the mouse heart, Atg7 mRNA levels increased 2.3-fold after four weeks of angiotensin II infusion (which activates the $G\alpha_q$-coupled AT_1 receptor) (81). Moreover, we observed increased protein expression of Lamp-2 and increased cathepsin D proteolytic cleavage. These data suggest that $G\alpha_q$ enhances the expression of key proteins in organelles at every level of the autophagy pathway.

p62 is considered to be an important mediator and substrate of autophagy, and thus is degraded upon autophagy activation in most cell systems. However, similar to what we observed in the $G\alpha_q$Q209L heart, p62 content increased in cardiac tissue in response to autophagic stimuli such as starvation and pressure overload (61,82,83). Upregulation of p62 expression and its localization in aggregates were also seen in two mouse models of cardiomyopathy caused by transgenic expression of misfolded

proteins (84). A major function of p62 is to self-oligomerize and forms protein aggregates to sequester harmful or toxic proteins. One such proteins is Keap-1, a negative regulator of the master antioxidant protein Nrf2 (85,86). p62 aggregation plays a critical role in promoting a cell's antioxidant response (56,87). As ROS burst is largely involved in pressure overload-induced heart failure and $G\alpha_q$-induced heart failure (21,88,89), it is possible that p62 expression and aggregation are induced to function as a stress response mechanism to alleviate the pathological condition.

I observed deformed mitochondria and an abnormal ultrastructure with multiple layers of membrane in $G\alpha_q$Q209L hearts (Fig. 2-4A & Fig. 2-4D). This ultrastructure resembles "myelin bodies" or "myelin figures" observed in a transgenic mouse heart failure model and a dilated cardiomyopathy patient sample, and have been proposed to be a result of damaged mitochondria (49-51). It has been demonstrated that $G\alpha_q$ causes loss of mitochondrial membrane potential, ROS production and cytochrome *c* release, which lead to apoptosis of cardiomyocytes (21,90). We did not observe significant apoptosis in the $G\alpha_q$Q209L heart; however, we cannot exclude the possibility that mitochondrial damage could trigger a global activation of autophagy.

I also observed an ultrastructure in which a mitochondrion is tightly wrapped in electronic dense membrane. Some researchers interpret it as autophagosome membrane (91); some think that it is a transition from damaged mitochondria to myelin bodies (50). I think it may be an indication of mitophagy. Current theory of mitophagy is that decrease of mitochondria membrane potential leads to accumulation of PINK1 on the mitochondria outer membrane; PINK1 then dimerizes and autophosphorylates itself and becomes active. PINK1 then activates Parkin which grows ubiquitin chains on mitochondria and recruit adaptor proteins, such as p62, and autophagosome membrane (140, 141). My data could be an evidence showing that autophagosome membrane is directly elongated on the outer membrane of a mitochondrion.

In summary, I observed increased autophagy activity in the mouse heart when $G\alpha_q$ signaling is enhanced. Increased Vps34-p150-Beclin1-Atg14 complex formation and increased Vps34 activity, increased Atg7 expression, and increased lysosome

activity may all contribute to this phenotype. However, more investigation is needed to uncover the detailed molecular mechanisms by which $G\alpha_q$ regulates autophagy.

Chapter 3. Calpain is not the key mediator of autophagy activation in the $G\alpha_qQ209L$ heart

3-1. Introduction

3-1-1. Calpain

Proteins in the *Cal*cium Ion-Dependent Pa*pain*-Like protease (calpain) family are cysteine proteases with significant substrate specificity which do not induce widespread degradation of proteins. Calpains have been shown to have regulatory roles in the cell cycle, contraction, apoptosis, cell migration, cell differentiation and cellular signal transduction in muscle (92). A calpain is composed of one large catalytic subunit and one small regulatory subunit. There are 16 human calpain genes discovered, 14 of which encode large subunits and two of which encode small regulatory subunits (93). Among the 14 catalytic subunits, calpain 1 (CAPN1) and calpain 2 (CAPN2) are the most studied, especially in heart. Calpain 4 (CAPNS1) is the small regulatory subunit for calpain 1 and calpain 2.

Calpains generally exist as inactive proenzymes that may be activated by increases in intracellular calcium (92). Calpains respond to calcium concentrations very differently: the concentration of Ca^{2+} giving half-maximal activity *in vitro*, $[Ca^{2+}]_{0.5}$, ranges from 2 to 75 μM for calpain 1 (μ-calpain), and 200-1000 μM for calpain 2 (m-calpain) (94). However, Ca^{2+} concentrations in non-contracting cells range from 50 to 300 nM normally, which is far lower than $[Ca^{2+}]_{0.5}$ *in vitro*. In cardiomyocytes, Ca^{2+} sparks can reach up to 1~2 μM to activate the contractile apparatus (25), but this is still at the lower limit of the activation concentration for calpains. One explanation for this discrepancy is that ancillary mechanisms or factors should enhance the affinity of calpains for calcium. For example, phosphatidylinositides reduced the Ca^{2+} demand for calpain activation (94). Another explanation is that calpain molecules are anchored to the cell membrane in the vicinity of Ca^{2+} channels where much higher Ca^{2+} concentrations could form than the cytoplasmic average (25,94).

Besides calcium concentration, calpain activity is regulated in two other ways *in vivo*. First, calpastatin is an endogenous calpain inhibitor that acts in a substrate

competitive manner on calpain 1 and calpain 2 (95). Second, phosphorylation by protein kinase A reduces calpain activity (92). Pharmacologically, there are several calpain inhibitors that are often used in calpain research.

3-1-2. Calpain's role in autophagy

Calpain has been reported to be essential for or inhibitory to autophagy in different systems. In CAPNS1$^{-/-}$ mouse embryo fibroblasts, autophagosome formation, lysosome function and long-lived protein degradation were all hampered upon starvation or rapamycin treatment (70). Autophagy was increased in chronic myeloid leukemia cells when imatinib treatment was used to induce ER stress and activate calpain (96). However, calpain was also reported to cleave Atg5, Atg3, Beclin1 and other autophagy-related proteins in different systems (97-99), and calpain inhibition induced autophagy (71,99,100).

In the heart, calpain tends to upregulate or positively correlate with autophagy. In the rat cardiac myoblast cell line H9c2, viral infection caused activation of calpain and induction of autophagy, which impaired apoptosis of host cells and allowed viral replication; application of a calpain inhibitor downregulated autophagy (101). Ischemia/reperfusion induced cell death in neonatal rat cardiomyocytes and increased calpain activity and autophagy activity at the same time (102). Exercise induced the downregulation of calpain activity and autophagy activity in the hearts of both wild type and hypertensive rats (103).

3-1-3. Calpain's role in heart failure

The majority of studies of calpain in the heart focus on pathologic conditions. There was one study showing that at baseline, only calpain 1 is active and affects the ubiquitination of certain proteins, but does not change ubiquitination globally. In different CVDs and CVD models, increased calpain activity in the heart was observed (92).

In our $G\alpha_q$Q209L heart failure mouse model, calpain activity was 2-fold higher in $G\alpha_q$Q209L hearts than wild type hearts after 7 days of tamoxifen treatment (47). Administration of Calpain Inhibitor III (which is selective for Calpains 1 and 2)

successfully prevented the development of several $G\alpha_q$Q209L phenotypes: phosphorylation of PLB, SERCA-2 activity, T-tubule organization and contractility were all normal. These results indicate that calpain plays an important role in $G\alpha_q$Q209L-induced heart failure.

I decided to examine the role that calpain may play in the increased autophagy in our $G\alpha_q$Q209L heart failure model. Because both calpain activity and autophagy are increased at the same time in several models of heart failure (101-103), I decided to examine calpain's role in autophagy at an early time point before significant contractility dysfunction develops.

3-2. Results

3-2-1. Calpain activity is increased in the heart early upon $G\alpha_q$ activation

Calpain activity was examined in $G\alpha_q$Q209L hearts after tamoxifen injection for 3 days, when cardiac contractility was not significantly reduced (fractional shorting of 50.0% ± 3.1% in WT hearts and 45.5% ± 3.9% in $G\alpha_q$Q209L hearts, $p > 0.05$, n = 4 for each group). Consistent with what we found before, calpain activity increased ~1.7- fold in $G\alpha_q$Q209L hearts compared to WT (Fig. 3-1A). This indicates that calpain is activated by $G\alpha_q$Q209L signaling, but is not secondary to heart failure.

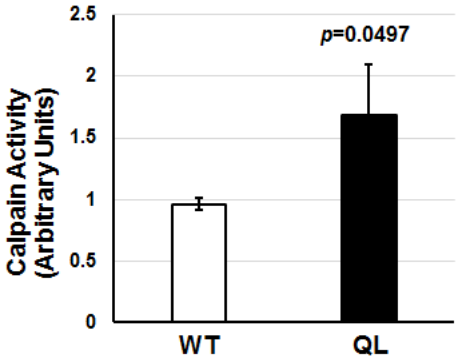

Figure 3-1. Calpain activation in $G\alpha_q$Q209L hearts. WT and $G\alpha_q$Q209L (QL) mice were injected with tamoxifen for 3 days, and calpain activity in ventricular lysates was measured. n=5 for each group. Significance was determined by Student's *t*-test.

3-2-2. Calpain inhibition has different effects on p62 and LC3-II in $G\alpha_q$Q209L heart

We have demonstrated that administration of Calpain Inhibitor III prevents $G\alpha_q$Q209L-induced heart failure (47). To determine the effect of calpain inhibition on the $G\alpha_q$Q209L-induced increase in autophagy, we applied Calpain Inhibitor III to tamoxifen injected WT and $G\alpha_q$Q209L mice and examined autophagic protein level in the $G\alpha_q$Q209L heart. Heart weight tended to increase in control $G\alpha_q$Q209L mice after 3 days of tamoxifen injections, and calpain inhibitor treatment tended to impede the process; however, the changes were not significant (Fig. 3-2A).

As observed in Chapter 2, p62 and LC3-II protein levels were increased after 3 days of tamoxifen injections in $G\alpha_q$Q209L hearts (Fig. 2-1), but to our surprise, calpain

inhibitor administration did not prevent the increase (Figure 3-2B & Fig. 3-2C). Moreover, in $G\alpha_q$Q209L mice that were injected with tamoxifen for 14 days, although the heart failure phenotype was prevented (47) and the p62 level was lowered by calpain inhibition, the increase in LC3-II was only partially reversed (Fig. 3-2D). These results suggest that calpain activation and the increase in autophagy are probably parallel responses induced by $G\alpha_q$ activation, and the increase in autophagy is not the direct cause of heart failure.

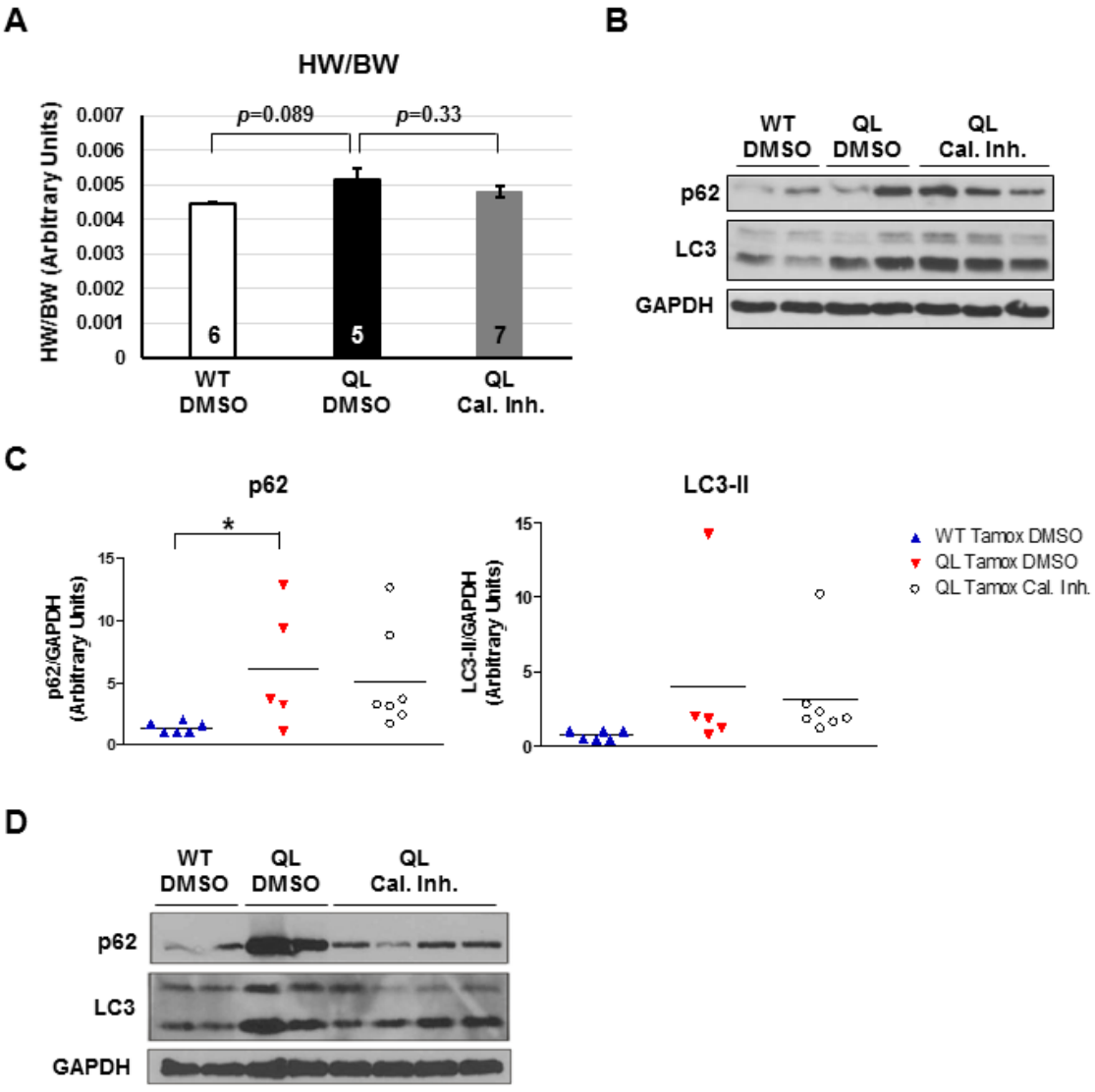

Figure 3-2. Effect of calpain inhibition on p62 and LC3-II levels. (A-C) WT and $G\alpha_q$Q209L (QL) mice were pretreated with DMSO or calpain inhibitor (Cal. Inh.) for 6 hours, and then injected with tamoxifen plus DMSO (DMSO) or tamoxifen plus calpain inhibitor

(Cal. Inh.) for 3 days. (A) Heart weight normalized to body weight (HW/BW) was calculated. N is indicated inside each column. Significance was determined by Student's *t*-test. (B) The expression of p62 and LC3 in ventricular tissue was determined by western blotting. GAPDH is a loading control. (C) Experiment in (B) was repeated twice and quantification of p62 and LC3-II protein levels (normalized to GAPDH) is shown. Each point indicates data of one mouse. *, $p<0.05$, Student's *t*-test. (D) WT and $G\alpha_q$Q209L (QL) mice were treated the same way as in (A) but for 14 days. Autophagy-related proteins in ventricular lysates of mice were detected by western blotting. GAPDH is a loading control.

3-3. Discussion

Due to several reports suggesting that calpain activity and autophagy may be enhanced in heart failure, I chose to study these two phenotypes at an early time point after $G\alpha_q$ activation to minimize the possible confounding effects of heart failure or contractile dysfunction. The results showed that both calpain activity and autophagy increased because of $G\alpha_q$ signaling, not heart failure. Calpain could be activated because of increased intracellular calcium concentration due to $G\alpha_q$ activation. However, there is not enough evidence to show that autophagy is directly activated by $G\alpha_q$; it could be secondary to other cellular changes induced by $G\alpha_q$ activation.

Calpain inhibition prevented heart failure and the increase in p62 in $G\alpha_q$Q209L mice injected with tamoxifen for 14 days, but did not change the p62 increase when mice were injected with tamoxifen for 3 days. This may indicate that p62 upregulation is an adaptive response to cellular stress. It is possible that the early increase in p62 expression is caused by $G\alpha_q$-induced stress (i.e., ROS production) independent of calpain, but calpain induces sustained p62 upregulation and aggregation at a later stage. When calpain is inhibited, high p62 expression is not sustained, and the p62 level goes back to the level induced by $G\alpha_q$ alone.

When the calpain inhibitor was applied, LC3-II conversion was only partially reduced. This indicates that calpain activation and the autophagy increase are probably parallel responses induced by $G\alpha_q$ activation, and the autophagy increase might be an adaptive response. The autophagy protein levels remained higher than in WT hearts while heart failure was prevented, demonstrating that the increase in autophagy is not a direct cause of heart failure in the $G\alpha_q$Q209L heart.

Chapter 4. Future directions

4-1. Possible molecular mechanisms for $G\alpha_q$ activation of autophagy

Although I demonstrated that autophagy activity is increased in the $G\alpha_q$Q209L heart, the signaling event and molecular mechanism that activate autophagy is not clear. Based on some preliminary data and literature, I would like to propose several directions that may be pursued in the future.

4-1-1. Post-translational modification of autophagic proteins

1) Phosphorylation of Atg14

In my Atg14 western blots, I often observed a band that is detected by Atg14 antibody but runs higher than the normal Atg14 band in both $G\alpha_q$Q209L heart lysates and $G\alpha_q$Q209L cardiomyocyte lysates (Fig. 4-1A & Fig. 4-1B). Moreover, in Beclin1 IP products, the Atg14 co-precipitated with Beclin1 was this higher molecular weight form. I propose that it is either an unknown isoform of Atg14, or post-translational modified Atg14.

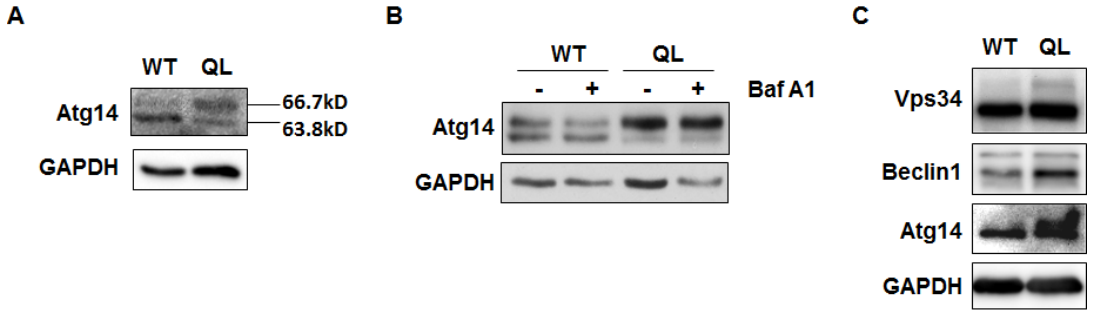

Figure 4-1. Possible post-translational modification on autophagic proteins in the $G\alpha_q$Q209L heart and cardiomyocytes. WT and $G\alpha_q$Q209L (QL) mice were injected with tamoxifen for 7 days. (A) Ventricle lysates were analyzed using indicated antibodies; GAPDH is a loading control. (B) Cardiomyocytes isolated from both groups were treated with dimethyl sulfoxide (DMSO) or 100 nM bafilomycin A1 (Baf A1) in ACCIT medium for 6 h. Cell lysates were then analyzed by western blotting using the indicated antibodies. (C) Ventricle lysates were analyzed using indicated antibodies; GAPDH is a loading control.

Atg14 seems to be one of the limiting factors regulating autophagic activity (34). Atg14 is reported to be phosphorylated by mTORC1 and ULK1. At high nutritional condition, mTORC1 phosphorylates Atg14 at multiple sites (Ser3, Thr233, Ser383, Ser440, and possible Ser223), and inhibits Vps34 activity (104). At low nutritional condition, mTORC1 activity is diminished, Atg14 phosphorylation by mTORC1 is removed, which allows activated ULK1 (which is also inhibited by mTROC1) to phosphorylate Atg14 at Ser29 site. The phosphorylation at Ser29 of Atg14 greatly increases Vps34's kinase activity and PI(3)P production, thus stimulates autophagosome formation (105).

Thus, studies can be done to determine if the upper band detected by Atg14 antibody is due to phosphorylation by ULK1. This could be done by pulling down Atg14 and detecting by p-Atg14-S29 antibody.

A more complete analysis is to do a Mass Spectrometry and analyze all the phosphorylation sites on this protein. This analysis could also provide clues if the post-translational modification is not due to phosphorylation.

2) Post-translational modification of other autophagic proteins

In my western blots, several autophagic proteins often showed upper bands similar to that was observed in Atg14 blots (Fig. 4-1C). This may indicates that a post-translational modification mechanism is upregulated globally on autophagic proteins upon $G\alpha_q$ activation. Similar studies can be performed to determine if post-translational modifications are present in other proteins.

4-1-2. $G\alpha_q$ interaction with autophagic proteins

In yeast, Gpa1 (the only Gα protein) binds to both Vps34 and Vps15; Gpa1-GDP form has higher affinity towards Vps15, while GTP form has higher affinity for Vps34. Sequence similarity analysis shows that Vps15 resembles Gβ and Atg14 is proposed to be similar to Gγ (76). BLAST analysis on Gpa1 (yeast) shows that mouse $G\alpha_i$s have highest similarity with Gpa1 (yeast); mouse $G\alpha_q$ also has high similarity with Gpa1, but lacks ~ 120 amino acids which are present in the middle region of Gpa1. To test whether G protein interacts with Vps34 in mouse cardiac tissues,

reciprocal co-immunoprecipitation using Vps34, $G\alpha_i$ and $G\alpha_q$ antibodies should be done.

In a test co-immunoprecipitation experiment, both Beclin1 and $G\alpha_q$ antibody pulled down Atg14 in WT heart lysate; however, only Beclin1 antibody pulled down Atg14 in $G\alpha_q$Q209L heart lysate (Fig. 4-2). This may indicate that $G\alpha_q$ interacts with Atg14 at basal state; upon $G\alpha_q$ activation, Atg14 is released and engages in the formation of Class III PI3K complex to initiate autophagy. Although the $G\alpha_q$ antibody did not successfully pull down endogenous $G\alpha_q$, which makes the interpretation of the result difficult, I think this is a direction worth trying. Reciprocal co-immunoprecipitation using Atg14 and $G\alpha_q$ antibodies should be done to test this hypothesis.

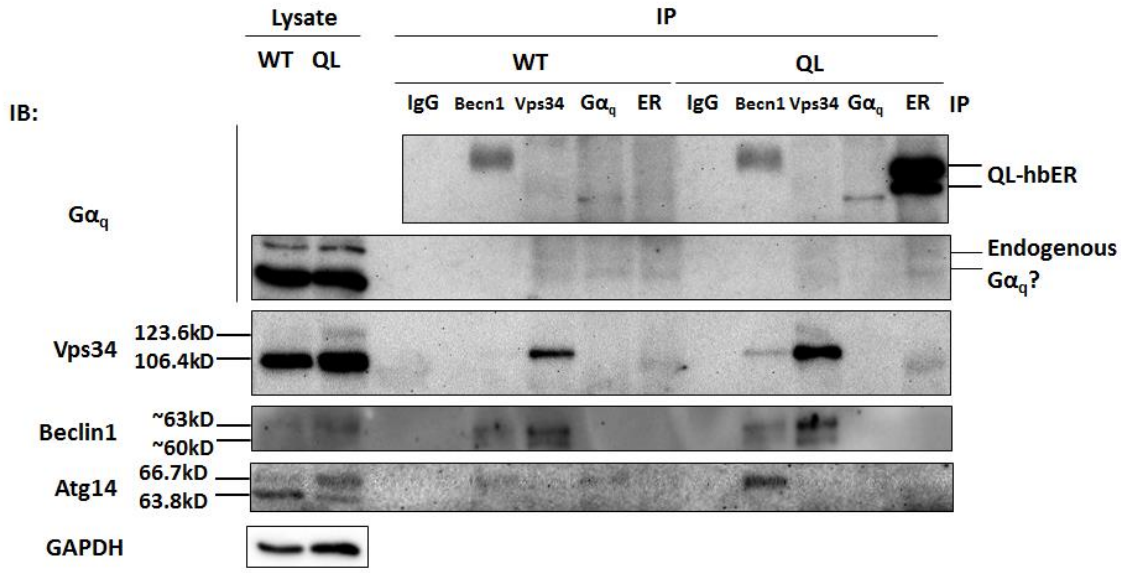

Figure 4-2. Protein interactions in the heart. WT and $G\alpha_q$Q209L (QL) mice were injected with tamoxifen for 7 days. Ventricle lysates were incubated with different antibodies (as indicated in the top) and the IP products were analyzed by western blotting.

4-1-3. IP_3R downregulation

In non-cardiac cells, elevation of intracellular IP_3 decreased autophagic flux by an unknown mechanism, while the IP_3R was shown to block autophagy by binding to and sequestering Beclin1 in a complex that cannot initiate autophagosome formation (45, 46). Similar observations were made in neonatal rat cardiomyocytes (47). Since

IP_3R is an important molecule in the $G\alpha_q$ signaling pathway, it will be worth checking if similar mechanism is true in the $G\alpha_q$Q209L heart.

4-1-4. Upstream signaling

Recent studies indicate that mTORC1, ULK1 and AMPK are the most important nutrients and energy sensors. The activity of these kinases in the $G\alpha_q$Q209L heart would be a direct link from $G\alpha_q$Q209L to autophagy induction. The activity of these kinases and how their activity may be regulated by $G\alpha_q$Q209L should be further investigated.

4-2. Autophagy is protective

According to several studies (97,100), autophagy is protective under stress conditions and inhibition of autophagy could lead to apoptosis. Mitochondria damage has been observed in many $G\alpha_q$ activation models but was not obvious in the $G\alpha_q$Q209L heart (no change in mitochondria proteins, no caspase cleavage), which may indicates that autophagy activation in the $G\alpha_q$Q209L heart may actively remove damaged mitochondria and protect cardiomyocytes from deleterious signals being released.

To test my hypothesis that autophagy is protective, agents that inhibit autophagy could be applied in $G\alpha_q$Q209L heart together with tamoxifen. If increased cell death is observed, then the result would support my hypothesis.

4-3. p62's role in cardiac health

4-3-1. p62 level may be an indicator of cardiac health

I observed that p62 protein level in heart correlates with heart weight (Fig. 4-3). If this correlation is true, it would be worth studying if p62 could be an indicator of cardiac heath and be used for cardiac disease prognosis.

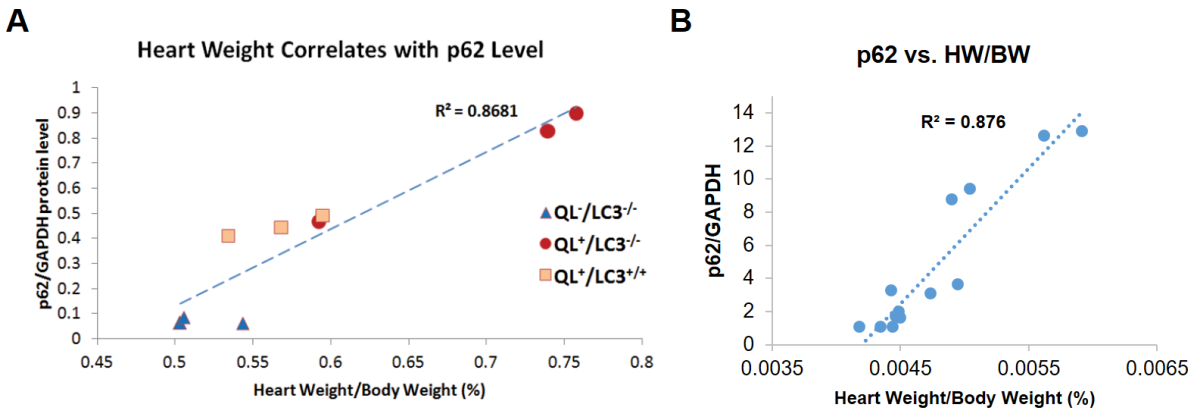

Figure 4-3. p62 level correlates with heart weight. (A) $G\alpha_qQ209L$ (QL) mice were crossed with a whole body LC3KO mice. Offspring with indicated genotypes were injected with tamoxifen for 7 days. Heart weight and body weight were measured; p62 level in ventricle lysates was determined by western blotting and normalized by GAPDH. p62 level was plotted against heart weight/body weight, and a linear regression was performed. (B) WT and QL mice were injected with tamoxifen, tamoxifen with DMSO, or tamoxifen with calpain inhibitor for 3 days. A linear regression analysis was done in the same way as in (A).

4-3-2. p62 upregulation is a compensatory response

In Chapter 2, I discussed that p62 upregulation and aggregation may be a compensatory and protective response to alleviate ROS stress upon $G\alpha_qQ209L$ activation. To further investigate this hypothesis, ROS level and ROS responsive proteins in the $G\alpha_qQ209L$ heart can be measured. Also, p62 knockdown or knockout in $G\alpha_qQ209L$ cardiomyocytes/hearts could be done to see if these manipulations change the ROS level, worsen the contractile defect, and lead to myocyte death.

4-4. Increased ubiquitinated protein level

We observed an increased level of ubiquitinated proteins in the $G\alpha_q$Q209L heart, which would normally be a result of blockade of proteasome activity or autophagy. However, autophagy is enhanced, as I showed in Chapter 2. To determine if proteasome activity might be blocked, $G\alpha_q$Q209L cardiomyocytes were treated with the proteasome inhibitor MG132. I found that ubiquitinated proteins accumulated (data not shown), indicating that proteasome activity is present in the $G\alpha_q$Q209L hearts.

My observation is supported by other studies in which increased global ubiquitination was observed in mouse heart with pressure-overload–induced hypertrophy and in NRCM activated by phenylephrine; MG132 treatment further increased ubiquitinated protein levels in NRCM treated with phenylephrine (106). Similarly, ischemia/reperfusion induced autophagy activation in mouse heart, but increased ubiquitinated protein levels were also observed (107).

Similar to upregulation of p62 expression, the ubiquitin-proteasome system (UPS) might be transcriptionally upregulated in the $G\alpha_q$Q209L heart. In pressure-overload–induced hypertrophy of rat heart, 5 out of 6 examined proteins in the UPS, including ubiquitin B, were upregulated transcriptionally (108). Thus, it might be worth measuring mRNA levels of key proteins in the UPS to explain the increase in ubiquitinated proteins in the $G\alpha_q$Q209L heart.

4-5. Find a cell line to study the molecular mechanism of $G\alpha_qQ209L$ inducing autophagy

Autophagy is a dynamic process, which makes it hard to completely study its mechanism in animal models. I tried several widely used cell lines to study the mechanism, but these cell lines failed to replicate what I saw in $G\alpha_qQ209L$ heart. I finally found some clues in HL-1 cells, a mouse atrial cardiomyocyte cell line. Future cell biology and molecular studies could be carried out using this cell line.

4-5-1. MEF

We first tried to study the molecular mechanism in mouse embryonic fibroblasts (MEFs). Not resembling what I saw in the $G\alpha_qQ209L$ heart, at basal level, $G\alpha_qQ209L$ expression did not change LC3-II or ubiquitinated protein level; nor did it increase autophagic flux. However, when the cells were serum starved to induce autophagy, $G\alpha_qQ209L$ caused a great increase of LC3-II level and ubiquitinated protein accumulation (Fig. 4-4A). This indicates that $G\alpha_qQ209L$ enhanced starvation induced autophagy in MEFs.

I utilized a GFP-FYVE MEF cell line to study Vps34 activity upon $G\alpha_qQ209L$ expression. FYVE domain is a PI(3)P binding domain; by conjugating FYVE to GFP, PI(3)P generation could be easily visualized in cells. If there is not high level of PI(3)P, overexpressed GFP-FYVE is diffused in cytosol; if PI(3)P is actively synthesized, GFP-FYVE will localize to PI(3)P generation sites which are small vesicles, and appear as "puncta" when visualized using fluorescent microscope. To our surprise, $G\alpha_qQ209L$ expression tended to decrease GFP-FYVE puncta formation. Moreover, the AA mutant which cannot activate PLCβ and did not cause $G\alpha_qQ209L$ phenotype in heart, inhibited GFP-FYVE puncta formation even more (Fig. 4-4B & Fig. 4-4C). This is opposite to the increased Vps34 activity I observed in the $G\alpha_qQ209L$ heart. Thus, MEF is not a good model to study the molecular mechanism of $G\alpha_qQ209L$-induced autophagy in heart.

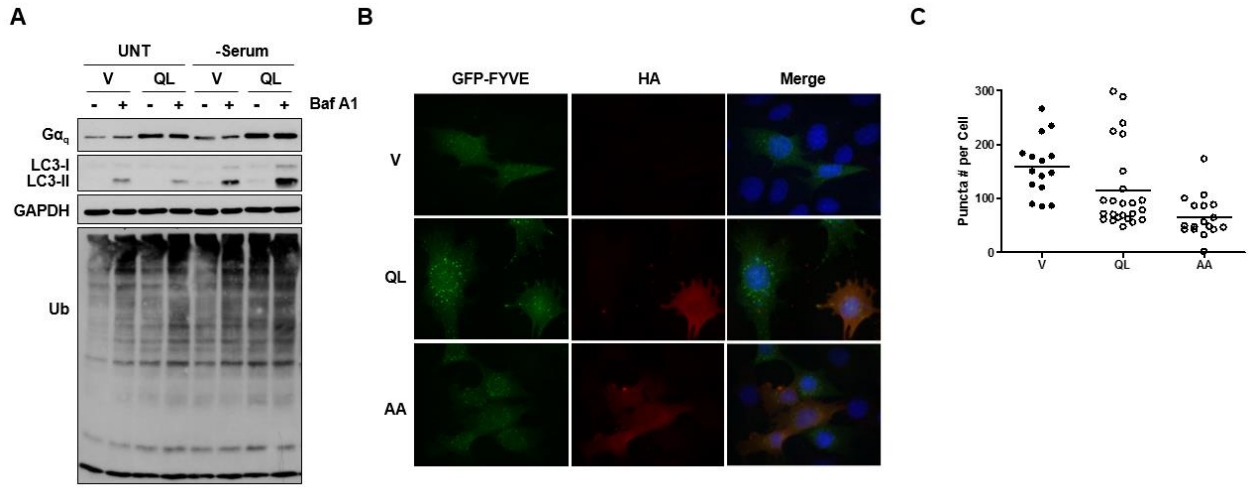

Figure 4-4. Autophagy activity and Vps34 activity in $G\alpha_qQ209L$ expressing MEFs. (A) MEFs were transiently transfected with a construct expressing $G\alpha_qQ209L$ (QL) protein or an empty vector. 42 hour post transfection, cells were either untreated (UNT) or serum starved (-Serum) for 6 h. Meanwhile, cells were treated with dimethyl sulfoxide (DMSO) or 100 nM bafilomycin A1 (Baf A1). Cell lysates were then analyzed by western blotting using the indicated antibodies. (B) MEFs stably expressing GFP-FYVE protein were transiently transfected with vector, HA-$G\alpha_qQ209L$, or HA-$G\alpha_qQ209L$-AA (AA) proteins. 48 hour post transfection, cells were fixed, immunostained for HA tag, and visualized by deconvolution microscopy (Zeiss; 60x magnification). GFP-FYVE puncta in vector transfected cells or HA positive cells were quantified by CellProfiler 2.0 and shown in (C). Bars indicate average of each group. p=0.0684 for QL vs. V, and p<0.0001 for AA vs. V; student t-test.

4-5-2. α_{1A}-AR expressing Rat-1

Our laboratory previously established a cell line in which α_{1A}-adrenergic receptor (α_{1A}-AR) was expressed in Rat-1 cell, a rat fibroblast cell line. Treatment of this cell line with phenylephrine (PE) specifically stimulates α_{1A}-AR which couples to $G\alpha_q$.

To see whether Vps34 activity is also increased by $G\alpha_q$ activation in this cell line, I treated α_{1A}-AR Rat-1 cells with PE for different durations (0.5 h to 24 h). As shown in Fig. 4-5B, Vps34 activity began to decrease after 1 h of PE treatment and kept at lower than basal level up to 24 h post treatment. This might be due to desensitization of the receptor (109). Repeated experiments showed that Vps34 activity was not increased by $G\alpha_q$ activation at 30 min (Fig. 4-5C). Protein levels of p62, LC3-II and Beclin1 were not elevated as I saw in the $G\alpha_qQ209L$ heart (Fig. 4-5A). Thus, α_{1A}-AR Rat-1 cell line is not suitable for studying $G\alpha_q$ regulation of autophagy.

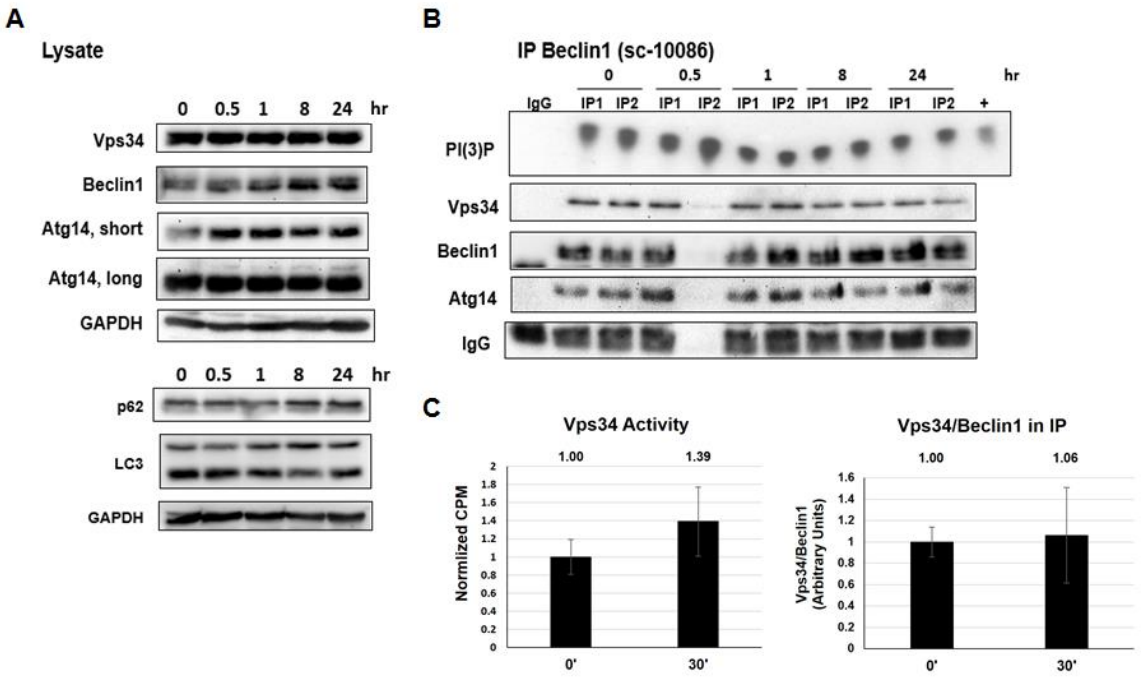

Figure 4-5. Vps34 activity in phenylephrine (PE) activated Rat-1 α_{1A}-AR cells. (A-B) Rat-1 α_{1A}-AR cells was treated with 10 μM PE for indicated time. Cells were collected in Vps34 lysis buffer and performed Vps34 activity assay as described in Methods. (A) Protein content in lysates was analyzed using western blotting. GAPDH is a loading control. (B) 75% of each IP was subjected to a Vps34 activity assay. The top panel shows an autoradiograph of ^{32}P-labeled PI(3)P produced in the assays. "+" indicates a positive control with human Vps34 protein. The remainder of each IP was subjected to immunoblotting using the indicated antibodies (lower panels). IgG is a loading control. (C) Same experiment as in (A-B) was done for three times, but with different PE treatment time. Only assays 30 min after PE treatment were quantified. Left panel: ^{32}P-labeled PI(3)P were quantified by scintillation counting and normalized to the WT mean. Error bars show standard error of the mean. Right panel: Protein bands from Beclin1 IP/western blots were quantified by densitometry. Normalized Vps34/Beclin1 ratio is shown. Error bars show standard error of the mean. Not significant for both panels, Student's *t*-test. * Note: I forgot to mix 0.5 hr IP2 beads before split them into western tube and Vps34 assay tube. So there was little protein in IP samples and I used ¾ of CPM to calculate average CPM for that group.

4-5-3. HL-1

I then looked for cells of cardiac origin. HL-1 cells were derived from the AT-1 mouse atrial cardiomyocyte tumor lineage. HL-1 cells can be serially passaged, yet they maintain the ability to contract and retain differentiated cardiac morphological, biochemical, and electrophysiological properties (110).

To create a model mimicking our $G\alpha_q$Q209L heart, I made a lentiviral construct carrying $G\alpha_q$Q209L-hbER gene to deliver this fusion protein into HL-1 cells at relatively higher efficiency. Because HL-1 cells need to be maintained at high cellular density in order not to lose their spontaneous beating character, puromycin selection was not performed. Thus, experiments were done using a heterogeneous pool of cells, with $G\alpha_q$Q209L expressing cells accounting for ~50% of the cells. Western blotting of membrane fraction shows that upon adding 4-hydroxytamoxifen (4-OHT), PKCα is mobilized to cell membrane and phosphorylated (Fig. 4-6A); thus, the construct works and 4-OHT activates the $G\alpha_q$ signal. A time course showed that $G\alpha_q$ activation led to increase of LC3-II level two days after $G\alpha_q$ activation, and a slight increase of Beclin1 protein level six days after $G\alpha_q$ activation. 4-OHT also led to increase of LC3-II on Day 2 in parental cells; this is consistent with reports that 4-OHT (tamoxifen) activates autophagy (Fig. 4-6B). Nevertheless, $G\alpha_q$Q209L led to a higher increase of LC3-II level. Because p62 level in HL-1 cells is originally high, the slight increase of p62 level is not mimicking heart $G\alpha_q$Q209L phenotype.

One method to test autophagic activity is to check LC3 puncta formation and delivery to lysosomes using mCherry-GFP-LC3 fusion protein. Upon autophagy induction, mCherry-GFP-LC3 localizes to autophagosome membrane and form yellow puncta (red and green); if autophagosomes successfully fuse with lysosomes and lysosomal pH is acidic as normal, the GFP fluorescence is quenched by low pH while mCherry red fluorescence is not, thus red puncta are viewed. I transiently transfected HL-1 cells with mCherry-GFP-LC3 and HA-tagged $G\alpha_q$Q209L proteins. In HA-$G\alpha_q$Q209L positive cells, there are more yellow and red puncta formed at both basal level and starvation, which demonstrates that autophagy activity is higher in $G\alpha_q$Q209L expressing HL-1 cells compared to control cells (Fig. 4-7).

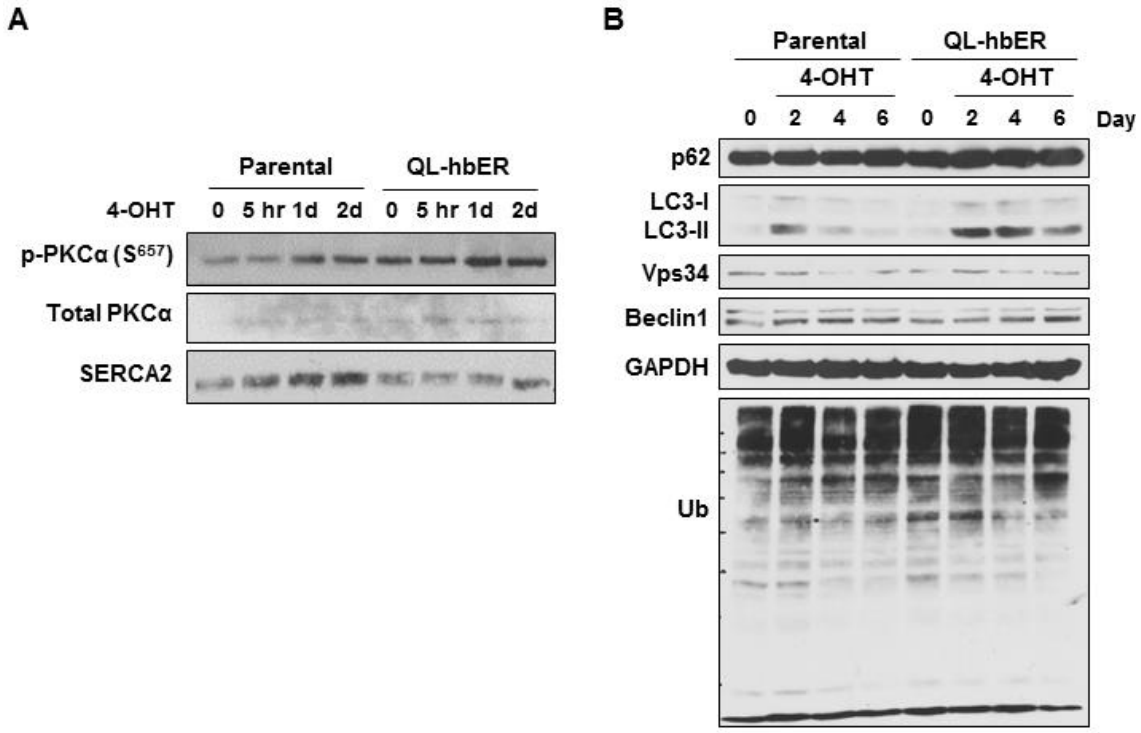

Figure 4-6. Autophagic protein level in $G\alpha_qQ209L$ expressing HL-1 cells. HL-1 cells were transduced with lentivirus carrying $G\alpha_qQ209L$-hbER gene, the transduction efficiency was about 50%. Experiments were done using this heterogeneous pool of cells. (A) After stimulation with 4-hydroxytamoxifen (4-OHT), membrane fraction of cells was prepared and protein content was analyzed by western blotting using indicated antibodies. (B) Parental and QL-hbER expressing HL-1 cells were treated with 4-OHT for indicated time; 4-OHT was refreshed every day. Cell lysates were collected and analyzed by western blotting using indicated antibodies.

4-5-4. Cultured adult mouse cardiomyocytes

This model is discussed in Chapter 5, Section 5-1-1.

4-5-5. Discussion

The different results from MEFs and α_{1A}-AR Rat-1 cells suggest that *in vitro* cell lines are not suitable for cardiac autophagy study. Thus far, HL-1 is the best cell line I have found that somewhat mimics $G\alpha_qQ209L$ induced autophagic activity in heart. However, high endogenous level of p62 in HL-1 cells may miss important molecular mechanisms related to p62. Cultured adult mouse cardiomyocyte is a better model to reflect *in vivo* condition. However, this system is limited by our ability to conduct molecular manipulation. Future studies will need a combination of HL-1 and cultured

cardiomyocytes to further delineate the molecular mechanism of $G\alpha_qQ209L$-induced autophagic response.

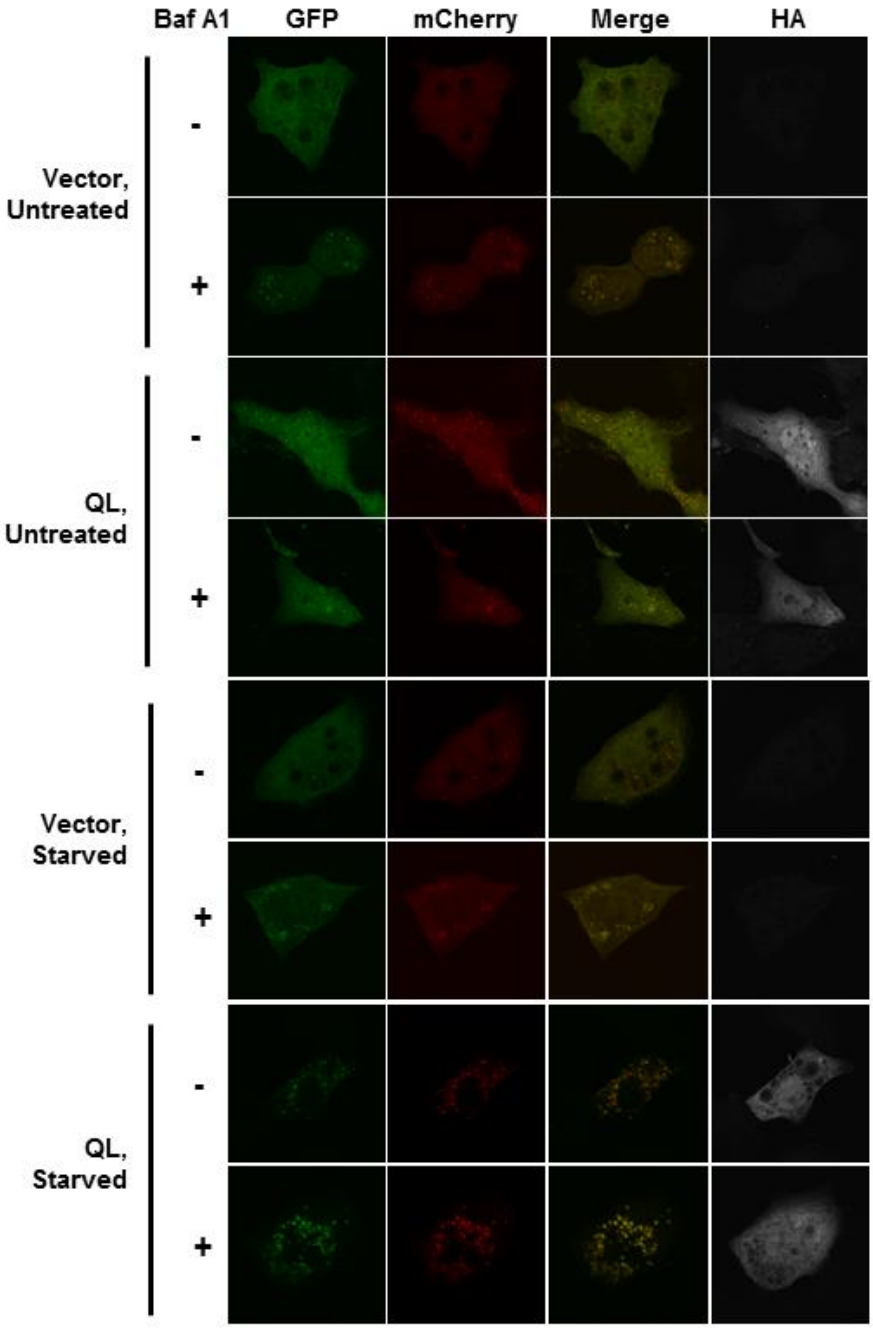

Figure 4-7. Autophagic activity in $G\alpha_qQ209L$ expressing HL-1 cells. HL-1 cells were transiently transfected with mCherry-GFP-LC3 and either vector or HA-$G\alpha_qQ209L$ constructs. 24 h post transfection, cells were re-plated at a lower density; 42 h post transfection, cells were either untreated or serum starved for 6 h; 48 h post transfection, cells were fixed, immunostained with HA antibody, and viewed under a confocal microscope (63X magnification).

4-6. Overview

Figure 4-8 is an illustration of the molecular events occurring in the heart upon activation of $G\alpha_q$. I propose that in the heart, $G\alpha_q$ activation leads to the activation of calpain and other calcium responsive molecules, which may contribute to mitochondria damage and its subsequent events. Increased p62 expression and activation of autophagy may be a direct result of $G\alpha_q$ signaling, or may function to clear out those detrimental damages as a compensatory response. Further investigations are needed to precisely identify which regulatory signals are responsible for the increased autophagy upon activation of $G\alpha_q$, and confirm the role increased autophagy plays in this heart failure model.

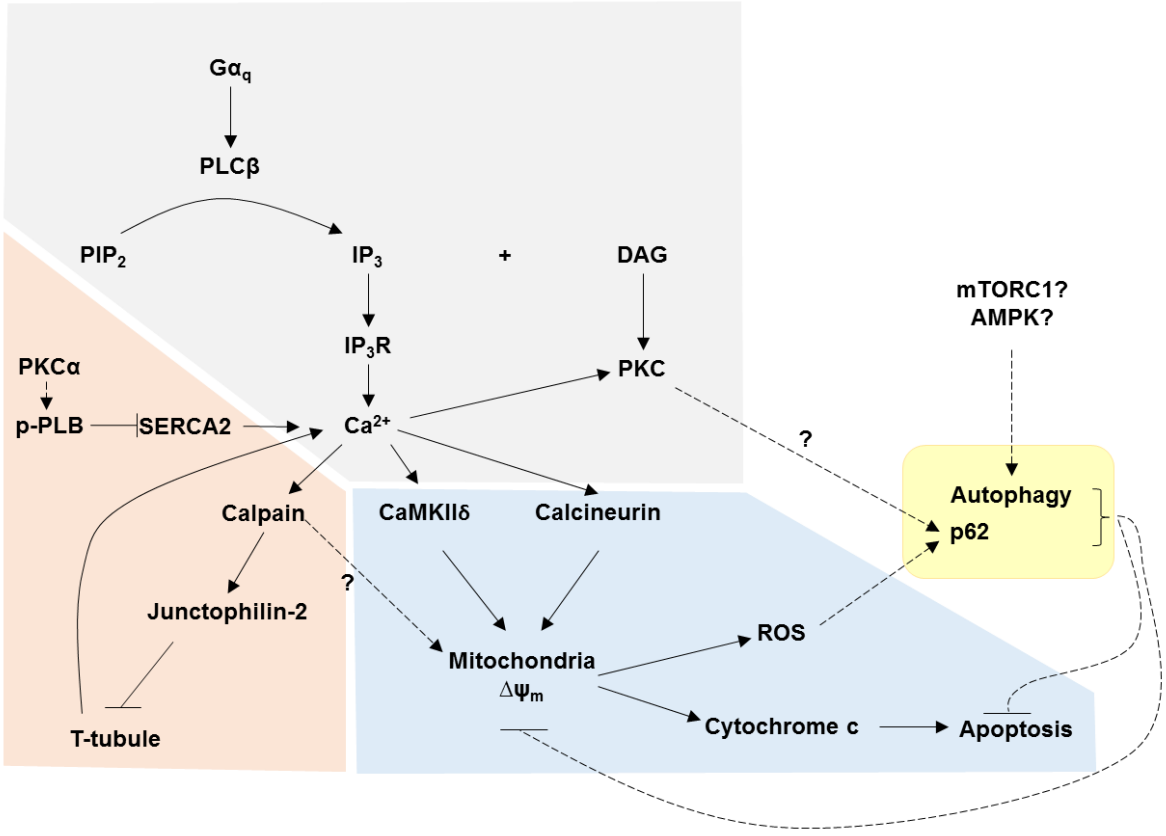

Figure 4-8. An illustration of molecular events in the $G\alpha_qQ209L$ heart. Grey background: canonical $G\alpha_q$ signaling; orange background: events identified by our laboratory; blue background: events identified by other laboratories (not yet confirmed in our $G\alpha_qQ209L$ model); yellow background: events identified by me. Dash line indicates links proposed yet to be confirmed in our $G\alpha_qQ209L$ model.

Chapter 5. Methods

5-1. Development of protocols

Autophagy research in cardiac tissue is not new, but has been restrained by the limitations of animal models and lack of a good cell line model. A shortcoming of small animal models is that animals need to be sacrificed for sample collection, which only allows samples at one time point to be examined. In addition, systematic error due to animal variance and human manipulation is much larger in animal models than in cell lines. In my research, I adopted some methods that have been published and optimized them for autophagy research in cardiomyocytes.

5-1-1. Adult mouse cardiomyocyte culture

No cell line has been demonstrated to perfectly mimic cardiac tissue behaviors (111). Thus, the best experiment would be done directly using adult cardiomyocytes. The length of adult cardiomyocyte culture varies depending on the technician's technique and many unknown factors. Cultured adult mouse cardiomyocytes can live for up to 96 h (112). Cardiomyocytes of adult rabbit and rat were reported to be viable for up to 6 days and 14 days in culture, respectively, although changed morphology or reduced ion channel performance took place at later stages of culture (113-117). Thus, in most studies, experiments are performed on cultured adult cardiomyocytes between 24 h and 72 h after isolation (118-121).

Figure 5-1. Adult mouse cardiomyocytes in culture. Cardiomyocytes were isolated from one adult wild type mouse and cultured in ACCIT medium for 2 days. Representative differential interference contrast (DIC) images taken using a confocal microscope are shown. Left panel: 20x magnification; Right panel: 60x magnification.

Based on a protocol provided by Dr. Caimei Zhang in Dr. Long-Sheng Song's laboratory, I established a protocol for culturing ventricular cardiomyocytes isolated from adult mice 8 to 12 weeks old. Cardiomyocytes remained viable and showed a striated pattern for up to 3 days (Fig. 5-1). The cultured cardiomyocytes were responsive to insulin stimulation (Fig. 5-2), were capable of ectopically expressing proteins transduced by adenoviral infection (Fig. 5-3A), and were able to execute lentiviral shRNA-mediated protein knockdown (Fig. 5-3B). We used adenoviral delivery of a constitutively active PI3K catalytic subunit, p110α, to show that p110α regulates the electrophysiologic properties of a sodium channel in cultured adult mouse cardiomyocytes (122). In summary, this culture protocol will be a powerful tool to study the cell biology of adult cardiomyocytes. The detailed protocol is described in Section 5-2.

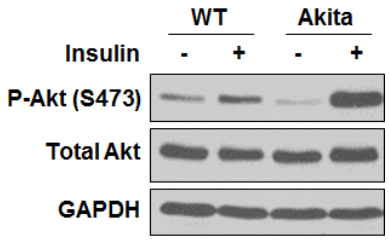

Figure 5-2. Cultured adult mouse cardiomyocytes are responsive to growth factor stimulation. Cardiomyocytes were isolated from WT and type 1 diabetic *Ins2*^{Akita} (Akita) mice and cultured in ACCIT medium. Cells were incubated in insulin-free ACCIT medium for 3 h, and then stimulated with or without 100 nM insulin for 5 min. Cell lysates were collected and analyzed by western blotting using the indicated antibodies. GAPDH is a loading control.

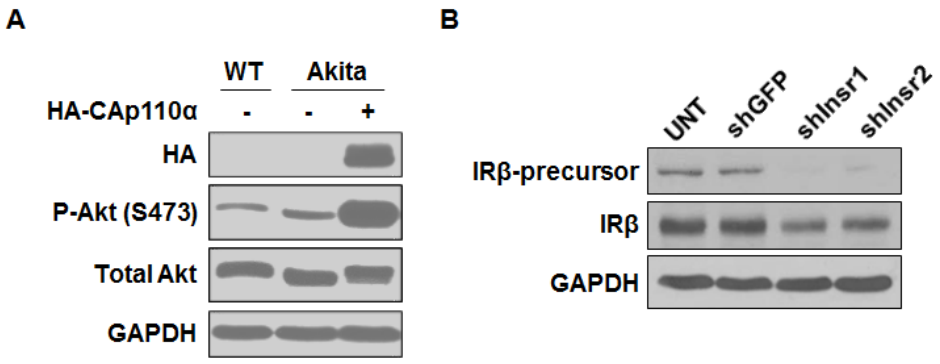

Figure 5-3. Protein expression and knockdown in adult mouse cardiomyocytes. (A) Cardiomyocytes were isolated from WT and Akita mice and cultured in ACCIT medium. Adenoviruses expressing GFP or HA-tagged constitutively active p110α (HA-CAp110α) were added to the culture medium 4 h after recovery. Cell lysates were collected 48 h post-transduction and analyzed by western blotting using the indicated antibodies. GAPDH is a loading control. (B) Cardiomyocytes were isolated from one adult WT mouse and plated in ACCIT medium. After ~16 h of recovery, the cells were left untreated (UNT) or infected with lentiviruses carrying shRNA to GFP or to insulin receptor β (gene name Insr; two different shRNAs were used) for 16 h. Then the medium was changed to fresh ACCIT medium. The cells were lysed in General Lysis Buffer 72 h post-transduction. Lysates were analyzed by western blotting using an anti-insulin receptor β (IRβ) antibody which detects both precursor and mature forms of IRβ. GAPDH is a loading control.

5-1-2. PI(3)P level measurement in cardiac tissue

Based on the protocol from the PI(3)P ELISA kit and several publications (123-126), I developed the current protocol for phospholipid extraction from cardiac tissue and PI(3)P ELISA. Utilizing $Vps34^{fl/fl}$ mice from our collaborator, Dr. Wei-Xing Zong, I was able to validate this assay. $Vps34^{fl/fl}$ mice were crossed with αMHC-MerCreMer mice (127) to generate $Vps34^{fl/fl}$ animals with or without the tamoxifen-activated Cre recombinase (MerCreMer) expressed specifically in cardiomyocytes. Injection of tamoxifen results in deletion of the Vps34 genes in the heart of $Vps34^{fl/fl}$/MerCreMer animals but not in control $Vps34^{fl/fl}$ mice that do not express MerCreMer. As shown in Fig. 5-4, two independent experiments showed that Vps34 knockout (KO) hearts have a lower level of PI(3)P than control hearts. PI(3)P levels appeared to be sensitive to long-term storage of the tissue at -80 °C, so in subsequent experiments the frozen heart tissue was stored for no longer than 2 weeks before processing. Also, it seems that it takes more than one week for Vps34 protein to be completely turned over, as the PI(3)P level decreased to a larger degree in cardiac tissue of Vps34 KO mice collected 19 days *vs.* 8 days after tamoxifen treatment.

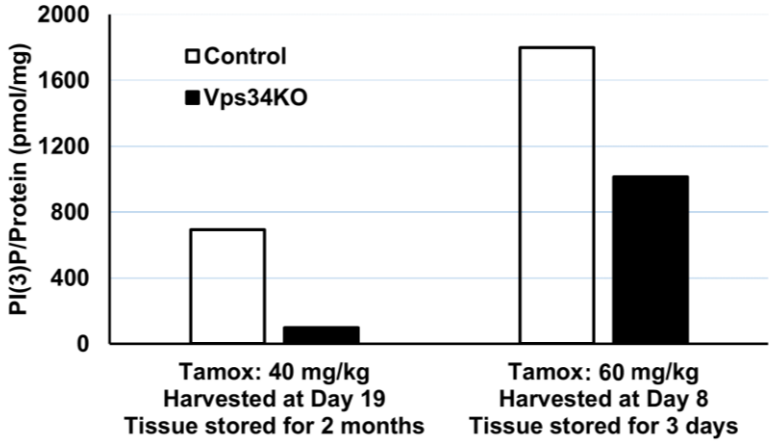

Figure 5-4. PI(3)P ELISA validation using Vps34 knockout (KO) hearts. At 5 weeks of age, Vps34$^{fl/fl}$/MerCreMer mice (Vps34 KO) and Vps34$^{fl/fl}$ mice (Control) were injected with tamoxifen (Tamox) at the indicated dose for 5 days. Day 1 is the day of the first injection. At the day of harvest, the hearts were quickly excised, trimmed of atria and aorta, frozen in liquid nitrogen, and stored at -80 °C. Phospholipids were extracted from frozen ventricles and analyzed by PI(3)P ELISA. The amount of PI(3)P was normalized by protein mass in the same amount of tissue used to extract phospholipids. Two experiments were done with different experimental conditions as indicated in the graph.

5-1-3. PI(3)P immunofluorescence microscopy

Fluorescence microscopy is a powerful tool to detect the subcellular localization as well as qualitative amounts of molecules. Localization of exogenous GFP-FYVE protein to membranes is a standard method to detect PI(3)P generation in cells (as discussed in Chapter 4). However, the lack of a readily available adenovirus expressing GFP-FYVE and resistance to other gene transfer methods make it hard to utilize GFP-FYVE in cardiomyocytes. Moreover, ectopically expressed lipid-binding fusion proteins such as GFP-FYVE may interfere with endogenous lipid function and are potentially toxic (128). Thus, determining the amount and subcellular localization of PI(3)P in cardiomyocytes is a challenge. I have developed a PI(3)P staining protocol based on Dr. Gerald R. V. Hammond's publication in 2009 (129). I validated this protocol in Vps34 KO MEFs.

MEFs derived from Vps34$^{fl/fl}$ mice were infected with adenoviruses expressing GFP or Cre recombinase with GFP to generate control or Vps34 KO MEFs, respectively. After 7 days of infection, Vps34 protein was undetectable by western

blotting in Vps34 KO cells and residual GFP fluorescence was very low (41). These cells were used to detect PI(3)P utilizing a commercially available antibody to PI(3)P and immunofluorescence microscopy. As shown in Fig. 5-5A, PI(3)P-positive signals in control cells localized to the perinuclear region, while the signal in Vps34 KO cells was absent or very much reduced. Moreover, when control cells were treated with 300 nM wortmannin (WM) to inhibit Vps34 activity, PI(3)P staining was essentially abolished, as expected. Interestingly, PI(3)P staining was still seen in control cells treated with 1 μM WM; the reason for this is not clear. PI(3)P staining was not seen in Vps34 KO cells treated with either concentration of WM.

Because adenoviruses do not infect $Vps34^{fl/fl}$ cells at 100% efficiency, the Vps34 KO MEFs I used are a mixed population of Vps34-expressing and Vps34 KO cells. Vps34 KO cells grow more slowly than control cells, so after 7 days of culture the percentage of control cells in a mixed culture will have increased. One distinguishing characteristic of Vps34 KO MEFs is that they have numerous enlarged vacuoles (41). The results in Fig. 5-5B show that cells full of vacuoles (i.e., Vps34 KO cells) had diminished PI(3)P staining, while cells with normal morphology (i.e., Vps34-expressing cells) had obvious PI(3)P-positive perinuclear staining. This indicates that the PI(3)P staining protocol successfully detects endogenous PI(3)P.

Optimization of the protocol for PI(3)P staining in cardiomyocytes would be the next step.

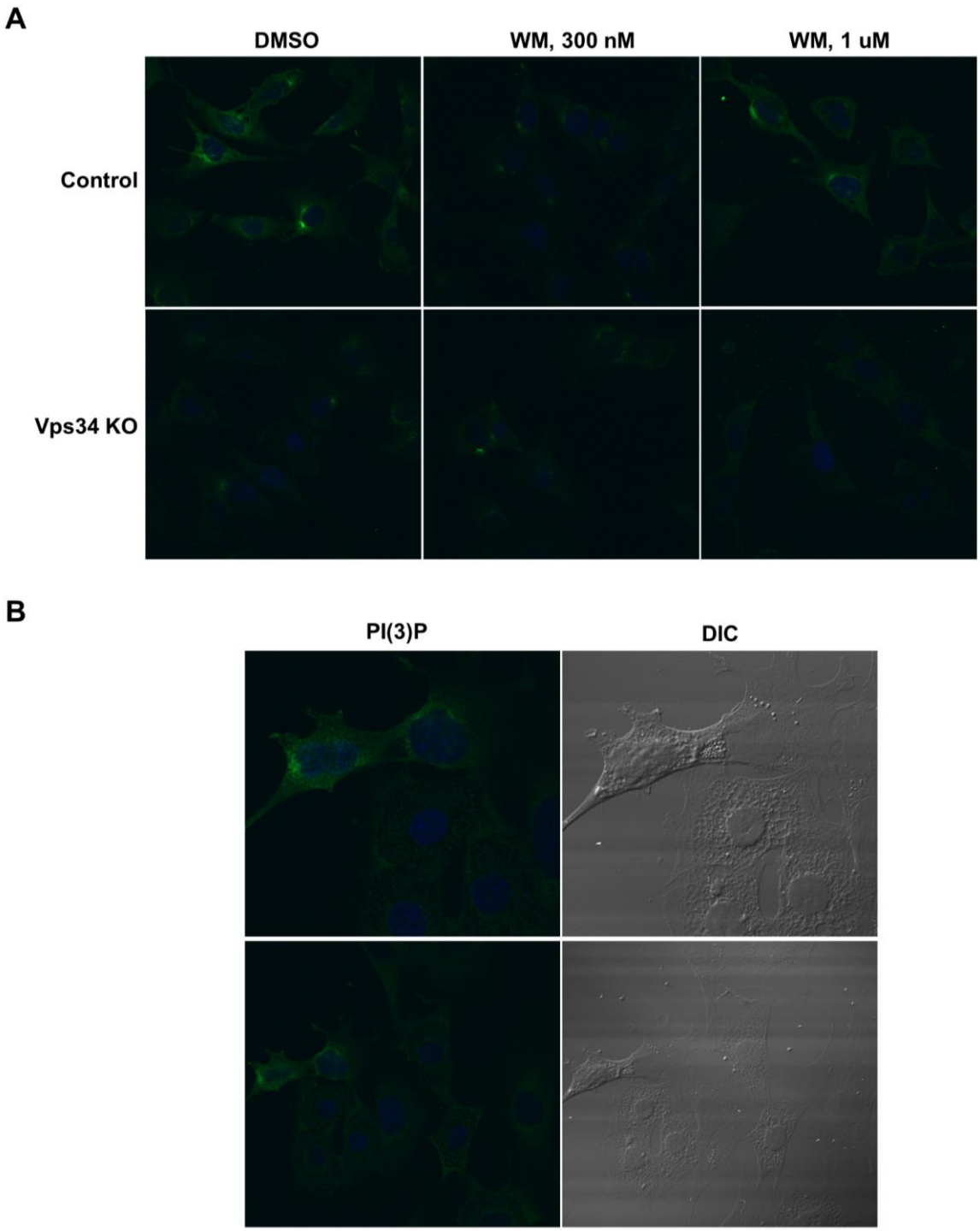

Figure 5-5. PI(3)P immunofluorescence microscopy in Vps34 KO MEFs. Vps34$^{fl/fl}$ MEFs were infected with adenoviruses expressing GFP (Control) or Cre recombinase with GFP (Vps34 KO). Immunostaining of PI(3)P was carried out 7 days after infection when GFP signal was undetectable. (A) Cells were treated with DMSO, 300 nM wortmannin (WM), or 1 µM WM for 1 h, and then were fixed and immunostained with anti-PI(3)P antibody. DAPI was used as a counter stain. Images were taken using a confocal microscope at 63x magnification. (B) Vps34 KO MEFs were fixed and immunostained with

anti-PI(3)P antibody and visualized under a confocal microscope at 100x magnification. DAPI was used as a counter stain. Left panels, immunofluorescence microscopy; right panels, differential interference contrast (DIC) microscopy.

5-2. List of Methods

Animals

C57BL/6J mice were purchased from the Jackson Laboratory and used as wild type (WT) controls. Generation and characterization of transgenic $G\alpha_qQ209L$ mice in the C57BL/6J background were described previously (9,46,47,130). GFP-LC3 transgenic mice and $Vps34^{fl/fl}$ mice were provided by Dr. Wei-Xing Zong's laboratory. *Ins2*^{Akita} (Akita) mice were purchased from the Jackson Laboratory. αMHC-MerCreMer mice were provided by Dr. Jeffery D. Molkentin's laboratory. All protocols for animal experiments were approved by the Stony Brook University Animal Care and Use Committee.

Materials

Antibodies were obtained from the following sources: p62 (Abnova H00008878-M01), LC3 (Cell Signaling 2775), Vps34 (Cell Signaling 4263), Beclin1 (Santa Cruz sc-10086), Atg7 (Cell Signaling 2631), Atg14 (a gift from Dr. Zhenyu Yue, Icahn School of Medicine at Mount Sinai), GAPDH (Sigma G8795), $G\alpha_{q/11}$ (Santa Cruz sc-392), normal goat IgG (Santa Cruz sc-2028), normal goat serum (Jackson Immuno Research 005-000-121), cathepsin D (Santa Cruz sc-6486), PI(3)P (Echelon Z-P003), insulin receptor β (Santa Cruz sc-711), ubiquitin (Santa Cruz sc-8017), and Alexa Fluor 647-conjugated goat anti-mouse IgG secondary antibody (Invitrogen A21236). The monoclonal antibodies against Lamp-1 (1D4B) and Lamp-2 (ABL-93), developed by J.T. August, were obtained from the Developmental Studies Hybridoma Bank, created by the NICHD of the NIH and maintained at the University of Iowa, Department of Biology, Iowa City, IA 52242. Specialty chemicals were obtained from the following sources: blebbistatin (Sigma B0560), bafilomycin A1 (Enzo BML-CM110), protease inhibitor cocktail (Sigma P8340), tamoxifen (Sigma T5648), Medium 199 (Sigma M4530), LysoTracker Red (Invitrogen L7528), laminin (Invitrogen 23017-015), insulin-transferrin-selenium (Gibco 41400), Liberase TM Research Grade (Roche 05401127001), and Calpain Inhibitor III (Bachem N-1535).

Cell culture, transfection and serum starvation

Generation of mouse embryonic fibroblasts (MEFs) (131), GFP-FYVE MEFs (131), Vps34 KO MEFs (41), and Rat-1 fibroblasts stably transfected with the human α_{1A}-adrenergic receptor (132) were described previously. Cells were maintained in DMEM supplemented with 10% fetal bovine serum, 100 units/ml penicillin and 100 μg/ml streptomycin, and cultured in a 5% CO_2 atmosphere at 37 °C. Transfections were done using Lipofectamine 2000 (Invitrogen) according to the manufacturer's protocol. To serum starve cells, cells were washed in PBS twice and then incubated in DMEM without serum for 6 h.

Viral constructs

Adenoviral HA-CAp110α was constructed by Dr. Eileen So Carpenter in our laboratory (122). shRNA constructs to IRβ in the lentiviral pLKO.1 vector were purchased from Sigma Aldrich (SHCLNG-NM_010568; shInsr1: TRCN0000023574; shInsr2: TRCN0000023575TRC). Lentiviral packaging constructs Δ8.91 and vesicular stomatitis virus G protein (VSV-G) were provided by Dr. Wei-Xing Zong's laboratory.

Tamoxifen treatment

Tamoxifen was sonicated in autoclaved peanut oil at 10 mg/ml. WT or $G\alpha_qQ209L$ mice 8 to 12 weeks old were injected with tamoxifen intraperitoneally at 1 mg per day for 3, 7 or 14 days as indicated.

Adult mouse cardiomyocyte isolation and culture

The basic protocol was provided by Dr. Long-Sheng Song (University of Iowa) and a few modifications were made (112,133). Mice were anesthetized under 3% isoflurane, and hearts were removed and mounted on a Langendorff apparatus. Retrograde perfusion was performed by gravity pressure. Hearts were first perfused with MyoBuffer (137 mM NaCl, 5.4 mM KCl, 2 mM $MgSO_4$, 0.33 mM NaH_2PO_4, 10 mM HEPES, 10 mM taurine, 10 mM glucose, and 100 U-100 μg/ml penicillin-

streptomycin, pH 7.4) for 3 min and then with 5 μg/ml Liberase TM in MyoBuffer plus 0.1 mM $CaCl_2$. When the hearts became soft, they were dismounted and perfused manually with Stop Buffer (MyoBuffer plus 1% bovine serum albumin (BSA)) with 0.2 mM $CaCl_2$. The tissue was minced and disrupted in Stop Buffer with 0.2 mM $CaCl_2$ using a Pasteur pipet. The suspension was filtered through 200 μm nylon mesh into a 15 ml centrifuge tube. Cardiomyocytes of good quality quickly settled to the bottom and the supernatant was removed. Cardiomyocytes were washed sequentially with Stop Buffer containing 0.5 mM $CaCl_2$ and 1.0 mM $CaCl_2$, then resuspended in Plating Medium (ACCIT medium (Medium 199, 2 mM L-carnitine, 5 mM creatine, 5 mM taurine, 2 mg/ml BSA, 100 U-100 μg/ml penicillin-streptomycin, 10 μl/ml insulin-transferrin-selenium, 2 mM glutamine, and 25 μM blebbistatin) (134) with 5% fetal bovine serum). Cardiomyocytes were plated onto laminin-coated cell culture dishes and incubated in a 5% CO_2 atmosphere at 37°C for 2 h. After incubation, healthy, rod-shaped cardiomyocytes adhered to the dish; dead and unhealthy cells were aspirated and fresh ACCIT medium was added. Treatments were carried out after a 2-h incubation in ACCIT medium.

Transmission electron microscopy (TEM)

Mice were anesthetized under 3% isoflurane, and hearts were quickly removed and retrograde perfused manually with 7 ml MyoBuffer and then 7 ml fixative (2% paraformaldehyde (PFA) and 2.5% glutaraldehyde in phosphate-buffered saline (PBS), pH 7.4). The endocardium was cut into ~1 mm^3 cubes in fixative at room temperature and stored overnight in fixative at 4°C. Later procedures were done as described previously (131). In short, fixed samples were placed in 2% osmium tetroxide in PBS, pH 7.4, for 1 h, then dehydrated in a graded series of ethanol, and embedded in Embed 812 resin. Ultra-thin sections of 80 nm were placed on formvar-coated copper grids or mesh. Sections were counterstained with uranyl acetate and lead citrate and viewed with an electron microscope (FEI Tecnai12 BioTwinG^2) at 80 kV. Images were acquired with a CCD digital camera system (model XR-60; Advanced Microscopy Techniques Corp.). 10-15 pictures were taken from each section using a uniform random sampling method (135) at a magnification of 9300x. Images to show detailed

structure were taken at a magnification of 30,000x or higher. Organelles were counted using 9300x images and normalized by an area of 156.75 μm^2 per image.

Western blotting

Mice were anesthetized under 3% isoflurane and killed by cervical dislocation. Hearts were quickly removed and the atria and aorta were trimmed off. Ventricles were homogenized in General Lysis Buffer (10 mM sodium pyrophosphate, 50 mM HEPES, pH 7.5, 1% Triton X-100, 50 mM NaCl, 50 mM NaF, 5 mM EDTA, pH 8.0, 200 μM sodium orthovanadate, 0.2 mM phenylmethanesulfonyl fluoride (PMSF), and 1 μl/ml protease inhibitor cocktail) using a glass dounce homogenizer on ice. Crude lysates were centrifuged at 13,500 rpm for 20 min at 4°C. Supernatants were collected and protein concentration was quantified using a Bradford assay (Bio-Rad). Proteins were separated by SDS-PAGE and electrophoretically transferred onto PVDF. The membranes were blocked with 5% non-fat dry milk in Tris-buffered saline plus 0.1% Tween 20 for 1 h, incubated with primary antibody overnight at 4°C, and incubated with horse radish peroxidase-conjugated secondary antibody for 1-2 h at room temperature. Enhanced chemiluminescence substrate (Thermo Pierce) was then applied to the blot, and signals were captured using a FluorChem E system (ProteinSimple). The density of each band was analyzed using AlphaView software (ProteinSimple).

Cultured cardiomyocytes were lysed in Lysis Buffer B (1% sodium deoxycholate, 1% SDS, 1% Triton X-100, 10 mM Tris, pH 8.0, and 0.14 M NaCl) and sonicated to fragment DNA. Crude lysates were centrifuged at 13,500 rpm for 15 min at 4°C, and the protein concentration of the supernatant was quantified using a BCA assay (Thermo Scientific). Proteins were then analyzed by western blotting.

RNA extraction and real-time quantitative PCR (RT-qPCR)

RNA was isolated from pieces of fresh ventricle weighing 40-50 mg using the RNeasy kit (QIAGEN) following the manufacturer's protocol. cDNA was made from 1.6 μg of RNA using the iScript cDNA synthesis kit (Bio-Rad), and cDNA made from 40 ng of RNA was added to each qPCR reaction. Reactions were done in triplicate.

RT-qPCR was carried out using TaqMan gene expression assays (Applied Biosystems), and gene expression relative to GAPDH was calculated using the ΔΔCq method (136,137). For each gene, the value obtained for one of the WT animals was assigned as 1, and values obtained for the other WT and $G\alpha_q$Q209L animals were normalized to it. Quality controls were performed following MIQE guidelines (137). Relative standard curves were performed for each TaqMan assay to ensure that PCR efficiency was between 90% and 110% and that the cDNA did not contain factors that inhibit PCR. The TaqMan assays used were: p62, Mm00448091_m1; LC3, Mm00782868_sH; Vps34, Mm00619489_m1; Beclin1, Mm01265461_m1; Atg14, Mm00553733_m1; Atg7, Mm00512209_m1; and p150, Mm00661451_m1.

PI(3)P level

Fresh ventricles were snap frozen in liquid nitrogen and stored at -80°C. The tissue was pulverized using a liquid nitrogen-cooled stainless steel mortar and pestle, and phospholipids were extracted following the protocol in the PI(3)P Mass ELISA Kit (Echelon) with modifications (124-126). The powder was transferred to a 15 ml glass tube and incubated on ice for 5 min in 7 ml 0.5 M trichloroacetic acid (TCA). The powder was then washed with 5 ml of 5% TCA containing 1 mM EDTA and then with 5 ml water. 8% of the suspension was then removed for the purpose of protein amount normalization. The powder was centrifuged down, sonicated in Lysis Buffer B, and the protein was quantified using the BCA assay. The rest of the powder was pelleted and depleted of neutral lipids by extracting with 6 ml of methanol:chloroform (2:1) for 10 min at room temperature. Acidic lipids were obtained by extracting the tissue with 4.5 ml of methanol:chloroform:HCl (80:40:1) for 15 min at room temperature. PI(3)P in this fraction was then extracted by adding 1.5 ml of chloroform and 2.7 ml of 0.1 M HCl. The lower organic phase was transferred into a 1.5 ml tube, dried under vacuum, and stored at -20°C. PI(3)P was measured using the PI(3)P Mass ELISA Kit following the manufacturer's protocol. The amount of PI(3)P was normalized to the amount of protein extracted from tissue of an equal mass.

Beclin1 immunoprecipitation (IP) and Vps34 activity assay

Freshly collected ventricles were homogenized on ice in Vps34 Lysis Buffer (20 mM Tris, pH 7.5, 137 mM NaCl, 1 mM $MgCl_2$, 1 mM $CaCl_2$, 100 mM NaF, 10 mM sodium pyrophosphate, 1% NP-40, 10% glycerol, 0.1 mM sodium orthovanadate, 0.2 mM PMSF, and 1 μl/ml protease inhibitor cocktail) and centrifuged at 13,500 rpm for 20 min at 4°C. The protein concentration of the supernatants was quantified by Bradford assay. Samples containing 50 μg of protein were used for western blotting, and samples containing 2 mg of protein were used for Beclin1 IP/western blots and Vps34 activity assays. Vps34 was co-precipitated with anti-Beclin1 antibody overnight at 4°C, and the precipitates were pulled down with protein G agarose beads for 1-2 h at 4°C. For Beclin1 IP/western blots, the beads were washed with Vps34 Lysis Buffer, boiled in SDS sample buffer, and subjected to western blotting. For Vps34 assays, the beads were washed 3 times with Vps34 Lysis Buffer and then twice with a buffer containing 50 mM Hepes, pH 7.5, 100 mM NaCl and 1 mM EGTA. 25% of each sample was boiled in SDS sample buffer and subjected to western blotting. The remainder was assayed for Vps34 activity by measuring incorporation of ^{32}P into L-α-phosphatidylinositol as previously described (131). For each heart sample, duplicate IPs were performed and average radioactivity from both Vps34 assays was calculated.

LysoTracker Red staining and confocal microscopy

Cardiomyocytes isolated as described above were plated on laminin-coated glass-bottom dishes (MatTek Corporation). After incubation in ACCIT medium for 2 h, cardiomyocytes were loaded with 67 nM LysoTracker Red for 30 min. Cells were washed twice with ACCIT medium and images were taken using an Olympus Fluoview FV1000 system. The same voltage and magnification were used for each image. Images were exported into TIFF files using FluoView2.0 software (Olympus). The number and area of LysoTracker Red-positive puncta in each cardiomyocyte were analyzed using CellProfiler 2.0 (Broad Institute) (138,139), and statistical analysis was done using GraphPad Prism 4.0.

Immunofluorescence (IF) microscopy for proteins

Cardiomyocytes were isolated as described above, except that Ca^{2+}-free Tyrode Buffer (137.7 mM NaCl, 2.3 mM NaOH, 1 mM $MgCl_2$, 10 mM glucose, 5 mM HEPES, and 5.4 mM KCl) was used instead of MyoBuffer solutions during the Langendorff perfusions, and Ca^{2+}-free KB solution (83 mM KCl, 30 mM K_2HPO_4, 5 mM $MgSO_4$, 5 mM sodium pyruvate, 5 mM β-hydroxy-butyric acid (sodium salt), 5 mM creatine, 20 mM taurine, 10 mM glucose, 0.5 mM EGTA, and 5 mM HEPES) was used instead of Stop Buffer solutions for the manual perfusion, mincing and washing steps. Cardiomyocytes were plated on laminin-coated glass coverslips. After 45 min at room temperature, the KB solution was aspirated and the cells were fixed using 4% PFA in PBS for 20 min. The cells were then permeablized using 0.1% Triton X-100 in PBS, blocked using 5% normal goat serum in PBS, and incubated with mouse anti-p62 antibody in 5% goat serum in PBST (PBS with 0.1% Tween 20) at 4°C overnight. The samples were then incubated with goat anti-mouse IgG secondary antibody conjugated to Alexa Fluor 647 (1:300) in PBST at room temperature for 1 h. Nuclei were stained with DAPI (1 μg/ml in PBS) for 5 min at room temperature. Coverslips were mounted using Immu-Mount and dried overnight. Images were acquired and analyzed using the same method as for LysoTracker Red staining.

For IF microscopy of tissue sections, hearts were retrograde perfused with Ca^{2+}-free Tyrode Buffer and then with 4% PFA. Tissue was fixed for 24 h at 4°C, and then the PFA was removed by four PBS washes over 3-4 h. The tissue was then soaked in 30% sucrose in PBS overnight, equilibrated in 30% sucrose and OCT (1:1) for 30 min, and then embedded in OCT and stored at -80°C. IF staining of 7 μm cryosections was then performed.

IF microscopy for PI(3)P

Control and Vps34 KO MEFs were plated on 0.02% gelatin-coated cover slips and cultured overnight. Cells were fixed in a 1:1 solution of 8% PFA:PBS for 15 min. Cells were washed with PBS containing 50 mM NH_4Cl, and then permeabilized with 20 μM digitonin in Buffer A (20 mM PIPES, pH 6.8, 137 mM NaCl, and 2.7 mM KCl) for 3 min. After washing, cells were blocked with 5% normal goat serum (NGS) and

50 mM NH_4Cl in Buffer A for 45 min, and then incubated with PI(3)P antibody at a 1:50 dilution in 5% NGS in Buffer A for 1 h. goat anti-mouse IgG secondary antibody conjugated to Alexa Fluor 488 (1:200) in 5% NGS in Buffer A was added and incubated for 1 h. After washing, samples were post-fixed for 5 min with 2% PFA, and washed with 50 mM NH_4Cl in Buffer A. Nuclei were stained with DAPI (1 μg/ml in Buffer A) for 5 min. Coverslips were mounted using Immu-Mount and dried overnight. All procedures were done at room temperature. Images were acquired and analyzed using the same method as for LysoTracker Red staining.

Statistical analysis

Student's *t*-test was performed in Microsoft Excel 2013; Mann-Whitney test was performed in Prism GraphPad4.0.

References

1. Houser, S. R., Margulies, K. B., Murphy, A. M., Spinale, F. G., Francis, G. S., Prabhu, S. D., Rockman, H. A., Kass, D. A., Molkentin, J. D., Sussman, M. A., Koch, W. J., American Heart Association Council on Basic Cardiovascular Sciences, C. o. C. C., Council on Functional, G., and Translational, B. (2012) Animal models of heart failure: a scientific statement from the American Heart Association. *Circ Res* **111**, 131-150

2. Mendis, S., Puska, P., and Norrving, B. (2011) Global Atlas on cardiovascular disease prevention and control - Policies, strategies and interventions.

3. Taylor, C. J., Roalfe, A. K., Iles, R., and Hobbs, F. D. (2012) Ten-year prognosis of heart failure in the community: follow-up data from the Echocardiographic Heart of England Screening (ECHOES) study. *Eur J Heart Fail* **14**, 176-184

4. Go, A. S., Mozaffarian, D., Roger, V. L., Benjamin, E. J., Berry, J. D., Borden, W. B., Bravata, D. M., Dai, S., Ford, E. S., Fox, C. S., Franco, S., Fullerton, H. J., Gillespie, C., Hailpern, S. M., Heit, J. A., Howard, V. J., Huffman, M. D., Kissela, B. M., Kittner, S. J., Lackland, D. T., Lichtman, J. H., Lisabeth, L. D., Magid, D., Marcus, G. M., Marelli, A., Matchar, D. B., McGuire, D. K., Mohler, E. R., Moy, C. S., Mussolino, M. E., Nichol, G., Paynter, N. P., Schreiner, P. J., Sorlie, P. D., Stein, J., Turan, T. N., Virani, S. S., Wong, N. D., Woo, D., Turner, M. B., American Heart Association Statistics, C., and Stroke Statistics, S. (2013) Executive summary: heart disease and stroke statistics--2013 update: a report from the American Heart Association. *Circulation* **127**, 143-152

5. Luttrell, L. M. (2006) Transmembrane signaling by G protein-coupled receptors. *Methods Mol Biol* **332**, 3-49

6. Wettschureck, N., and Offermanns, S. (2005) Mammalian G proteins and their cell type specific functions. *Physiol Rev* **85**, 1159-1204

7. Satagopam, V. P., Theodoropoulou, M. C., Stampolakis, C. K., Pavlopoulos, G. A., Papandreou, N. C., Bagos, P. G., Schneider, R., and Hamodrakas, S. J. (2010) GPCRs, G-proteins, effectors and their interactions: human-gpDB, a database employing visualization tools and data integration techniques. *Database : the journal of biological databases and curation* **2010**, baq019

8. Satagopam, V. P., , M. C. T., , C. K. S., Georgios A. Pavlopoulos, N. C. P., , P. G. B., , and Hamodrakas, R. S. a. S. J. (2010) Human-gpDB. Database

9. Fan, G., Jiang, Y. P., Lu, Z., Martin, D. W., Kelly, D. J., Zuckerman, J. M., Ballou, L. M., Cohen, I. S., and Lin, R. Z. (2005) A transgenic mouse model of heart failure using inducible Galpha q. *J. Biol. Chem.* **280**, 40337-40346

10. Pearse, S. G., and Cowie, M. R. (2014) Heart failure: classification and pathophysiology. *Medicine* **42**, 556–561

11. How is heart failure treated? National Heart, Lung and Blood Institute. Webpage, accessed on May 15, 2016.

12. Liggett, S. B., Kelly, R. J., Parekh, R. R., Matkovich, S. J., Benner, B. J., Hahn, H. S., Syed, F. M., Galvez, A. S., Case, K. L., McGuire, N., Odley, A. M., Sparks, L., Kardia, S. L., and Dorn, G. W., 2nd. (2007) A functional polymorphism of the Galphaq (GNAQ) gene is associated with accelerated mortality in African-American heart failure. *Hum Mol Genet* **16**, 2740-2750

13. Frey, U. H., Lieb, W., Erdmann, J., Savidou, D., Heusch, G., Leineweber, K., Jakob, H., Hense, H. W., Lowel, H., Brockmeyer, N. H., Schunkert, H., and Siffert, W. (2008) Characterization of the GNAQ promoter and association of increased Gq expression with cardiac hypertrophy in humans. *Eur Heart J* **29**, 888-897

14. D'Angelo, D. D., Sakata, Y., Lorenz, J. N., Boivin, G. P., Walsh, R. A., Liggett, S. B., and Dorn, G. W., 2nd. (1997) Transgenic Galphaq overexpression induces cardiac contractile failure in mice. *Proc Natl Acad Sci U S A* **94**, 8121-8126

15. Wettschureck, N., Rutten, H., Zywietz, A., Gehring, D., Wilkie, T. M., Chen, J., Chien, K. R., and Offermanns, S. (2001) Absence of pressure overload induced myocardial hypertrophy after conditional inactivation of Galphaq/Galpha11 in cardiomyocytes. *Nat Med* **7**, 1236-1240

16. Pahlavan, S., Oberhofer, M., Sauer, B., Ruppenthal, S., Tian, Q., Scholz, A., Kaestner, L., and Lipp, P. (2012) Galphaq and Galpha11 contribute to the maintenance of cellular electrophysiology and Ca^{2+} handling in ventricular cardiomyocytes. *Cardiovasc Res* **95**, 48-58

17. Sharif-Naeini, R., Folgering, J. H., Bichet, D., Duprat, F., Delmas, P., Patel, A., and Honore, E. (2010) Sensing pressure in the cardiovascular system: Gq-coupled mechanoreceptors and TRP channels. *J Mol Cell Cardiol* **48**, 83-89

18. Kruse, M., Hammond, G. R., and Hille, B. (2012) Regulation of voltage-gated potassium channels by $PI(4,5)P_2$. *J Gen Physiol* **140**, 189-205

19. Miyamoto, S., Howes, A. L., Adams, J. W., Dorn, G. W., 2nd, and Brown, J. H. (2005) Ca^{2+} dysregulation induces mitochondrial depolarization and apoptosis: role of Na^{+}/Ca^{2+} exchanger and AKT. *J Biol Chem* **280**, 38505-38512

20. Braz, J. C., Gregory, K., Pathak, A., Zhao, W., Sahin, B., Klevitsky, R., Kimball, T. F., Lorenz, J. N., Nairn, A. C., Liggett, S. B., Bodi, I., Wang, S., Schwartz, A., Lakatta, E. G., DePaoli-Roach, A. A., Robbins, J., Hewett, T. E., Bibb, J. A., Westfall, M. V., Kranias, E. G., and Molkentin, J. D. (2004) PKC-alpha regulates cardiac contractility and propensity toward heart failure. *Nat Med* **10**, 248-254

21. Dai, D. F., Johnson, S. C., Villarin, J. J., Chin, M. T., Nieves-Cintron, M., Chen, T., Marcinek, D. J., Dorn, G. W., 2nd, Kang, Y. J., Prolla, T. A., Santana, L. F., and Rabinovitch, P. S. (2011) Mitochondrial oxidative stress mediates angiotensin II-induced cardiac hypertrophy and Galphaq overexpression-induced heart failure. *Circ Res* **108**, 837-846

22. Westenbrink, B. D., Ling, H., Divakaruni, A. S., Gray, C. B., Zambon, A. C., Dalton, N. D., Peterson, K. L., Gu, Y., Matkovich, S. J., Murphy, A. N., Miyamoto, S., Dorn, G. W., 2nd, and Heller Brown, J. (2015) Mitochondrial reprogramming induced by CaMKIIdelta mediates hypertrophy decompensation. *Circ Res* **116**, e28-39

23. Chu, C. H., Tzang, B. S., Chen, L. M., Liu, C. J., Tsai, F. J., Tsai, C. H., Lin, J. A., Kuo, W. W., Bau, D. T., Yao, C. H., and Huang, C. Y. (2009) Activation of insulin-like growth factor II receptor induces mitochondrial-dependent apoptosis through G(alpha)q and downstream calcineurin signaling in myocardial cells. *Endocrinology* **150**, 2723-2731

24. Mende, U., Kagen, A., Cohen, A., Aramburu, J., Schoen, F. J., and Neer, E. J. (1998) Transient cardiac expression of constitutively active Galphaq leads to hypertrophy and dilated cardiomyopathy by calcineurin-dependent and independent pathways. *Proc Natl Acad Sci U S A* **95**, 13893-13898

25. Goonasekera, S. A., and Molkentin, J. D. (2012) Unraveling the secrets of a double life: contractile versus signaling Ca^{2+} in a cardiac myocyte. *J Mol Cell Cardiol* **52**, 317-322

26. Kundu, M., and Thompson, C. B. (2008) Autophagy: basic principles and relevance to disease. *Annu Rev Pathol* **3**, 427-455

27. Rabinowitz, J. D., and White, E. (2010) Autophagy and metabolism. *Science* **330**, 1344-1348

28. Essick, E. E., and Sam, F. (2010) Oxidative stress and autophagy in cardiac disease, neurological disorders, aging and cancer. *Oxid Med Cell Longev* **3**, 168-177

29. He, C., Bassik, M. C., Moresi, V., Sun, K., Wei, Y., Zou, Z., An, Z., Loh, J., Fisher, J., Sun, Q., Korsmeyer, S., Packer, M., May, H. I., Hill, J. A., Virgin, H. W., Gilpin, C., Xiao, G., Bassel-Duby, R., Scherer, P. E., and Levine, B. (2012) Exercise-induced BCL2-regulated autophagy is required for muscle glucose homeostasis. *Nature* **481**, 511-515

30. Ohsumi, Y. (2014) Historical landmarks of autophagy research. *Cell Res* **24**, 9-23

31. Noda, N. N., and Inagaki, F. (2015) Mechanisms of Autophagy. *Annu Rev Biophys* **44**, 101-122

32. Gatica, D., Chiong, M., Lavandero, S., and Klionsky, D. J. (2015) Molecular mechanisms of autophagy in the cardiovascular system. *Circ Res* **116**, 456-467

33. Gallagher, L. E., and Chan, E. Y. (2013) Early signalling events of autophagy. *Essays Biochem* **55**, 1-15

34. Obara, K., and Ohsumi, Y. (2011) Atg14: a key player in orchestrating autophagy. *Int J Cell Biol* **2011**, 713435

35. Bento, C. F., Renna, M., Ghislat, G., Puri, C., Ashkenazi, A., Vicinanza, M., Menzies, F. M., and Rubinsztein, D. C. (2016) Mammalian Autophagy: How Does It Work? *Annu Rev Biochem*

36. Pankiv, S., Clausen, T. H., Lamark, T., Brech, A., Bruun, J. A., Outzen, H., Overvatn, A., Bjorkoy, G., and Johansen, T. (2007) p62/SQSTM1 binds directly to Atg8/LC3 to facilitate degradation of ubiquitinated protein aggregates by autophagy. *J Biol Chem* **282**, 24131-24145

37. Ganley, I. G. (2013) Autophagosome maturation and lysosomal fusion. *Essays Biochem* **55**, 65-78

38. Settembre, C., Fraldi, A., Medina, D. L., and Ballabio, A. (2013) Signals from the lysosome: a control centre for cellular clearance and energy metabolism. *Nat Rev Mol Cell Biol* **14**, 283-296

39. Xu, H., and Ren, D. (2015) Lysosomal physiology. *Annu Rev Physiol* **77**, 57-80

40. Lipinski, M. M., Hoffman, G., Ng, A., Zhou, W., Py, B. F., Hsu, E., Liu, X., Eisenberg, J., Liu, J., Blenis, J., Xavier, R. J., and Yuan, J. (2010) A genome-

wide siRNA screen reveals multiple mTORC1 independent signaling pathways regulating autophagy under normal nutritional conditions. *Dev Cell* **18**, 1041-1052

41. Jaber, N., Dou, Z., Chen, J. S., Catanzaro, J., Jiang, Y. P., Ballou, L. M., Selinger, E., Ouyang, X., Lin, R. Z., Zhang, J., and Zong, W. X. (2012) Class III PI3K Vps34 plays an essential role in autophagy and in heart and liver function. *Proc Natl Acad Sci U S A* **109**, 2003-2008

42. Taneike, M., Yamaguchi, O., Nakai, A., Hikoso, S., Takeda, T., Mizote, I., Oka, T., Tamai, T., Oyabu, J., Murakawa, T., Nishida, K., Shimizu, T., Hori, M., Komuro, I., Takuji Shirasawa, T. S., Mizushima, N., and Otsu, K. (2010) Inhibition of autophagy in the heart induces age-related cardiomyopathy. *Autophagy* **6**, 600-606

43. Nakai, A., Yamaguchi, O., Takeda, T., Higuchi, Y., Hikoso, S., Taniike, M., Omiya, S., Mizote, I., Matsumura, Y., Asahi, M., Nishida, K., Hori, M., Mizushima, N., and Otsu, K. (2007) The role of autophagy in cardiomyocytes in the basal state and in response to hemodynamic stress. *Nat Med* **13**, 619-624

44. Yan, L., Vatner, D. E., Kim, S. J., Ge, H., Masurekar, M., Massover, W. H., Yang, G., Matsui, Y., Sadoshima, J., and Vatner, S. F. (2005) Autophagy in chronically ischemic myocardium. *Proc Natl Acad Sci U S A* **102**, 13807-13812

45. Zhu, H., Tannous, P., Johnstone, J. L., Kong, Y., Shelton, J. M., Richardson, J. A., Le, V., Levine, B., Rothermel, B. A., and Hill, J. A. (2007) Cardiac autophagy is a maladaptive response to hemodynamic stress. *J Clin Invest* **117**, 1782-1793

46. Jiang, Y. P., Ballou, L. M., Lu, Z., Li, W., Kelly, D. J., Cohen, I. S., and Lin, R. Z. (2006) Reversible heart failure in G alpha(q) transgenic mice. *J. Biol. Chem.* **281**, 29988-29992

47. Wu, C. Y., Chen, B., Jiang, Y. P., Jia, Z., Martin, D. W., Liu, S., Entcheva, E., Song, L. S., and Lin, R. Z. (2014) Calpain-dependent cleavage of junctophilin-2 and T-tubule remodeling in a mouse model of reversible heart failure. *J Am Heart Assoc* **3**, e000527

48. Eskelinen, E. L. (2005) Maturation of autophagic vacuoles in Mammalian cells. *Autophagy* **1**, 1-10

49. Fidzianska, A., Bilinska, Z. T., Walczak, E., Witkowski, A., and Chojnowska, L. (2010) Autophagy in transition from hypertrophic cardiomyopathy to heart failure. *J Electron Microsc (Tokyo)* **59**, 181-183

50. Frerichs, F. C., Dingemans, K. P., and Brinkman, K. (2002) Cardiomyopathy with mitochondrial damage associated with nucleoside reverse-transcriptase inhibitors. *The New England journal of medicine* **347**, 1895-1896

51. Gupta, A., Gupta, S., Young, D., Das, B., McMahon, J., and Sen, S. (2010) Impairment of ultrastructure and cytoskeleton during progression of cardiac hypertrophy to heart failure. *Laboratory investigation; a journal of technical methods and pathology* **90**, 520-530

52. Ylä-Anttila, P., Vihinen, H., Jokitalo, E., and Eskelinen, E. L. (2009) Chapter 10 Monitoring Autophagy by Electron Microscopy in Mammalian Cells. **452**, 143-164

53. Jain, A., Lamark, T., Sjottem, E., Larsen, K. B., Awuh, J. A., Overvatn, A., McMahon, M., Hayes, J. D., and Johansen, T. (2010) p62/SQSTM1 is a target gene for transcription factor NRF2 and creates a positive feedback loop by inducing antioxidant response element-driven gene transcription. *J Biol Chem* **285**, 22576-22591

54. Duran, A., Linares, J. F., Galvez, A. S., Wikenheiser, K., Flores, J. M., Diaz-Meco, M. T., and Moscat, J. (2008) The signaling adaptor p62 is an important NF-kappaB mediator in tumorigenesis. *Cancer Cell* **13**, 343-354

55. Puissant, A., Robert, G., Fenouille, N., Luciano, F., Cassuto, J. P., Raynaud, S., and Auberger, P. (2010) Resveratrol promotes autophagic cell death in chronic myelogenous leukemia cells via JNK-mediated p62/SQSTM1 expression and AMPK activation. *Cancer Res* **70**, 1042-1052

56. Komatsu, M., Kurokawa, H., Waguri, S., Taguchi, K., Kobayashi, A., Ichimura, Y., Sou, Y. S., Ueno, I., Sakamoto, A., Tong, K. I., Kim, M., Nishito, Y., Iemura, S., Natsume, T., Ueno, T., Kominami, E., Motohashi, H., Tanaka, K., and Yamamoto, M. (2010) The selective autophagy substrate p62 activates the stress responsive transcription factor Nrf2 through inactivation of Keap1. *Nat Cell Biol* **12**, 213-223

57. Pan, J. A., Sun, Y., Jiang, Y. P., Bott, A. J., Jaber, N., Dou, Z., Yang, B., Chen, J. S., Catanzaro, J. M., Du, C., Ding, W. X., Diaz-Meco, M. T., Moscat, J., Ozato, K., Lin, R. Z., and Zong, W. X. (2016) TRIM21 Ubiquitylates SQSTM1/p62 and Suppresses Protein Sequestration to Regulate Redox Homeostasis. *Mol Cell* **61**, 720-733

58. Zaidi, N., Maurer, A., Nieke, S., and Kalbacher, H. (2008) Cathepsin D: a cellular roadmap. *Biochem Biophys Res Commun* **376**, 5-9

59. Kim, J., Kim, Y. C., Fang, C., Russell, R. C., Kim, J. H., Fan, W., Liu, R., Zhong, Q., and Guan, K. L. (2013) Differential regulation of distinct Vps34 complexes by AMPK in nutrient stress and autophagy. *Cell* **152**, 290-303

60. Wauson, E. M., Dbouk, H. A., Ghosh, A. B., and Cobb, M. H. (2014) G protein-coupled receptors and the regulation of autophagy. *Trends Endocrinol Metab* **25**, 274-282

61. Qipshidze, N., Tyagi, N., Metreveli, N., Lominadze, D., and Tyagi, S. C. (2012) Autophagy mechanism of right ventricular remodeling in murine model of pulmonary artery constriction. *Am J Physiol Heart Circ Physiol* **302**, H688-696

62. Tannous, P., Zhu, H., Nemchenko, A., Berry, J. M., Johnstone, J. L., Shelton, J. M., Miller, F. J., Jr., Rothermel, B. A., and Hill, J. A. (2008) Intracellular protein aggregation is a proximal trigger of cardiomyocyte autophagy. *Circulation* **117**, 3070-3078

63. Zhang, T., Dong, K., Liang, W., Xu, D., Xia, H., Geng, J., Najafov, A., Liu, M., Li, Y., Han, X., Xiao, J., Jin, Z., Peng, T., Gao, Y., Cai, Y., Qi, C., Zhang, Q., Sun, A., Lipinski, M., Zhu, H., Xiong, Y., Pandolfi, P. P., Li, H., Yu, Q., and Yuan, J. (2015) G-protein-coupled receptors regulate autophagy by ZBTB16-mediated ubiquitination and proteasomal degradation of Atg14L. *Elife* **4**, e06734

64. Sarkar, S., Floto, R. A., Berger, Z., Imarisio, S., Cordenier, A., Pasco, M., Cook, L. J., and Rubinsztein, D. C. (2005) Lithium induces autophagy by inhibiting inositol monophosphatase. *J Cell Biol* **170**, 1101-1111

65. Vicencio, J. M., Ortiz, C., Criollo, A., Jones, A. W., Kepp, O., Galluzzi, L., Joza, N., Vitale, I., Morselli, E., Tailler, M., Castedo, M., Maiuri, M. C., Molgo, J., Szabadkai, G., Lavandero, S., and Kroemer, G. (2009) The inositol 1,4,5-trisphosphate receptor regulates autophagy through its interaction with Beclin 1. *Cell Death Differ* **16**, 1006-1017

66. Wong, A., Grubb, D. R., Cooley, N., Luo, J., and Woodcock, E. A. (2013) Regulation of autophagy in cardiomyocytes by Ins(1,4,5)P(3) and IP(3)-receptors. *J Mol Cell Cardiol* **54**, 19-24

67. Law, B. Y., Wang, M., Ma, D. L., Al-Mousa, F., Michelangeli, F., Cheng, S. H., Ng, M. H., To, K. F., Mok, A. Y., Ko, R. Y., Lam, S. K., Chen, F., Che, C. M., Chiu, P., and Ko, B. C. (2010) Alisol B, a novel inhibitor of the sarcoplasmic/endoplasmic reticulum Ca(2+) ATPase pump, induces autophagy, endoplasmic reticulum stress, and apoptosis. *Mol Cancer Ther* **9**, 718-730

68. Vingtdeux, V., Giliberto, L., Zhao, H., Chandakkar, P., Wu, Q., Simon, J. E., Janle, E. M., Lobo, J., Ferruzzi, M. G., Davies, P., and Marambaud, P. (2010) AMP-activated protein kinase signaling activation by resveratrol modulates amyloid-beta peptide metabolism. *J Biol Chem* **285**, 9100-9113

69. Harr, M. W., McColl, K. S., Zhong, F., Molitoris, J. K., and Distelhorst, C. W. (2010) Glucocorticoids downregulate Fyn and inhibit IP(3)-mediated calcium signaling to promote autophagy in T lymphocytes. *Autophagy* **6**, 912-921

70. Demarchi, F., Bertoli, C., Copetti, T., Tanida, I., Brancolini, C., Eskelinen, E. L., and Schneider, C. (2006) Calpain is required for macroautophagy in mammalian cells. *J Cell Biol* **175**, 595-605

71. Williams, A., Sarkar, S., Cuddon, P., Ttofi, E. K., Saiki, S., Siddiqi, F. H., Jahreiss, L., Fleming, A., Pask, D., Goldsmith, P., O'Kane, C. J., Floto, R. A., and Rubinsztein, D. C. (2008) Novel targets for Huntington's disease in an mTOR-independent autophagy pathway. *Nat Chem Biol* **4**, 295-305

72. Petiot, A., Ogier-Denis, E., Blommaart, E. F., Meijer, A. J., and Codogno, P. (2000) Distinct classes of phosphatidylinositol 3'-kinases are involved in signaling pathways that control macroautophagy in HT-29 cells. *J Biol Chem* **275**, 992-998

73. Levine, B., and Kroemer, G. (2008) Autophagy in the pathogenesis of disease. *Cell* **132**, 27-42

74. Ballou, L. M., Chattopadhyay, M., Li, Y., Scarlata, S., and Lin, R. Z. (2006) Galphaq binds to p110alpha/p85alpha phosphoinositide 3-kinase and displaces Ras. *Biochem J* **394**, 557-562

75. Ballou, L. M., Lin, H. Y., Fan, G., Jiang, Y. P., and Lin, R. Z. (2003) Activated G alpha q inhibits p110 alpha phosphatidylinositol 3-kinase and Akt. *J Biol Chem* **278**, 23472-23479

76. Slessareva, J. E., Routt, S. M., Temple, B., Bankaitis, V. A., and Dohlman, H. G. (2006) Activation of the phosphatidylinositol 3-kinase Vps34 by a G protein alpha subunit at the endosome. *Cell* **126**, 191-203

77. Kihara, A., Noda, T., Ishihara, N., and Ohsumi, Y. (2001) Two distinct Vps34 phosphatidylinositol 3-kinase complexes function in autophagy and carboxypeptidase Y sorting in Saccharomyces cerevisiae. *J Cell Biol* **152**, 519-530

78. Thoresen, S. B., Pedersen, N. M., Liestol, K., and Stenmark, H. (2010) A phosphatidylinositol 3-kinase class III sub-complex containing VPS15, VPS34, Beclin 1, UVRAG and BIF-1 regulates cytokinesis and degradative endocytic traffic. *Exp Cell Res* **316**, 3368-3378

79. Fogel, A. I., Dlouhy, B. J., Wang, C., Ryu, S. W., Neutzner, A., Hasson, S. A., Sideris, D. P., Abeliovich, H., and Youle, R. J. (2013) Role of membrane association and Atg14-dependent phosphorylation in beclin-1-mediated autophagy. *Mol Cell Biol* **33**, 3675-3688

80. Ambrosini, G., Pratilas, C. A., Qin, L. X., Tadi, M., Surriga, O., Carvajal, R. D., and Schwartz, G. K. (2012) Identification of unique MEK-dependent genes in GNAQ mutant uveal melanoma involved in cell growth, tumor cell invasion, and MEK resistance. *Clin Cancer Res* **18**, 3552-3561

81. Kang, B. Y., Hu, C., Ryu, S., Khan, J. A., Biancolella, M., Prayaga, S., Seung, K. B., Novelli, G., Mehta, P., and Mehta, J. L. (2010) Genomics of cardiac remodeling in angiotensin II-treated wild-type and LOX-1-deficient mice. *Physiol Genomics* **42**, 42-54

82. Schlossarek, S., Englmann, D. R., Sultan, K. R., Sauer, M., Eschenhagen, T., and Carrier, L. (2012) Defective proteolytic systems in Mybpc3-targeted mice with cardiac hypertrophy. *Basic Res Cardiol* **107**, 235

83. Reichelt, M. E., Mellor, K. M., Curl, C. L., Stapleton, D., and Delbridge, L. M. (2013) Myocardial glycophagy - a specific glycogen handling response to metabolic stress is accentuated in the female heart. *J Mol Cell Cardiol* **65**, 67-75

84. Zheng, Q., Su, H., Ranek, M. J., and Wang, X. (2011) Autophagy and p62 in cardiac proteinopathy. *Circ Res* **109**, 296-308

85. Zhang, D. D., Lo, S. C., Cross, J. V., Templeton, D. J., and Hannink, M. (2004) Keap1 is a redox-regulated substrate adaptor protein for a Cul3-dependent ubiquitin ligase complex. *Mol Cell Biol* **24**, 10941-10953

86. Kobayashi, A., Kang, M. I., Okawa, H., Ohtsuji, M., Zenke, Y., Chiba, T., Igarashi, K., and Yamamoto, M. (2004) Oxidative stress sensor Keap1 functions as an adaptor for Cul3-based E3 ligase to regulate proteasomal degradation of Nrf2. *Mol Cell Biol* **24**, 7130-7139

87. Lau, A., Wang, X. J., Zhao, F., Villeneuve, N. F., Wu, T., Jiang, T., Sun, Z., White, E., and Zhang, D. D. (2010) A noncanonical mechanism of Nrf2 activation by autophagy deficiency: direct interaction between Keap1 and p62. *Mol Cell Biol* **30**, 3275-3285

88. Date, M. O., Morita, T., Yamashita, N., Nishida, K., Yamaguchi, O., Higuchi, Y., Hirotani, S., Matsumura, Y., Hori, M., Tada, M., and Otsu, K. (2002) The antioxidant N-2-mercaptopropionyl glycine attenuates left ventricular hypertrophy in in vivo murine pressure-overload model. *J Am Coll Cardiol* **39**, 907-912

89. Lancel, S., Qin, F., Lennon, S. L., Zhang, J., Tong, X., Mazzini, M. J., Kang, Y. J., Siwik, D. A., Cohen, R. A., and Colucci, W. S. (2010) Oxidative posttranslational modifications mediate decreased SERCA activity and myocyte dysfunction in Galphaq-overexpressing mice. *Circ Res* **107**, 228-232

90. Adams, J. W., Pagel, A. L., Means, C. K., Oksenberg, D., Armstrong, R. C., and Brown, J. H. (2000) Cardiomyocyte apoptosis induced by Galphaq signaling is mediated by permeability transition pore formation and activation of the mitochondrial death pathway. *Circ Res* **87**, 1180-1187

91. Das, S., Mitrovsky, G., Vasanthi, H. R., and Das, D. K. (2014) Antiaging properties of a grape-derived antioxidant are regulated by mitochondrial balance of fusion and fission leading to mitophagy triggered by a signaling network of Sirt1-Sirt3-Foxo3-PINK1-PARKIN. *Oxid Med Cell Longev* **2014**, 345105

92. Patterson, C., Portbury, A. L., Schisler, J. C., and Willis, M. S. (2011) Tear me down: role of calpain in the development of cardiac ventricular hypertrophy. *Circ Res* **109**, 453-462

93. Bukowska, A., Lendeckel, U., Bode-Boger, S. M., and Goette, A. (2012) Physiologic and pathophysiologic role of calpain: implications for the occurrence of atrial fibrillation. *Cardiovascular therapeutics* **30**, e115-127

94. Friedrich, P. (2004) The intriguing Ca^{2+} requirement of calpain activation. *Biochem Biophys Res Commun* **323**, 1131-1133

95. Demarchi, F., and Schneider, C. (2007) The calpain system as a modulator of stress/damage response. *Cell Cycle* **6**, 136-138

96. Mancini, M., Leo, E., Campi, V., Castagnetti, F., Zazzeroni, L., Gugliotta, G., Santucci, M. A., and Martinelli, G. (2014) A calpain-cleaved fragment of beta-catenin promotes BCRABL1+ cell survival evoked by autophagy induction in response to imatinib. *Cellular signalling* **26**, 1690-1697

97. Yousefi, S., Perozzo, R., Schmid, I., Ziemiecki, A., Schaffner, T., Scapozza, L., Brunner, T., and Simon, H. U. (2006) Calpain-mediated cleavage of Atg5 switches autophagy to apoptosis. *Nat Cell Biol* **8**, 1124-1132

98. Norman, J. M., Cohen, G. M., and Bampton, E. T. (2010) The in vitro cleavage of the hAtg proteins by cell death proteases. *Autophagy* **6**, 1042-1056

99. Russo, R., Berliocchi, L., Adornetto, A., Varano, G. P., Cavaliere, F., Nucci, C., Rotiroti, D., Morrone, L. A., Bagetta, G., and Corasaniti, M. T. (2011) Calpain-mediated cleavage of Beclin-1 and autophagy deregulation following retinal ischemic injury in vivo. *Cell death & disease* **2**, e144

100. Menzies, F. M., Garcia-Arencibia, M., Imarisio, S., O'Sullivan, N. C., Ricketts, T., Kent, B. A., Rao, M. V., Lam, W., Green-Thompson, Z. W., Nixon, R. A., Saksida, L. M., Bussey, T. J., O'Kane, C. J., and Rubinsztein, D. C. (2015) Calpain inhibition mediates autophagy-dependent protection against polyglutamine toxicity. *Cell death and differentiation* **22**, 433-444

101. Li, M., Wang, X., Yu, Y., Yu, Y., Xie, Y., Zou, Y., Ge, J., Peng, T., and Chen, R. (2014) Coxsackievirus B3-induced calpain activation facilitates the progeny virus replication via a likely mechanism related with both autophagy enhancement and apoptosis inhibition in the early phase of infection: an in vitro study in H9c2 cells. *Virus research* **179**, 177-186

102. Pedrozo, Z., Sanchez, G., Torrealba, N., Valenzuela, R., Fernandez, C., Hidalgo, C., Lavandero, S., and Donoso, P. (2010) Calpains and proteasomes mediate degradation of ryanodine receptors in a model of cardiac ischemic reperfusion. *Biochim Biophys Acta* **1802**, 356-362

103. McMillan, E. M., Pare, M. F., Baechler, B. L., Graham, D. A., Rush, J. W., and Quadrilatero, J. (2015) Autophagic signaling and proteolytic enzyme activity in cardiac and skeletal muscle of spontaneously hypertensive rats following chronic aerobic exercise. *PLoS One* **10**, e0119382

104. Yuan, H. X., Russell, R. C., and Guan, K. L. (2013) Regulation of PIK3C3/VPS34 complexes by MTOR in nutrient stress-induced autophagy. *Autophagy* **9**, 1983-1995

105. Park, J. M., Jung, C. H., Seo, M., Otto, N. M., Grunwald, D., Kim, K. H., Moriarity, B., Kim, Y. M., Starker, C., Nho, R. S., Voytas, D., and Kim, D. H. (2016) The ULK1 complex mediates MTORC1 signaling to the autophagy initiation machinery via binding and phosphorylating ATG14. *Autophagy* **12**, 547-564

106. Jenie, R. I., Nishimura, M., Fujino, M., Nakaya, M., Mizuno, N., Tago, K., Kurose, H., and Itoh, H. (2013) Increased ubiquitination and the crosstalk of G protein signaling in cardiac myocytes: involvement of Ric-8B in Gs suppression by Gq signal. *Genes Cells* **18**, 1095-1106

107. Wang, Z. G., Wang, Y., Huang, Y., Lu, Q., Zheng, L., Hu, D., Feng, W. K., Liu, Y. L., Ji, K. T., Zhang, H. Y., Fu, X. B., Li, X. K., Chu, M. P., and Xiao, J. (2015) bFGF regulates autophagy and ubiquitinated protein accumulation induced by myocardial ischemia/reperfusion via the activation of the PI3K/Akt/mTOR pathway. *Sci Rep* **5**, 9287

108. Razeghi, P., Baskin, K. K., Sharma, S., Young, M. E., Stepkowski, S., Essop, M. F., and Taegtmeyer, H. (2006) Atrophy, hypertrophy, and hypoxemia induce transcriptional regulators of the ubiquitin proteasome system in the rat heart. *Biochem Biophys Res Commun* **342**, 361-364

109. Kelly, E., Bailey, C. P., and Henderson, G. (2008) Agonist-selective mechanisms of GPCR desensitization. *Br J Pharmacol* **153 Suppl 1**, S379-388

110. Claycomb, W. C., Lanson, N. A., Jr., Stallworth, B. S., Egeland, D. B., Delcarpio, J. B., Bahinski, A., and Izzo, N. J., Jr. (1998) HL-1 cells: a cardiac muscle cell line that contracts and retains phenotypic characteristics of the adult cardiomyocyte. *Proc Natl Acad Sci U S A* **95**, 2979-2984

111. Graham, E. L., Balla, C., Franchino, H., Melman, Y., del Monte, F., and Das, S. (2013) Isolation, culture, and functional characterization of adult mouse cardiomyoctyes. *J Vis Exp*, e50289

112. Kabaeva, Z., Zhao, M., and Michele, D. E. (2008) Blebbistatin extends culture life of adult mouse cardiac myocytes and allows efficient and stable transgene expression. *Am J Physiol Heart Circ Physiol* **294**, H1667-1674

113. Mitcheson, J. S., Hancox, J. C., and Levi, A. J. (1998) Cultured adult cardiac myocytes: future applications, culture methods, morphological and electrophysiological properties. *Cardiovasc Res* **39**, 280-300

114. Dispersyn, G. D., Geuens, E., Ver Donck, L., Ramaekers, F. C., and Borgers, M. (2001) Adult rabbit cardiomyocytes undergo hibernation-like dedifferentiation when co-cultured with cardiac fibroblasts. *Cardiovasc Res* **51**, 230-240

115. Louch, W. E., Sheehan, K. A., and Wolska, B. M. (2011) Methods in cardiomyocyte isolation, culture, and gene transfer. *J Mol Cell Cardiol* **51**, 288-298

116. Lang, S. E., and Westfall, M. V. (2015) Gene transfer into cardiac myocytes. *Methods Mol Biol* **1299**, 177-190

117. Driesen, R. B., Verheyen, F. K., Dispersyn, G. D., Thone, F., Lenders, M. H., Ramaekers, F. C., and Borgers, M. (2006) Structural adaptation in adult rabbit

ventricular myocytes: influence of dynamic physical interaction with fibroblasts. *Cell Biochem Biophys* **44**, 119-128

118. Blaauw, E., van Nieuwenhoven, F. A., Willemsen, P., Delhaas, T., Prinzen, F. W., Snoeckx, L. H., van Bilsen, M., and van der Vusse, G. J. (2010) Stretch-induced hypertrophy of isolated adult rabbit cardiomyocytes. *Am J Physiol Heart Circ Physiol* **299**, H780-787

119. Wei, S., Guo, A., Chen, B., Kutschke, W., Xie, Y. P., Zimmerman, K., Weiss, R. M., Anderson, M. E., Cheng, H., and Song, L. S. (2010) T-tubule remodeling during transition from hypertrophy to heart failure. *Circ Res* **107**, 520-531

120. Kumar, S. N., Konorev, E. A., Aggarwal, D., and Kalyanaraman, B. (2011) Analysis of proteome changes in doxorubicin-treated adult rat cardiomyocyte. *J Proteomics* **74**, 683-697

121. Blaauw, E., Lorenzen-Schmidt, I., Babiker, F. A., Munts, C., Prinzen, F. W., Snoeckx, L. H., van Bilsen, M., van der Vusse, G. J., and van Nieuwenhoven, F. A. (2013) Stretch-induced upregulation of connective tissue growth factor in rabbit cardiomyocytes. *J Cardiovasc Transl Res* **6**, 861-869

122. Lu, Z., Jiang, Y. P., Wu, C. Y., Ballou, L. M., Liu, S., Carpenter, E. S., Rosen, M. R., Cohen, I. S., and Lin, R. Z. (2013) Increased persistent sodium current due to decreased PI3K signaling contributes to QT prolongation in the diabetic heart. *Diabetes* **62**, 4257-4265

123. Fetalvero, K. M., Yu, Y., Goetschkes, M., Liang, G., Valdez, R. A., Gould, T., Triantafellow, E., Bergling, S., Loureiro, J., Eash, J., Lin, V., Porter, J. A., Finan, P. M., Walsh, K., Yang, Y., Mao, X., and Murphy, L. O. (2013) Defective autophagy and mTORC1 signaling in myotubularin null mice. *Mol Cell Biol* **33**, 98-110

124. Chilvers, E. R., Batty, I. H., Challiss, R. A., Barnes, P. J., and Nahorski, S. R. (1991) Determination of mass changes in phosphatidylinositol 4,5-bisphosphate and evidence for agonist-stimulated metabolism of inositol 1,4,5-trisphosphate in airway smooth muscle. *Biochem J* **275 (Pt 2)**, 373-379

125. Creba, J. A., Downes, C. P., Hawkins, P. T., Brewster, G., Michell, R. H., and Kirk, C. J. (1983) Rapid breakdown of phosphatidylinositol 4-phosphate and phosphatidylinositol 4,5-bisphosphate in rat hepatocytes stimulated by vasopressin and other Ca^{2+}-mobilizing hormones. *Biochem J* **212**, 733-747

126. Downes, C. P., Dibner, M. D., and Hanley, M. R. (1983) Sympathetic denervation impairs agonist-stimulated phosphatidylinositol metabolism in rat parotid glands. *Biochem J* **214**, 865-870

127. Sohal, D. S., Nghiem, M., Crackower, M. A., Witt, S. A., Kimball, T. R., Tymitz, K. M., Penninger, J. M., and Molkentin, J. D. (2001) Temporally regulated and tissue-specific gene manipulations in the adult and embryonic heart using a tamoxifen-inducible Cre protein. *Circ Res* **89**, 20-25

128. Balla, T., and Varnai, P. (2009) Visualization of cellular phosphoinositide pools with GFP-fused protein-domains. *Current protocols in cell biology / editorial board, Juan S. Bonifacino ... [et al.]* **Chapter 24**, Unit 24 24

129. Hammond, G. R., Schiavo, G., and Irvine, R. F. (2009) Immunocytochemical techniques reveal multiple, distinct cellular pools of PtdIns4P and PtdIns(4,5)P(2). *Biochem J* **422**, 23-35

130. Lu, Z., Jiang, Y. P., Ballou, L. M., Cohen, I. S., and Lin, R. Z. (2005) Galpha q inhibits cardiac L-type Ca^{2+} channels through phosphatidylinositol 3-kinase. *J Biol Chem* **280**, 40347-40354

131. Dou, Z., Chattopadhyay, M., Pan, J. A., Guerriero, J. L., Jiang, Y. P., Ballou, L. M., Yue, Z., Lin, R. Z., and Zong, W. X. (2010) The class IA phosphatidylinositol 3-kinase p110-beta subunit is a positive regulator of autophagy. *J Cell Biol* **191**, 827-843

132. Ballou, L. M., Cross, M. E., Huang, S., McReynolds, E. M., Zhang, B. X., and Lin, R. Z. (2000) Differential regulation of the phosphatidylinositol 3-kinase/Akt and p70 S6 kinase pathways by the alpha(1A)-adrenergic receptor in rat-1 fibroblasts. *J Biol Chem* **275**, 4803-4809

133. Zhou, Y. Y., Wang, S. Q., Zhu, W. Z., Chruscinski, A., Kobilka, B. K., Ziman, B., Wang, S., Lakatta, E. G., Cheng, H., and Xiao, R. P. (2000) Culture and adenoviral infection of adult mouse cardiac myocytes: methods for cellular genetic physiology. *Am J Physiol Heart Circ Physiol* **279**, H429-436

134. Ellingsen, O., Davidoff, A. J., Prasad, S. K., Berger, H. J., Springhorn, J. P., Marsh, J. D., Kelly, R. A., and Smith, T. W. (1993) Adult rat ventricular myocytes cultured in defined medium: phenotype and electromechanical function. *Am J Physiol* **265**, H747-754

135. Yla-Anttila, P., Vihinen, H., Jokitalo, E., and Eskelinen, E. L. (2009) Monitoring autophagy by electron microscopy in Mammalian cells. *Methods Enzymol* **452**, 143-164

136. Livak, K. J., and Schmittgen, T. D. (2001) Analysis of relative gene expression data using real-time quantitative PCR and the 2(-Delta Delta C(T)) Method. *Methods* **25**, 402-408

137. Bustin, S. A., Benes, V., Garson, J. A., Hellemans, J., Huggett, J., Kubista, M., Mueller, R., Nolan, T., Pfaffl, M. W., Shipley, G. L., Vandesompele, J., and Wittwer, C. T. (2009) The MIQE guidelines: minimum information for publication of quantitative real-time PCR experiments. *Clin Chem* **55**, 611-622

138. Carpenter, A. E., Jones, T. R., Lamprecht, M. R., Clarke, C., Kang, I. H., Friman, O., Guertin, D. A., Chang, J. H., Lindquist, R. A., Moffat, J., Golland, P., and Sabatini, D. M. (2006) CellProfiler: image analysis software for identifying and quantifying cell phenotypes. *Genome Biol* **7**, R100

139. Kamentsky, L., Jones, T. R., Fraser, A., Bray, M. A., Logan, D. J., Madden, K. L., Ljosa, V., Rueden, C., Eliceiri, K. W., and Carpenter, A. E. (2011) Improved structure, function and compatibility for CellProfiler: modular high-throughput image analysis software. *Bioinformatics* **27**, 1179-1180

140. Eiyama, A., and Okamoto, K. (2015) PINK1/Parkin-mediated mitophagy in mammalian cells. *Curr Opin Cell Biol* 33, 95-101

141. Yamano, K., and Youle, R. J. (2013) PINK1 is degraded through the N-end rule pathway. *Autophagy* 9, 1758-1769